

https://dspace.org/

Evaluation of glassfibre reinforced plastic pipe couplings for high pressure applications

Gutmayer, Johannes

1992

https://hdl.handle.net/10539/28740

Downloaded from a DSpace repository. https://dspace.org/

EVALUATION OF GLASSFIBRE REINFORCED PLASTIC PIPE COUPLINGS FOR HIGH PRESSURE APPLICATIONS

Johannes Gutmayer

A dissertation submitted to the Faculty of Engineering, University of the Witwatersrand, Johannesburg, in fulfilment of the requirements for the Degree of Master of Science in Engineering.

Johannesburg, February 1992

DECLARATION

I declare that this dissertation is my own, unaided work. It is being submitted for the Degree of Master of Science in Engineering in the University of the Witwatersrand, Johannesburg. It has not been submitted before for any degree or examination in any other University.

J GUTMAYER : candidate

JOHANNESBURG , 10 day of MARCH 1992

ABSTRACT

This research was conducted in order to establish the feasibility of manufacturing GRP pipe couplings for high pressure GRP piping systems. The use of GRP pipes in high pressure piping systems is desirable due to their light weight, high corrosion resistance and their extremely low friction factors.

To date no official standard exists that details the design of GRP pipes or GRP couplings for high pressure applications in excess of 7 MPa. In this report various existing steel and GRP couplings are discussed. From this the GRP coupling tested during the present investigation was developed.

Tensile testing of couplings was carried out at each stage of the development phase in order to assess design modifications and to obtain an overview of the behaviour of GRP couplings. The test specimens were made from 400 mm long E-glass/epoxy pipe sections with an internal diameter of 50 mm, a wall thickness of 8 mm and a fibre orientation of ±55°.

The most suitable design suggested in this report consists of a pipe with a machined step and a flange laid up directly onto the pipe. The load is transferred from the pipe to the flange via adhesive shear stresses and through a mechanical interaction between the pipe and the flange. The seal is made with a hydrostatic "U"-type rubber seal, which is located on the outside of the pipe. An outer split clamp clamps over the flanges on adjacent pipes, thus holding these together. A thin sleeve over the split clamp secures the clamp.

The maximum load bearing capacity for this coupling was 75 kN, which is equivalent to an internal pressure of 22 MPa. Three different failure modes occurred, viz. interlaminar shear of the pipe, buckling of the fibres on the inside of the pipe and compression of the fibres on the face of the step. The type of failure depended on the location and depth of the step on

the pipe. Since failure occurred only in the pipe, it was concluded that the pipe needs to be tailored at the ends in order to achieve higher pressure capabilities.

A finite element model was used to simulate one of the experimental pipe/coupling configurations. This allowed experimental and theoretical results to be correlated, and a prediction of the coupling performance to be made.

ACKNOWLEDGEMENTS

I wish to place on record my appreciation for the help rendered by the following persons, companies and institutions during the course of my research:

- Dr. H CHANDLER - project supervisor
- MECHANICAL ENGINEERING WORKSHOP - for the manufacture of all the necessary experimental equipment.
- AERODYNE - for the manufacture of the filament wound pipe sections.
- AFI - for the supply of the glass reinforcement.
- NCS - or the supply of resins and bulk moulding compound.
- CHAMBER OF MINES - for their comments and ideas concerning this research.
- PAT HARRIS - for his comments and ideas concerning this research.

CONTENTS

	Page
Abstract	i
Acknowledgements	iii
Contents	iv
List of Figures	vi
List of Tables	ix
1. INTRODUCTION	1
1.1 Problem statement and requirements	3
2. REVIEW OF COUPLINGS	6
2.1 Literature survey	6
2.1.1 Pipe joints and couplings	6
2.1.2 Standards for pipe and joint design	17
2.2 Suggested modifications	19
2.2.1 GRP flange joint	19
2.2.2 Adapted Viking Johnson coupling	20
2.2.3 Adapted victaulic coupling	23
3. CALCULATION OF THE INITIAL PIPE AND COUPLING DIMENSIONS	27
3.1 Thin cylinder theory	28
3.2 Classical lamination theory	30
3.3 Adhesive shear stresses	34
4. EXPERIMENTATION	36
4.1 Experimental program	37
4.1.1 Test specimens	37
4.1.2 Testing apparatus	42
4.2 Results	45
4.2.1 Experimental results	45
4.2.2 Finite element results	65
5. DISCUSSION	73
5.1 Coupling development	73
5.2 Factors affecting the coupling performance	90

Page

5.3 Correlation between experimental and theoretical results 97

5.4 Performance prediction using the finite element method 100

5.5 General considerations and recommendations 109

6. CONCLUSIONS 118

7. RECOMMENDATIONS 122

References

Appendices

LIST OF FIGURES

		Page
2.1	Butt and strap joint	7
2.2	Bell and spigot joint	8
2.3	Threaded connection	9
2.4	Bolted flange joint	10
2.5	Victaulic coupling with hydrostatic seal	11
2.6	Victaulic coupling adapted for PVC pipes	12
2.7	Viking Johnson c' mp-on joint	13
2.8	"Kwikey" quick-connect coupling	14
2.9	Flange bonded to pipe by scarf joint	15
2.10	Flanged joint in GRP	19
2.11	Self-locking flange	20
2.12	Viking Johnson coupling adapted for GRP pipes	21
2.13	Modified Viking Johnson coupling	22
2.14	Grooved Victaulic coupling	23
2.15	Flanged Victaulic coupling	24
2.16	Possible sealing arrangements for a Victaulic coupling	25
2.17	Victaulic coupling with modified split ring	26
3.1	Diagram showing the fibre orientation and loading condition	30
3.2	Relationship between first ply failure and fibre orientation	31
3.3	Relationship between pressure, endload, diameter and wall thickness	33
3.4	Typical shear stress distribution in a lap shear joint	35
3.5	Shear stress variation with length of shear joint	36
4.1	Load applied to flange	38
4.2	Best step geometry	39
4.3	Flange bonded to pipe by tubular lap joint	40
4.4	Split steel flange on GRP pipe	40
4.5	Flange bonded to pipe by scarf joint	41
4.6	Photo showing pipe and flange with tapered ends	42

		Page
4.7	Sketch of test jig	43
4.8	Photo of test jig	44
4.9	Split backing ring	45
4.10	Type I flange	47
4.11	Graph showing the loading of the Type I flange	47
4.12	Type II flange	48
4.13	Curve showing the loading and gradual failure of the Type II flange	49
4.14	Type III flange	50
4.15	Graph of test result for Type III flange	50
4.16	Type IV flange	51
4.17	Curve showing the load bearing capacity of the Type IV flange	52
4.18	Type V flange	53
4.19	Graph showing the load bearing capacity of the Type V (a) flange	54
4.20	Graph showing the load bearing capacity of the Type V (b) flange	54
4.21	Type VI flange	55
4.22	Graph showing the load bearing capacity of the Type Vi flange	56
4.23	Type VII flange	57
4.24	Graph showing the load bearing capacity of the Type VII flange	57
4.25	Type VIII flange	58
4.26	Graph showing the load bearing capacity of the Type VIII flange	58
4.27	Type IX flange	59
4.28	Graph showing the load bearing capacity of the Type IX flange	59
4.29	Type X flange	60
4.30	Graph showing the load bearing capacity of the Type X flange	60
4.31	Type XI flange	61
4.32	Graph showing the load bearing capacity of the Type XI (a) flange	62

		Page
4.33	Graph showing the load bearing capacity of the Type XI (b) flange	62
4.34	Type XII flange	63
4.35	Graph showing the load bearing capacity of the Type XII flange	63
4.36	Type XIII flange	64
4.37	Graph showing the load bearing capacity of the Type XIII flange	65
4.38	Self-locking flange	66
4.39	Radial displacement of GRP pipe with two outer stiffening rings	67
4.40	Pipe with a double flange attached to it	67
4.41	Axial stresses in a GRP pipe with two GRP flanges	68
4.42	Type IV and type Xii flange	69
4.43	Axial stresses in steel pipe with GRP flange (Type XII)	70
4.44	Axial stresses in GRP pipe with GRP flange (Type IV)	71
4.45	Axial stresses in a "pressurised" GRP pipe with GRP flange	72
4.46	Hoop stresses in a "pressurised" GRP pipe with GRP flange	73
5.1	Hydrostatic rubber seal	75
5.2	Load path in coupling	76
5.3	Bending of the pipe and coupling	76
5.4	Load transferral from flange to pipe	77
5.5	Load transferral method of quick-connect coupling	77
5.6	Cross-section of first test flange	78
5.7	Effects of step angle on force components	79
5.8	Resin wedge in corner of flange	81
5.9	Photograph of flange expanding and slipping over step	81
5.10	Photograph showing compressive failure of the pipe (step region)	83

		Page
5.11	Photograph showing interlaminar shear failure of the pipe	84
5.12	Displacement of flange after compression	85
5.13	Cross-section of flange showing lay-up	85
5.14	Photograph showing compressive failure of the pipe (new flange cross-section)	86
5.15	Photograph showing buckling failure of the pipe	88
5.16	Photograph showing the tapered section which makes up the scarf joint	90
5.17	Cross-section through one half of the GRP coupling	92
5.18	Step depth and shear length which affect coupling performance	93
5.19	Failure mechanism map of the GRP pipe and coupling	94
5.20	Photograph of pipe and flange superimposing the axial stress contours	101
5.21	Photograph of pipe and flange superimposing the hoop stress contours	102
5.22	Flange/pipe combinations modelled using NISA	105
5.23	Section of the test specimen modelled using the finite element technique	107
5.24	Deformation of flange after compression	108
5.25	Constraints in the pressurised model	111
5.26	Loads applied to the finite element model	112
5.27	Selected coupling and sealing method	115
6.1	3 pipe/flange combinations that were tested	118
C.1	Finite element mesh of flange and pipe	
C.2	Refined mesh at step	
D.1	Hoop stresses in GRP pipe with GRP flange (Type IV)	
D.2	Shear stresses in GRP pipe with GRP flange (Type IV)	

LIST OF TABLES

	Page
2.1 Methods of joining piping systems	16
2.2 GRP piping standards	18
5.1 Material properties used in FE analysis	106

1. INTRODUCTION

Composite materials have a unique combination of properties. They combine light weight with high strength and corrosion resistance. Initially fibre reinforced products were made by the labour intensive hand lay-up process. Nowadays mechanised processes such as filament winding are often used. This is particularly suited to manufacturing tubular products such as pipes, ducts, tanks or pressure vessels.

The use of fibreglass pipes has increased dramatically in recent years, especially since the cost difference between fibreglass pipes and the traditional steel pipes has decreased. Properties such as high corrosion and abrasion resistance, high strength and light weight, and low friction factors make fibreglass pipes suitable for many applications. Their low weight makes them particularly suitable in applications where handling is a problem, eg. where there is a lack of heavy handling equipment or in confined spaces such as in underground mines.

Fibreglass pipes have been used extensively in the chemical process industry to convey chemicals and other fluid materials (food and beverage, pulp and paper, fertilizer etc.). They have also been used in the oil industry for gathering lines, downhole tubing and casing and saltwater disposal.

A relatively new application for high pressure pipes is their use in hydropower schemes in South African mines. Advantages of using fibreglass pipes in this application are reduced installation costs (due to the light weight of the pipes) and excellent corrosion resistance, both internally and externally. Also the pipes have a higher flow capacity than conventional pipes of the same diameter, due to their extremely low friction factor. This provides pumping energy cost savings over the projected life of the installation, especially since the original surface smoothness can be maintained in most cases (ie. there is little or no build-up of material on the inside of the pipe).

Wherever pipes and pipelines are in use, one needs pipe joints or couplings to connect the pipes. For non-pressure applications a variety of jointing systems exists, from factory prepared bell and spigot joints to field overlays. A number of ASTM standards are available [Ref 1], which recommend procedures for joining fibreglass pipes of virtually any diameter. The maximum design pressure dealt with in these ASTM standards is less than 2 MPa, although pipes have been manufactured for higher pressures using similar procedures. However these pipe joints are normally unable to sustain high axial loads (caused by the internal pressure).

Besides the information listed in the various standards (these are discussed in the following chapter), which have a maximum operating pressure of less than 7 MPa (see table 2.2 for maximum design pressures of each standard), there is no other information on high pressure fibreglass pipes operating at pressures over 20 MPa. Even less information on the pipe couplings for these high pressures is available. Pipe couplings that can sustain the full axial load caused by the internal pressure are required. This will enable the pipeline itself to carry the axial tension and largely eliminates the need for anchorages. On top of these strength requirements the coupling should be easily and quickly installed in limited working space and with the minimum of individual adjustment.

This research is an evaluation of glass fibre reinforced polyester pipe couplings to be used on high pressure fibreglass pipes. The pipes were made by the filament winding process using epoxy resin with glass reinforcement. The lay-up angle of the reinforcement was ±55° throughout.

Existing pipe couplings were briefly analysed and an alternative design proposed. This research was aimed specifically at the interface between the pipe and the coupling, since this is the critical area where failure is most likely to occur. Tests were done up to failure on these experimental couplings. The type of

test performed was a tensile test from which an ultimate axial load for the piping system is obtained. Since these tests were performed without any internal pressure, a finite element model was set up and correlated with the experimental results. The finite element model could then be "pressurised" in order to see the effect of the internal pressure.

General trends and problems were discovered by testing couplings with slightly modified basic dimensions and properties (viz. length of interface between the pipe and the coupling, type of glass reinforcement used for the coupling etc.). Additional tests were done on steel couplings used on fibreglass pipes. These results were compared to those of a fibreglass coupling, and were also correlated with predictions made by the finite element technique.

1.1 PROBLEM STATEMENT AND REQUIREMENTS

It was the aim of this research to investigate pipe couplings manufactured entirely from GRP (except for the seal, which can be made from a different material). These couplings are to be used on plain-ended, filament wound GRP pipes (manufactured from either polyester or epoxy resin) with a fibre orientation of ±55°. The internal operating pressure of the pipe installation should not exceed 20 MPa. Including a safety factor of 1.5 for waterhammer (1.5 is the factor taken for flexible pipes) the design pressure for this pipe should be 30 MPa. The coupling was to be designed for a water transportation pipeline in a corrosive environment, with operating temperatures of between 8°C and approximately 40°C.

It is often said that the biggest deterrent to the widespread use of GRP piping systems is the joining system. The efficiency of a joint is determined by many factors, such as the cost of fabrication, the ease of assembly (and disassembly) and the type of labour (skilled or unskilled) that is necessary to make the connections.

There are a few guidelines to follow when designing or selecting a pipe coupling [Ref 2]:

a) The pipe's longitudinal strength at the joint should be at least equivalent to that of the pipe. This is especially necessary in high-pressure pipes which are not anchored. In such cases the coupling must be able to sustain the full axial thrust caused by the internal pressure.
b) The transverse stiffening, caused by the excess of material necessary to bring about the joint, should be reduced to a minimum in order not to alter the duct's static pattern.
c) The sealing function should be clearly separated from the mechanical coupling function by using, if necessary, different materials.
d) The coupling should permit, if possible, angular and axial movements of the pipes without damage to the pipes or loss of watertightness. It is also important to realise that misaligned pipes can cause the entire load to be distributed over as little as one quarter of the coupling.
e) The coupling should retain its efficiency throughout the lifetime of the pipeline. Hence the choice of a suitable material, which does not degrade considerably with time, is necessary.
f) The coupling must retain its efficiency under any vibration of the pipeline, and it must be resistant to external shocks (eg. falling stones or rocks).
g) The constant internal diameter of the pipe should be maintained at the coupling. This is necessary to avoid the build-up of deposits in pipelines with low flow velocities.

h) "Sexless" couplings, ie. couplings which are symmetrical and can be installed in either direction are desirable. This requires that the pipes have the same end configuration on either side. This is important where long pipes are used in very confined spaces and the pipes cannot be turned round if they are oriented in the wrong direction (eg. in a mine tunnel where the pipe length exceeds the diameter of the tunnel).

i) The coupling should be easily and quickly assembled or disassembled in limited working space, and with the minimum of individual adjustment. This will allow the use of semi-skilled or un-skilled labour in the laying or re-routing of a pipeline.

It is important to note that the axial load caused by a constant internal pressure is proportional to the square of the internal pipe diameter (ie. $F \propto d^2$). This means that some couplings may perform well when used on pipes with a small diameter, but may fail at larger diameters. This also explains why high-pressure piping is normally of a relatively small diameter (less than 100 mm).

With pressure piping manufactured from fibreglass it is essential that there are no exposed fibres. Water under high pressure can easily move along these fibres by capillary action. This causes the pipe to start weeping, ie. the water slowly moves from inside the pipe through the pipe wall to the outside. To prevent weeping it may be necessary to line the fibreglass pipe with either PVC (polyvinyl chloride) or polypropylene. In any case there should be no exposed fibres at the coupling since water can penetrate into the coupling here and cause degradation.

The aim of this research was to establish the feasibility of manufacturing GRP couplings for GRP pipes to meet some or all of the above-mentioned guidelines. The main criterion in this evaluation was the ultimate pressure capability of the joint.

2. REVIEW OF COUPLINGS

Many different types of joints and couplings are commercially available to connect pipes of different sizes and materials. Most of these joints and couplings however are only designed to work at relatively low internal pressures and can only sustain low axial loads. High pressure pipes and couplings were traditionally made from steel and are mostly still made from steel. One reason for this is that it is much easier to design with an isotropic material as opposed to an orthotropic or an anisotropic material. Also steel has a very high stiffness compared with plastics (typically one order of magnitude higher than fibreglass), which is important in strain limited designs.

Another reason why steel is being used extensively for many high pressure piping systems, is that sufficient Codes and Standards are available, which describe the design of pipes, joints and couplings in steel for extreme conditions.

2.1 LITERATURE SURVEY

The following two sections consist of a brief survey of different pipe joints and couplings that are in use, together with a review of the different standards for pipe and coupling design. Some of the couplings discussed are for use on steel pipes only, and are consequently manufactured entirely from steel. Advantages and disadvantages of each coupling are briefly mentioned.

2.1.1 PIPE JOINTS AND COUPLINGS

Although the terms "joints" and "couplings" are loosely applied, there is a distinction to be made. A joint is normally a watertight (airtight) connection which cannot sustain high axial loads. It is used in low-pressure systems or where the pipes are anchored and the anchor takes up the entire axial load.

anchored and the anchor takes up the entire axial load. Mechanical couplings on the other hand are able to sustain the full axial load caused by the internal pressure of the pipe. Couplings would thus normally be used to connect high-pressure pipes. The entire pipe system can thus sustain the axial load and the need for anchorages is reduced.

The most common technique used to join GRP (glass fibre reinforced plastic) pipes is the butt and strap arrangement [Ref 9], as illustrated in figure 2.1.

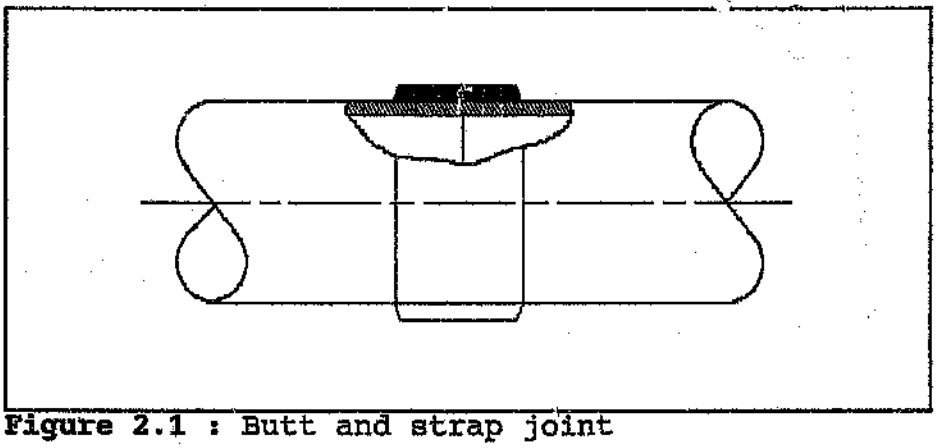

Figure 2.1 : Butt and strap joint

This method gives a strong joint that can be made readily in the field. Connections are made by butting two sections of pipe together and overwrapping the joint with successive layers of fibreglass reinforcement, saturated with the appropriate resin. The overwrap is normally made as thick as the pipe. This connection is essentially a tubular lap joint and derives its strength from the adhesive layer. There is no need for any elastomeric sealing rings, since the overwrap provides a watertight (and airtight) seal. A disadvantage of the butt and strap arrangement is that is takes some time to make the joint and allow it to cure. Such joints are permanent and hence not useful for temporary installations. The pipes can only be separated by cutting them apart.

Another common method of joining pipes is the bell and spigot joint [Ref 9, 10]. In this arrangement one end is socketed and the other end is plain. The male end has a rubber sealing gasket fitted over it and the socket (bell) is forced over the sealing ring. Bell and spigot joints with rubber rings can normally accommodate one or two degrees of deflection. This joint is illustrated in figure 2.2.

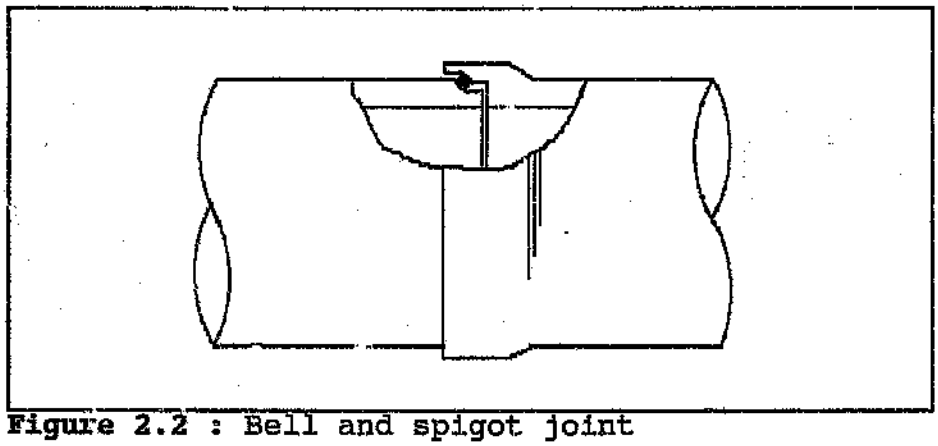

Figure 2.2 : Bell and spigot joint

Some reasons for the widespread use of bell and spigot joints are:

- Compliance with existing standards.
- It confers some longitudinal elasticity to rigid pipes.
- For materials subject to galvanic corrosion, the sealing gasket constitutes an insulating barrier which limits the circulation of electric currents in the piping.

Since GRP pipes are very flexible and are excellent electrical insulators, the above reasons for using the bell and spigot joint are no longer valid. Since sealing depends on the stability of the joint's configuration, ie. the uniformity of the gasket's compression against the wall, this type of joint is not particularly suitable for flexible pipes, especially if these operate under high pressures. Another practical disadvantage is that there is a "male" and a "female" end to each pipe. This means that the pipes can only be installed in one direction,

which can cause problems in confined spaces.

A variation of the bell and spigot joint is the threaded connection. Sealing is also accomplished with an elastomeric gasket. The female side has the rubber gasket about it and an outer coupling (threaded sleeve) tightens the female (bell) over the spigot, forcing the gasket to compress, thus effecting a seal. Often adhesives are used in conjunction with threaded connections. This type of pipe connection, shown in figure 2.3 below, is able to sustain the full axial load.

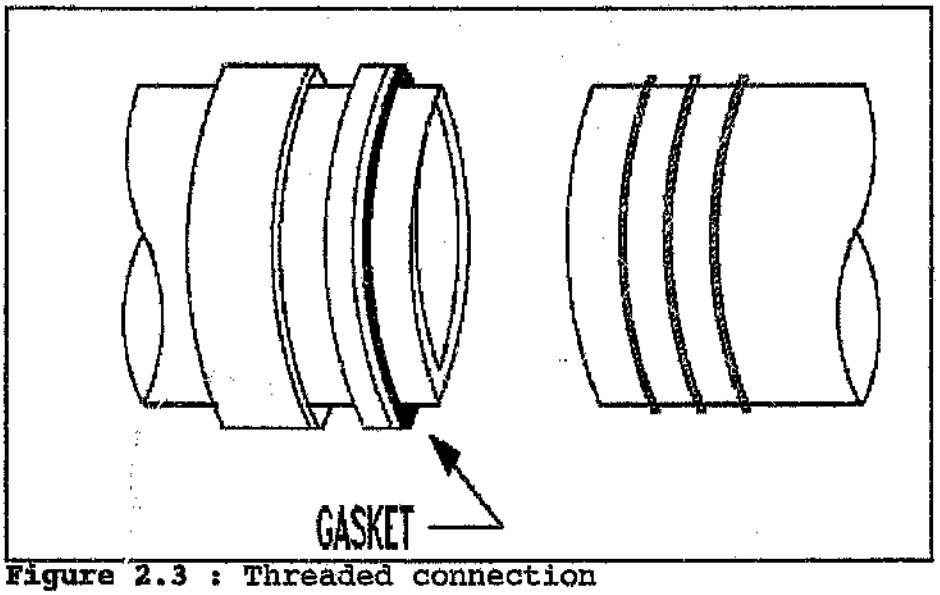

Figure 2.3 : Threaded connection

This joining method is designed for rapid field assembly of long runs and is often used for temporary installations (in which case no adhesive is used). The opportunity for installation errors is considerably reduced with this type of coupling, although there is still the disadvantage of having a male and a female end to each pipe.

A flanged connection is very common when pipes need to be connected to process equipment, valves, meters, pumps etc. Flanged connections are also often used where disassembly is anticipated. They can be used for medium-to-high pressure

systems as well as for large diameter pipes. Various types of gasketing materials can be used, including rubber, PVC and teflon. The connection is made by simply bolting two flanges together (with the gasket inbetween the flanges). A simple flanged joint is shown in the figure 2.4.

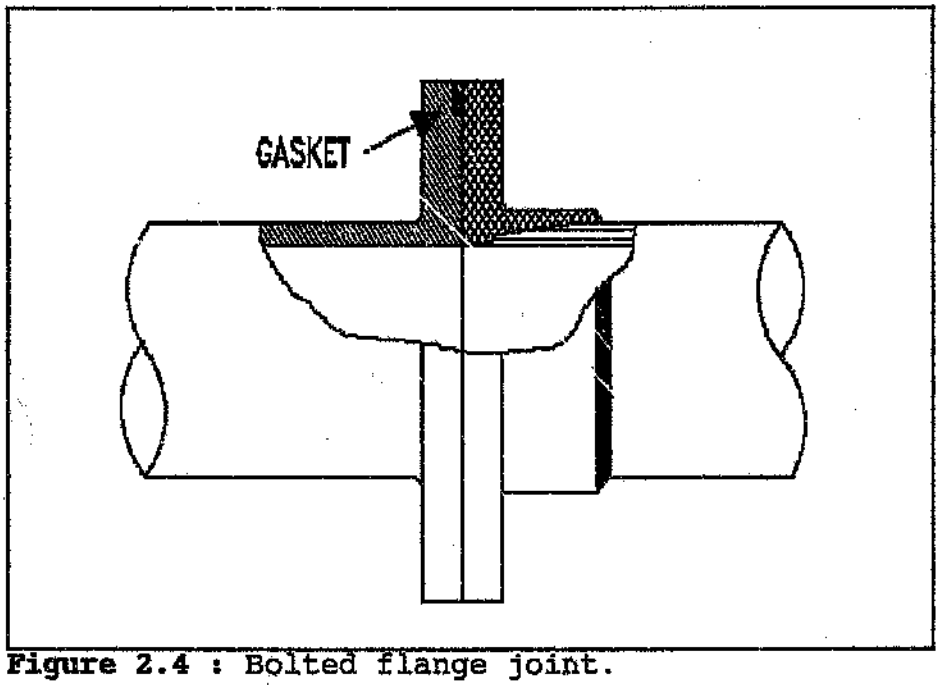

Figure 2.4 : Bolted flange joint.

The primary requirement of a flanged joint is that it should be capable of allowing sufficient force to be applied to the gasket to prevent leakage. This applies both initially, when the joint is assembled, as well as under operating conditions, when additional loadings due to pressure have to be supported. Due to the flexible nature of GRP two major disadvantages arise. The gasket tends to extrude away from the bolts during initial tightening, thus imposing a limit to the load that can be applied, and it tends to extrude out of the space between the bolts when subjected to internal pressure [Ref 3].

The Victaulic coupling [Ref 9] is used extensively for iron and steel pipes in high-pressure systems. It is normally manufactured from cast iron in the form of a split collar which

is secured by two tangential bolts. The pipe has either a small lip (flange) at its end or a recessed step machined into it. The coupling clamps around this step and thus holds the two pipes together. It is capable of sustaining the full axial load caused by the internal pressure. The seal is provided by a rubber "U"-ring which is located between the pipe outer surface and the inside of the split collar. This type of rubber seal is a hydrostatic seal. The internal pressure forces the two lips of the seal onto the ends of the pipe, thus increasing the sealing pressure as the internal pressure increases. The Victaulic coupling is depicted in figure 2.5.

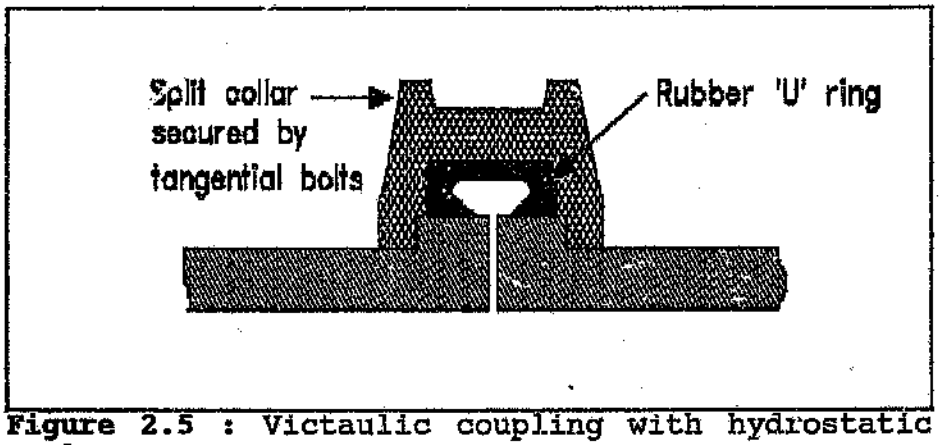

Figure 2.5 : Victaulic coupling with hydrostatic seal.

Some major advantages of this coupling immediately become apparent. The coupling is very easy and quick to fit with very little possibility of installation errors. It is extremely useful in temporary installations. The coupling does not have a male and a female side, ie. it is a "sexless" coupling. This is useful, as mentioned earlier, in confined spaces such as in underground mine tunnels, since the pipes do not have to arrive on site oriented in the correct direction.

The Victaulic coupling has been adapted for use on PVC pipes, as shown in figure 2.6 [Ref 11]. An injection moulded, high impact resistant uPVC (unplasticised polyvinyl chloride) collar, which

incorporates two flanges, is bonded onto the plain end of the PVC pipe. The flange nearest to the face of the collar is similar to a standard victaulic joint and seats the standard rubber "U" sealing ring. The other larger flange has a pronounced radius on the side furthest away from the face of the collar.

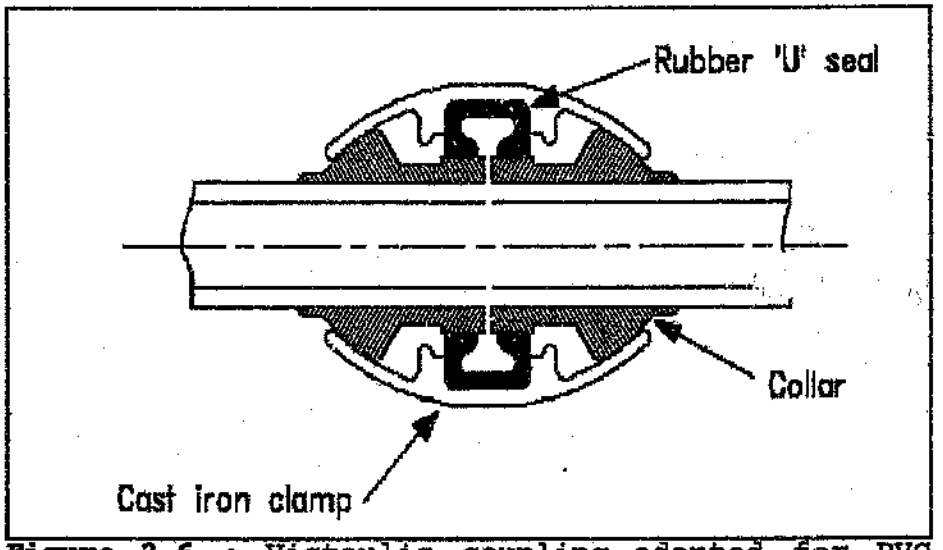

Figure 2.6 : Victaulic coupling adapted for PVC pipes

The clamp (outer split ring) encloses this flange when bolted into position, causing end thrust to be taken up as a compressive force over the area of the radius on the clamp. Due to the rounded collar and flange the coupling allows slight movement and angular deflection of the pipes.

The most widely used clamp-on joint is the proprietary Viking Johnson coupling [Ref 10, 11]. With this coupling it is possible to join plain ended pipes (non-pressure applications) or pipes with lips on the ends (pressure applications). It is however mainly used for steel and cast iron pipes. To make the joint, a rubber seal is clamped between each pipe barrel and a cover sleeve as shown in figure 2.7.

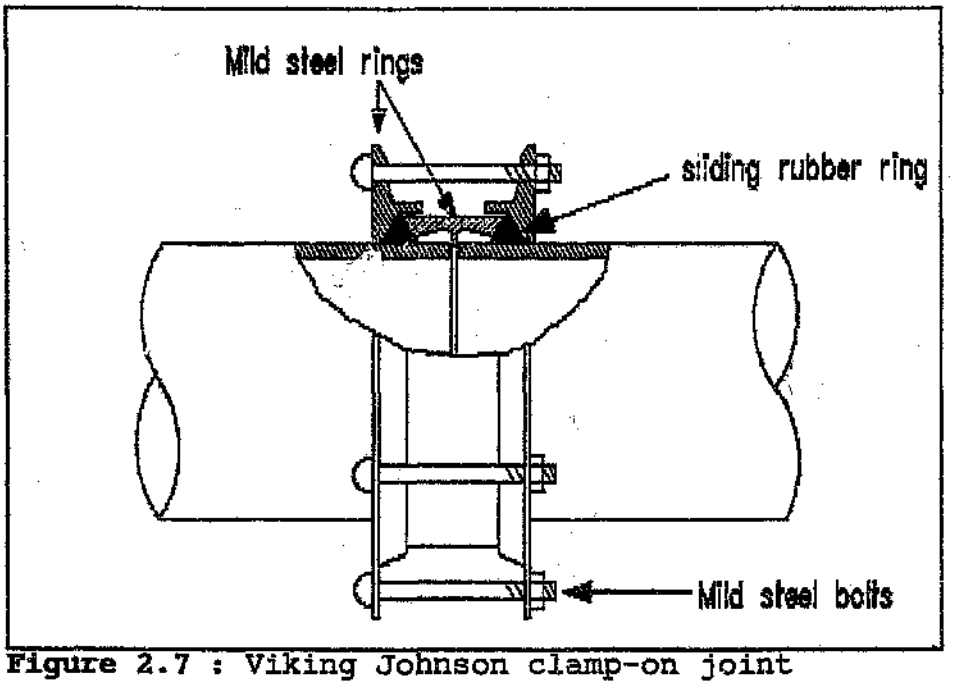

Figure 2.7 : Viking Johnson clamp-on joint

Such joints can accommodate movement easily, and may be designed to take several degrees of deflection between pipes as well as longitudinal movement. This joint is reusable and is useful in temporary installations.

Another coupling which is useful in temporary installations is the "Kwikey" quick-connect coupling ("Kwikey" is a trademark of Fibreglass Resources Corporation). This coupling consists of a sleeve with a double groove near the centre to locate two O-rings which provide the seal. Near the edges of the sleeve is a deep groove on each side which acts as a keyway. A similar groove exists in the pipes to be coupled (see figure 2.8).

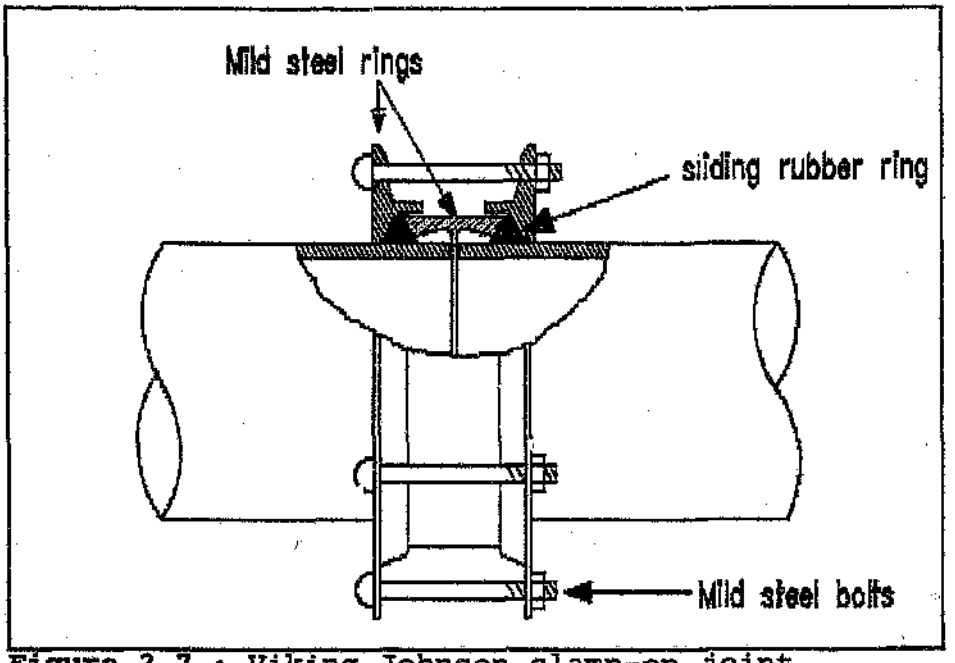

Figure 2.7 : Viking Johnson clamp-on joint

Such joints can accommodate movement easily, and may be designed to take several degrees of deflection between pipes as well as longitudinal movement. This joint is reusable and is useful in temporary installations.

Another coupling which is useful in temporary installations is the "Kwikey" quick-connect coupling ("Kwikey" is a trademark of Fibreglass Resources Corporation). This coupling consists of a sleeve with a double groove near the centre to locate two O-rings which provide the seal. Near the edges of the sleeve is a deep groove on each side which acts as a keyway. A similar groove exists in the pipes to be coupled (see figure 2.8).

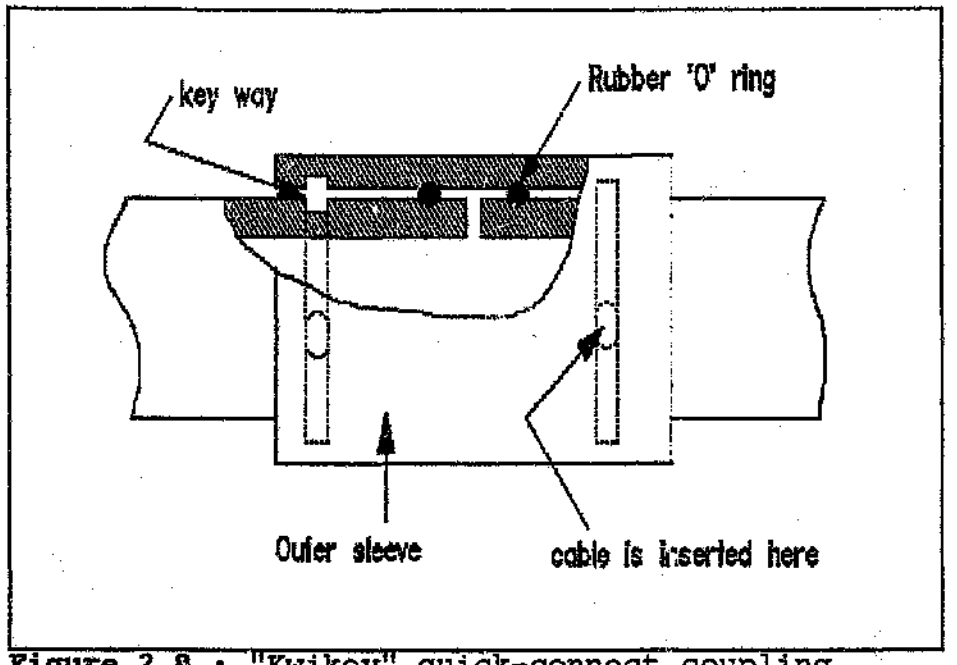

Figure 2.8 : "Kwikey" quick-connect coupling.

The pipes are pushed into the coupling (sleeve) with the rubber O-rings now compressed between the outside of the pipes and the sleeve. A cable rope which acts as a key is now pushed through a hole in the coupling into the groove at the interface between the sleeve and the pipe. This joint provides positive locking and can take up axial loads. It eliminates the need for adhesives and provides simple field assembly and disassembly. Like the Viking Johnson coupling this coupling is reusable and it can be installed in either direction because it is symmetrical (as opposed to the bell and spigot joint which can only be installed in one direction). The quick-connect coupling is the only reusable mechanical coupling that is manufactured entirely from GRP (except for the key which is made from steel, sometimes from polyethylene).

Another pipe coupling manufactured specifically for GRP pipes is shown in figure 2.9.

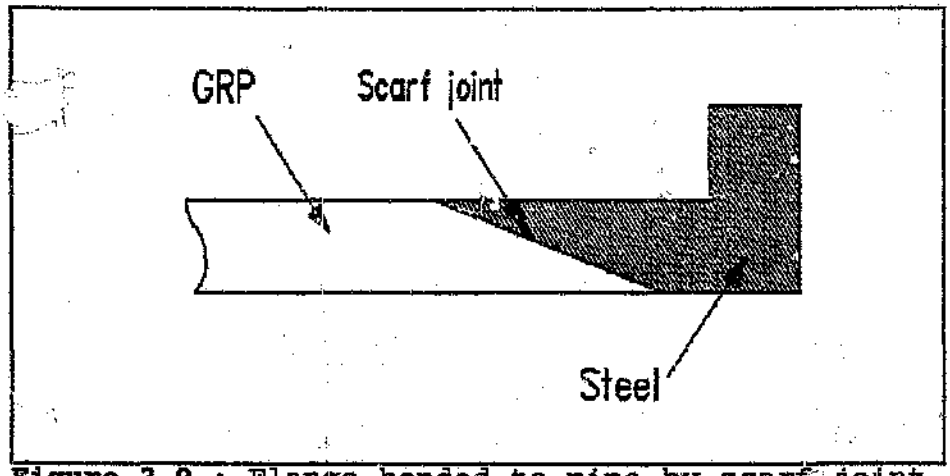

Figure 2.9 : Flange bonded to pipe by scarf joint

The end of the pipe is tapered with an angle of 6°. A steel sleeve with an opposite taper is adhesively bonded to the pipe. To add axial strength to the joint, the outside is overwrapped with successive lay rs of glass reinforcement impregnated in the appropriate resin. The steel sleeve has a flange at its end. Various joining methods can now be used, eg. a Viking Johnson coupling can be used with an O-ring inbetween the two flanges.

The following table is a summary of all the above couplings. It lists the advantages and disadvantages of each coupling.

Table 2.1 : Methods of joining piping systems

Type	Advantages	Disadvantages
Butt and strap	Strong, easy to install, cheaper than other joints for large diameters	Cannot be taken apart, limited to polyester hand laid-up pipe
Bell and spigot	Joint deflection of 2°-5° permissible, ideal for sewer service, resists earth movements and tremors.	Normally considered to be a sewer pipe and not recommended for pressure applications above ground
Threaded connection	Quick assembly, easy disassembly, inexpensive on small piping, satisfactory for water and mildly corrosive systems.	Commonly disappears in larger-size piping, not suited for highly corrosive systems
Bolted flange joint	Low-cost joint (if not hand laid-up), hand laid-up flanges are very strong	Must normally be used with a full-faced gasket, expensive if hand laid-up, cannot be overtorqued or failure will result
Victaulic coupling	Very simple to install, extremely strong	Not yet manufactured for fibreglass pipes

Viking Johnson coupling	Very simple to install	Not suited for high pressure applications, designed for steel pipes
Quick connect coupling "Kwikey"	Satisfactory for moderate chemical service, simple assembly and disassembly, reusable, good for temporary installations	not adapted to tough corrosive environments

2.1.2 STANDARDS FOR PIPE AND JOINT DESIGN

The existence of industry product standards greatly simplifies the engineer's task when designing certain components. It also allows the engineer to confidently and definitely specify a material.

The issuance of standards for fibreglass pipe has had a dramatic effect on the acceptance of fibreglass pipe. This appears to be most prevalent in the public works or municipal pipe markets, not so much in the mining industry yet.

Various product standards have been published by the American Society of Testing and Materials (ASTM), the American Water Works Association (AWWA) and the American Society of Mechanical Engineers (ASME). These standards however only cover the design of pipes for design pressures of 250 psi. The design of joints and couplings is not covered in detail, although stringent

performance requirements are laid down in these standards. Various types of joints are suggested or recommended which include most of the joints mentioned in the previous section. The American Petroleum Institute (API) has issued guidelines on the design of high pressure piping. This specification relies on and uses the long-term and short-term test methods developed by ASTM wherever applicable as part of its product specifications.

The table below lists several reinforced pipe specifications with the range of applicable diameters and pressures that each standard covers.

Table 2.2 : GRP piping standards.

Standard	Diameter range [mm]	Pressure range [MPa]
ASTM D2996	51 - 406	6.9 *
ASTM D3517/D3754	203 - 3,658	1.7
AWWA C950	203 - 3,658	1.7
API 15AR	38 - 242	20.6 *
API 15LR	51 - 406	6.9

Note that the pressures marked with an asterisk (*) are not listed operating pressures. However pipes made according to these standards are available to the pressures shown.

It can be clearly seen that there is a lack of design specifications for fibreglass joints and couplings, although the requirements of such pipe connections are clearly stipulated. Especially in the field of high-pressure fibre glass reinforced piping systems little information has been documented.

performance requirements are laid down in these standards. Various types of joints are suggested or recommended which include most of the joints mentioned in the previous section. The American Petroleum Institute (API) has issued guidelines on the design of high pressure piping. This specification relies on and uses the long-term and short-term test methods developed by ASTM wherever applicable as part of its product specifications.

The table below lists several reinforced pipe specifications with the range of applicable diameters and pressures that each standard covers.

Table 2.2 : GRP piping standards.

Standard	Diameter range [mm]	Pressure range [MPa]
ASTM D2996	51 - 406	6.9 *
ASTM D3517/D3754	203 - 3,658	1.7
AWWA C950	203 - 3,658	1.7
API 15AR	38 - 242	20.6 *
API 15LR	51 - 406	6.9

Note that the pressures marked with an asterisk (*) are not listed operating pressures. However pipes made according to these standards are available to the pressures shown.

It can be clearly seen that there is a lack of design specifications for fibreglass joints and couplings, although the requirements of such pipe connections are clearly stipulated. Especially in the field of high-pressure fibre glass reinforced piping systems little information has been documented.

2.2 SUGGESTED MODIFICATIONS

This section deals with some preliminary ideas for joint modifications for GRP applications based on the existing couplings mentioned in section 2.1.1. All these couplings described here are "sexless", ie. they are symmetrical. Thus the pipes as well as the couplings can be installed either way around.

2.2.1 GRP FLANGE JOINT

A flange joint is a very crude and normally structurally inefficient joint. However it is often essential in a system which contains valves and pumps, since these components normally have flanged connections. The primary requirement of the flanged joint is that it should be capable of applying sufficient pressure to a gasket to prevent leakage.

A GRP flange could be manufactured fairly easily, as shown in figure 2.10.

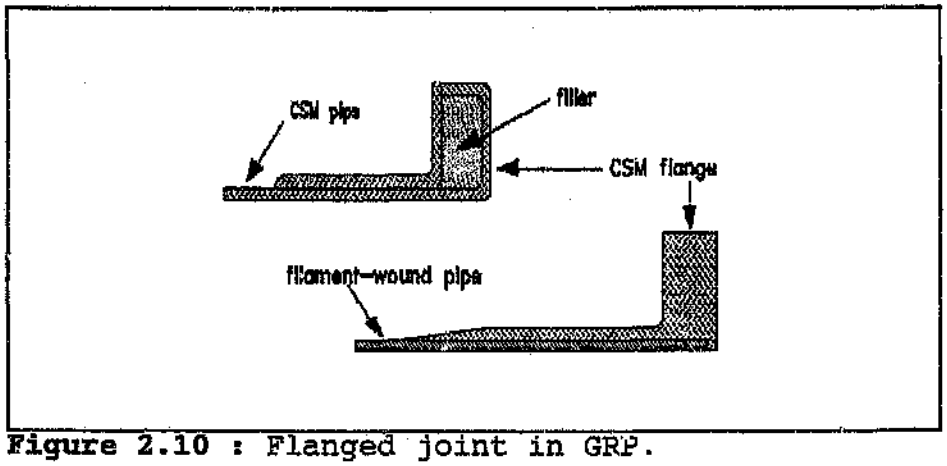

Figure 2.10 : Flanged joint in GRP.

However due to the high axial loads caused by the internal pressure, extremely high bending moments would result in the joint. An excessively high bolt torque would be required to

tighten the bolts, which could cause cracking of the GRP flange, unless a steel backing ring were used.

In addition to the danger of overtightening the bolts, there is also the disadvantage that the flange joint does not allow for any misalignment of the pipes. It would appear that the GRP flange joint would not generally be satisfactory in a high-pressure GRP piping installation.

If a steel flange were to be used, the difference in stiffnesses between steel and GRP could perhaps be utilised to make a self-locking flange, as shown in figure 2.11.

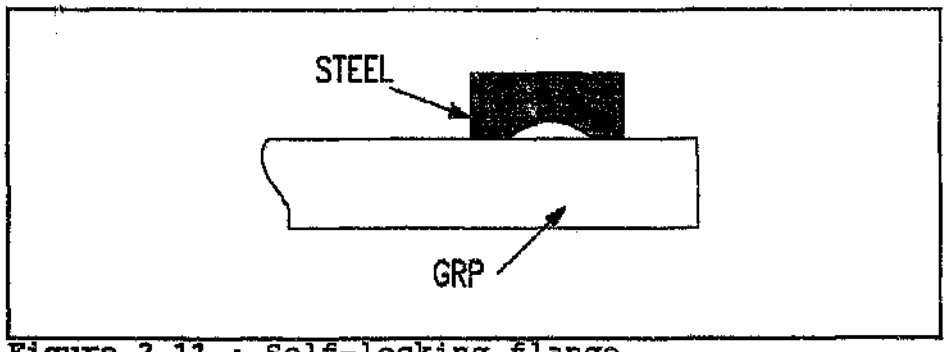

Figure 2.11 : Self-locking flange.

With an increase in pressure the pipe would bulge outwards, thus preventing the flange from slipping off the pipe. Two adjacent pipes could then be joined by bolting the flanges together or perhaps even using split collars, as used with the victaulic coupling.

2.2.2 ADAPTED VIKING JOHNSON COUPLING

A standard Viking Johnson coupling could be adapted fairly easily to join plain ended GRP pipes. For this coupling a method is needed to transfer the axial load from the pipe to the coupling. This can be accomplished by pushing a serrated metal sleeve onto the pipe. The serrations grip on the surface of the pipe to

transfer the axial force. In addition to this an epoxy adhesive can be used to give added strength to the joint (see figure 2.12).

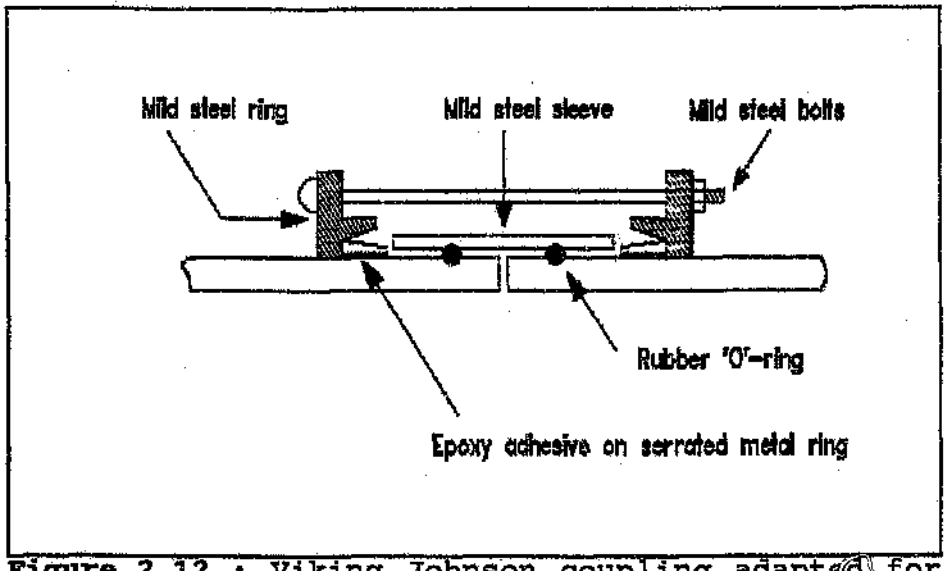

Figure 2.12 : Viking Johnson coupling adapted for GRP pipes.

The steel ring of the coupling must be slipped over the end of the pipe before the serrated metal sleeve is installed. Once installation has taken place the coupling cannot be re-used unless the pipe is cut behind the serrated sleeve.

The seal can be made by using two O-rings on each pipe end. The O-rings are compressed between the pipe wall and another steel sleeve which slips over the outside of the pipe. One drawback of this sealing method is that the gap between the pipe and the sleeve must be very small, otherwise the O-ring can quite easily be forced out from between the pipe and the sleeve at high pressures. The pipes are then joined by tightening tie bolts between the two metal rings.

The amount of axial and angular misalignment that can be taken up by this joint is negligible. This coupling is more efficient than the GRP flange joint from the point of view that a much

smaller bending moment is set up in the pipe. The primary loading on the interface between the coupling and the pipe (ie. the jagged adhesive line between the serrated ring and the pipe surface) is a shear loading. This is desirable in an adhesive joint.

The strength of the joint is essentially dependent on the strength of the adhesive. If the teeth of the serrated ring grip deep into the fibreglass, then the strength of the joint will also depend on the interlaminar shear strength of the pipe (this is the shear strength between adjacent layers in a laminate).

Another method of modifying the Viking Johnson coupling is to wind a very low flange onto the pipe end while it is being manufactured. A thin flange will ensure that the bending moment caused in the pipe is kept as low as possible. This flange would have to be manufactured with the metal sleeves on the pipe, which is very impractical. Alternatively a split ring could be used. Figure 2.13 illustrates this modification.

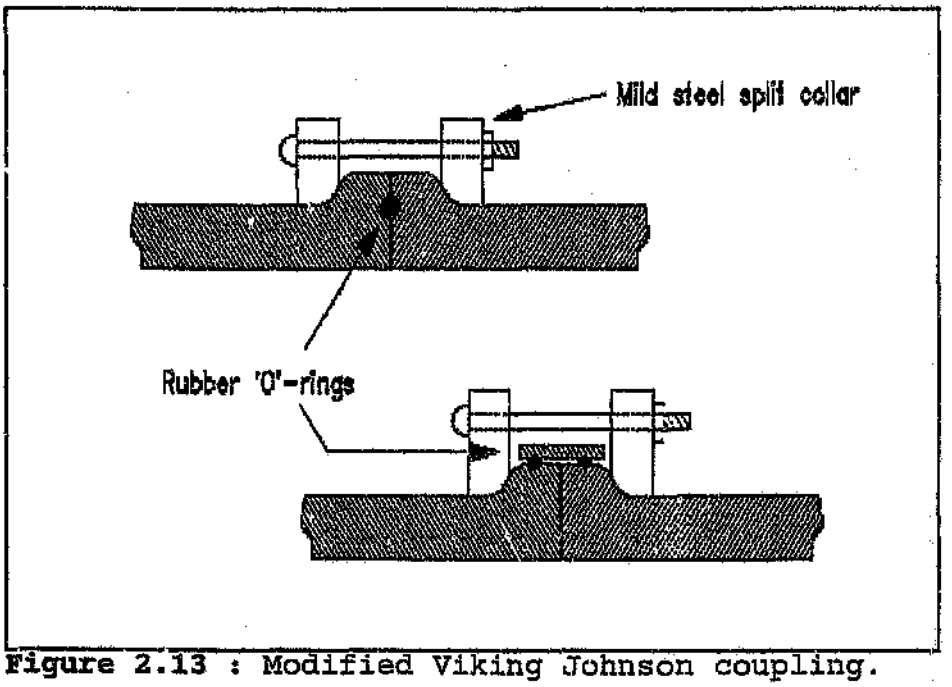

Figure 2.13 : Modified Viking Johnson coupling.

The seal could be similar to the one described for the previous coupling. Alternatively an O-ring could be seated between the flanges to provide a watertight seal. This coupling does also not allow for any angular or axial deflection of the pipes.

Both the modified Viking Johnson couplings previously described are made almost entirely from steel. To make them out of fibreglass, they would have to be substantially modified. However, the principle of these couplings can possibly be applied in a fibreglass coupling.

2.2.3 ADAPTED VICTAULIC COUPLING

The Victaulic coupling is ideally suited to the joining and sealing of high-pressure pipes. The hydrostatic seal increases its sealing pressure as the internal water pressure increases.

A groove could be machined into the fibreglass pipe, as is the case with the grooved Victaulic coupling. This groove would have to be located further away from the end of the pipe than it is on the steel pipe, to increase the shear area of the lip (because the shear strength of steel is much higher than the interlaminar shear strength of a fibreglass laminate). The two grooves on adjacent pipes would be relatively far apart and hence a steel split ring would be very bulky and heavy. But a GRP split ring could be manufactured which is light and easy to handle.

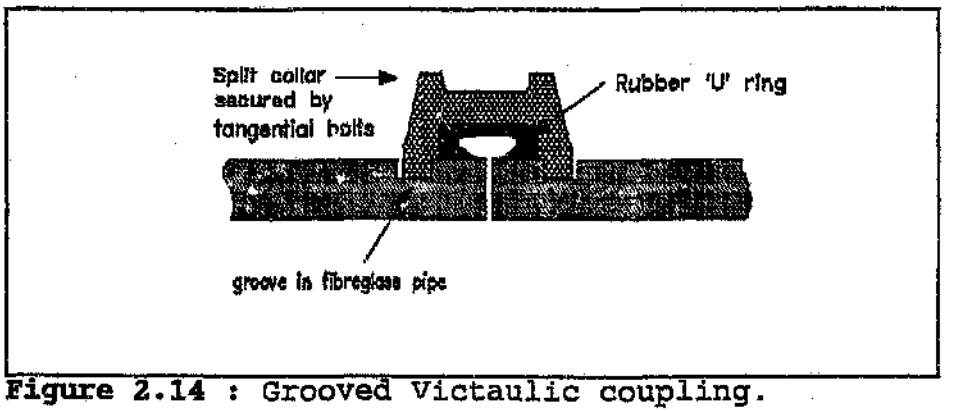

Figure 2.14 : Grooved Victaulic coupling.

Alternatively a pipe with a very flat flange could be used instead of the grooved arrangement. This flange would be manufactured together with the pipe. The flange could be located right at the end of the pipe. In this case the hydrostatic seal would be seated on top of the flanges. Alternatively the flange could be located further away from the end, in which case the hydrostatic seal would be located between adjacent flanges. This brings the seal much closer to the centre of the pipe.

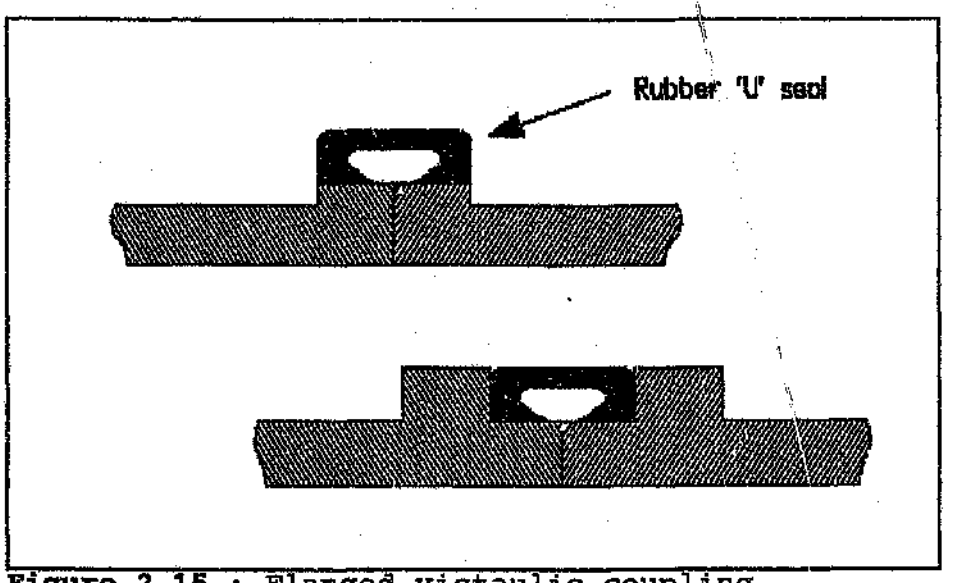

Figure 2.15 : Flanged victaulic coupling.

The sealing of the pipe can be done with O-rings instead of the "U"-type rubber seal. The O-rings can be located inbetween the flanges as in the modified Viking Johnson coupling. Alternatively two O-rings could be located in grooves on the outside of the flange. The O-rings would be squashed between an outer sleeve and the two flanges (see figure 2.16).

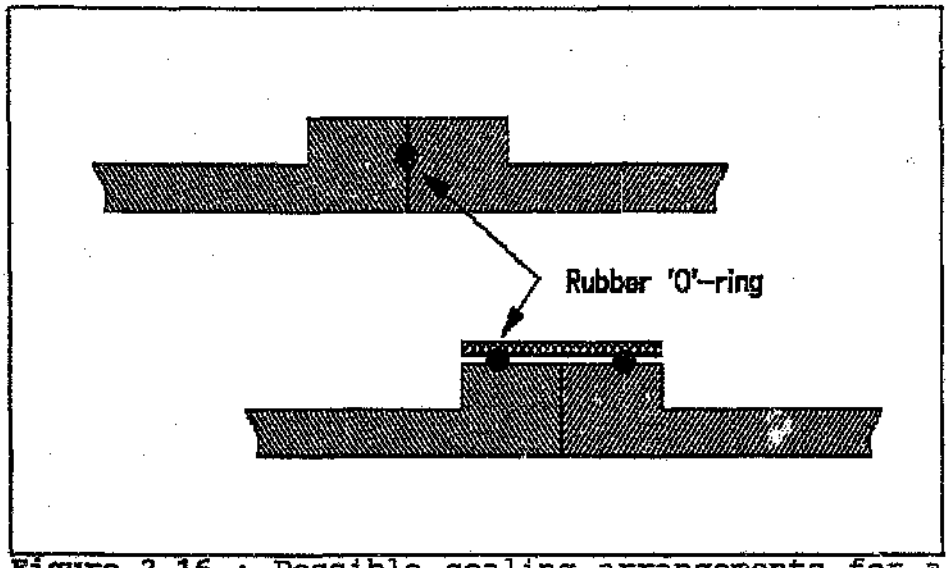

Figure 2.16 : Possible sealing arrangements for a Victaulic coupling.

The "U"-type rubber ring will provide the most reliable seal if misalignment of the pipes occurs. With an O-ring inbetween the flanges an uneven sealing pressure will occur if the pipes are misaligned.

A further modification to the victaulic-type coupling could be in the design of the split ring. A split ring with tightening bolts is both time consuming and, when manufactured in GRP, can easily be damaged by overtightening the bolts. A safer and faster method is to slide a thin tube (also manufactured from GRP) over the cylindrical split ring. This sleeve will hold the split ring together and will take up any hoop stresses. This arrangement is shown in the figure 2.17.

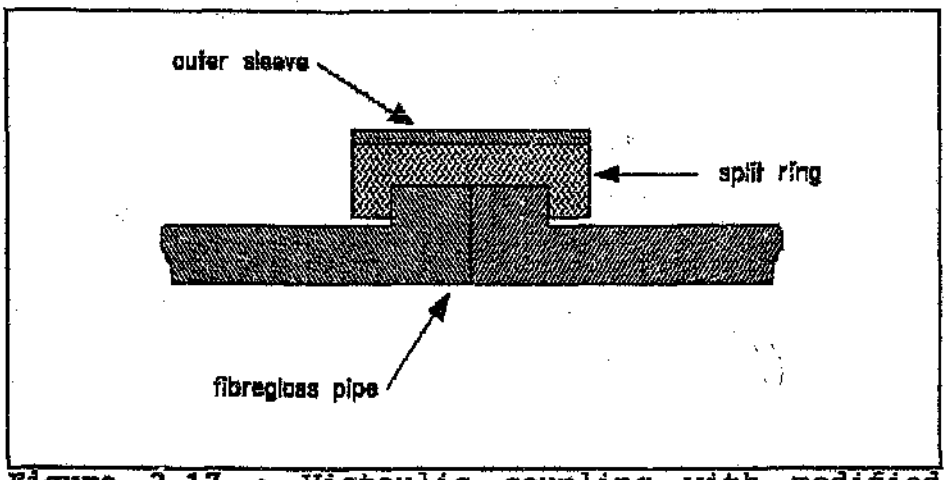

Figure 2.17 : Victaulic coupling with modified split ring.

3. CALCULATION OF THE INITIAL PIPE AND COUPLING DIMENSIONS

The initial sizing of the various components of the coupling, as well as the determination of the pipe wall thickness was calculated using the theory for thin cylinders [REF. 4] and the Classical Lamination Theory [REF. 5]. The adhesive shear stresses were estimated using an extension of Volkersen's theory [REF. 6]. The Finite Element Method was used to model the configuration used in the experiments. Hence a correlation between experimental and theoretical results was possible. By modelling the entire coupling, predictions of the pipe and coupling performance were made.

These theories are described in more detail in the following sections.

3.1 THIN CYLINDER THEORY [REF. 4]

The thin cylinder theory was used in conjunction with the Classical Lamination Theory to set up pipe design charts which show the relationship between the internal pipe diameter and the wall thickness for varying internal pressure, as well as the endloads caused by the internal pressure. These pipe dimensions were needed in order to size the coupling and to be able to perform initial design calculations (eg. the adhesive shear stress depends on the surface area which in turn depends on the pipe diameter and wall thickness).

The thin-cylinder theory was also used to establish the loading condition in a pressure pipe. The unit loads were derived and hence the ratio of hoop loading to axial loading, which was used in the Classical Lamination Theory, was found. This is the loading condition of any pressure pipe that is not restrained axially.

The three principal stresses in a thin cylinder are the circumferential (hoop) stress, the longitudinal (axial) stress and the radial stress. If the ratio of thickness to internal diameter is less than about 1/20, it may be assumed with reasonable accuracy that the hoop and axial stresses are constant throughout the thickness and that the radial stress is small and can be neglected.

The equation for the hoop stress in a thin cylinder is

$$\sigma_h = \frac{Pd}{2t}$$

and the equation for the axial stress in a thin cylinder is

$$\sigma_a = \frac{Pd}{4t}$$

where P is the internal pressure, d is the internal diameter and t is the wall thickness.

It is possible to convert the above stresses into unit loads, ie. a load per unit width. Using the relationship

$$\sigma = \frac{F}{A}$$

we get

$$\frac{F}{width} = N = \sigma \cdot t$$

where σ is a direct stress, A is the cross-sectional area, F is the applied load and N is the unit load (load per unit width).

Substituting the stresses from the Thin Cylinder theory into the above equations, the unit loads are defined as follows:

$$N_h = \frac{Pd}{2}$$

and

$$N_a = \frac{Pd}{4}$$

where N_h and N_a are the loads per unit width, P is the internal pressure and d is the internal diameter.

The loading ratio of thin walled pressure pipes is

$$\frac{N_h}{N_a} = 2$$

3.2 CLASSICAL LAMINATION THEORY [Ref. 5]

The theory assumes a plane stress state in the lamina, the stress perpendicular to the plane of the lamina assumed to be zero. The elastic stress-strain relations of the lamina can be expressed in matrix form as follows:

$$\{e_1\} = [S]\{\sigma_1\}$$

where *1* identifies lamina coordinates, and *[S]*, the compliance matrix, relates the stress and strain components in the principal material directions. (The Lamination Theory is described in more detail in appendix A).

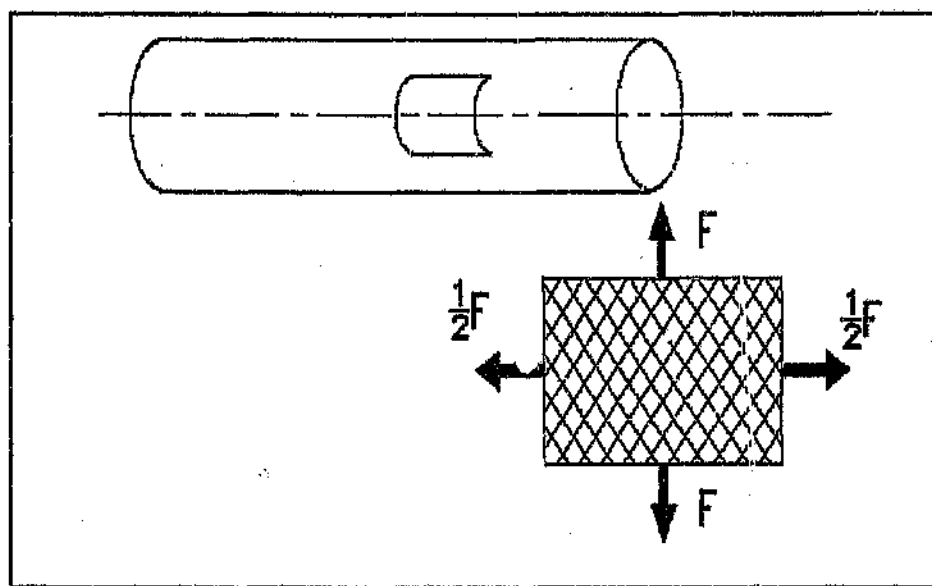

Figure 3.1 : Diagram showing the fibre orientation and loading condition.

The loading condition shown in the figure above was determined in section 3.1. Using the Classical Lamination Theory the optimum lay-up angle for a pressure pipe was found to be approximately 55° to the axis of the pipe (see figure 3.2).

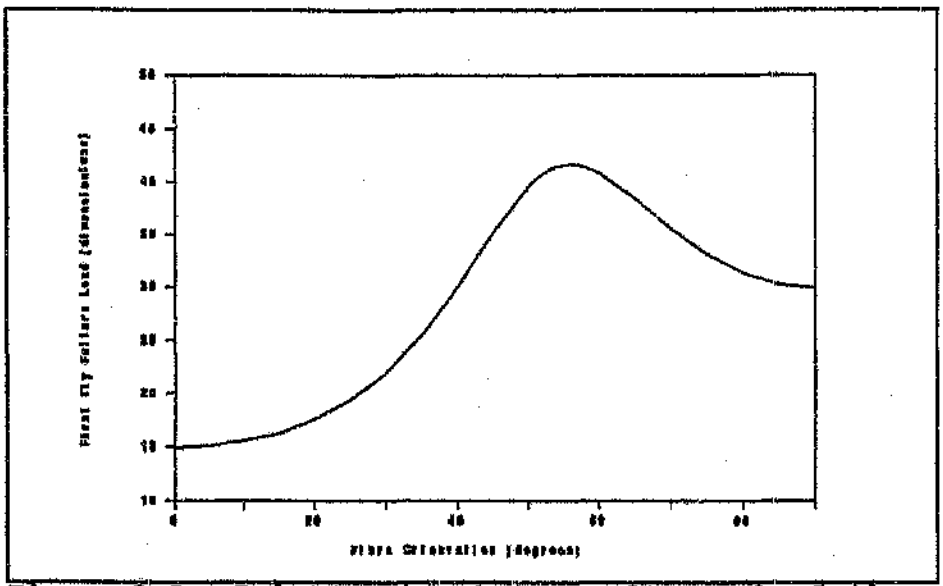

Figure 3.2 : Relationship between first ply failure and fibre orientation.

To draw the graph of endload versus pressure for various pipe diameters and wall thicknesses, the following procedure was adopted. The relationship

$$F = P \cdot A = P \cdot \frac{\Pi \cdot D_i^2}{4}$$

(where F is the endload, P is the internal pressure and D_i is the internal diameter) was used to plot a curve of endload versus pressure for some selected internal pipe diameters. These are the straight lines in figure 3.3.

From the thin cylinder theory the axial stress is

$$\sigma = \frac{P \cdot D_i}{4 \cdot t}$$

which can be rewritten as

$$t = k \cdot P \cdot D_i$$

where t is the wall thickness, k is a constant incorporating the ultimate failure stress, P is the internal pressure and D_i is the internal diameter.

Using the Classical Lamination Theory, the minimum wall thicknesses for a range of pipe diameters and pressures was calculated (see appendix B for table of results). Plotting this data on a graph of thickness versus pressure results in a series of straight lines for the various diameters. The equations for the straight lines yield a value

$$k = \frac{1}{455}$$

which is constant for all lines.

Substituting

$$D = \frac{t}{k \cdot p}$$

in the equation

$$F = \frac{P \cdot D^2 \cdot \pi}{4}$$

results in

$$F = \frac{\pi}{4 \cdot P} \cdot \left(\frac{t}{k}\right)^2$$

Figure 3.3 represents these relationships graphically.

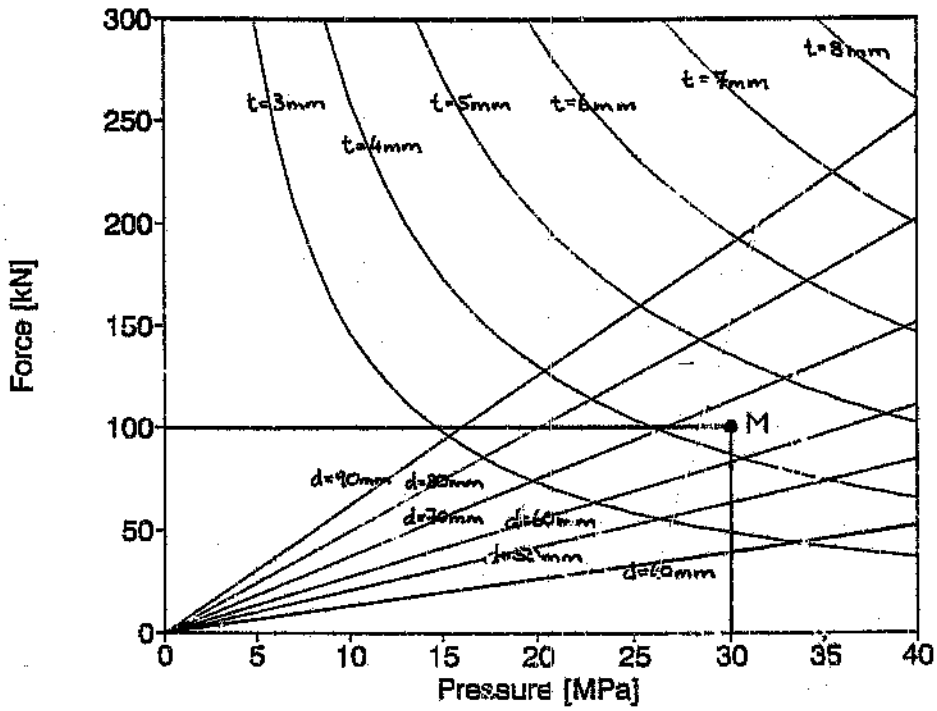

Figure 3.3 : Relationship between pressure, endload, diameter and wall thickness for a composite tube (material properties are shown in table 5.1, page 106).

From this figure a pipe diameter for the test specimens was selected. The point labelled ***M*** indicates the target pressure and the maximum force that the testing machine was able to supply. Various pipes with a diameter less than 65 mm would be suitable. In order to allow for a safety factor in the pipe and to minimise the cost of the test specimens, an internal pipe diameter of 50 mm was selected with a wall thickness of 8 mm.

3.3 ADHESIVE SHEAR STRESSES

From the calculated pipe dimensions it is possible to predict adhesive shear stresses and hence also to establish an optimum adhesive length for a certain pipe outside diameter. A lap shear joint of constant width (represented by the perimeter of the outside of the pipe) increases in strength with an increase in the length of the overlap. This effect however decreases until an optimum length is reached, after which an increase in length has no more effect on the strength of the lap joint. The optimum lap joint length for the selected pipe dimensions can then be calculated.

Volkerson's theory is used to estimate the shear stress distribution in an adhesive lap joint.

$$\frac{\tau(x)}{\tau_{(avg)}} = \frac{[\frac{\delta}{K}]^{0.5}}{\sinh(\delta * K)^{0.5}} [(K-1)\cosh((\delta * K)^{0.5}\frac{x}{l}) + \cosh((\delta * K)^{0.5}(1-\frac{x}{l}))$$

where

$$\delta = \frac{G_a l^2}{E t_2 t_a}$$

and

$$K = \frac{t_1 + t_2}{t_1}$$

Figure 3.4 shows a typical shear stress distribution along a lap shear joint of constant width.

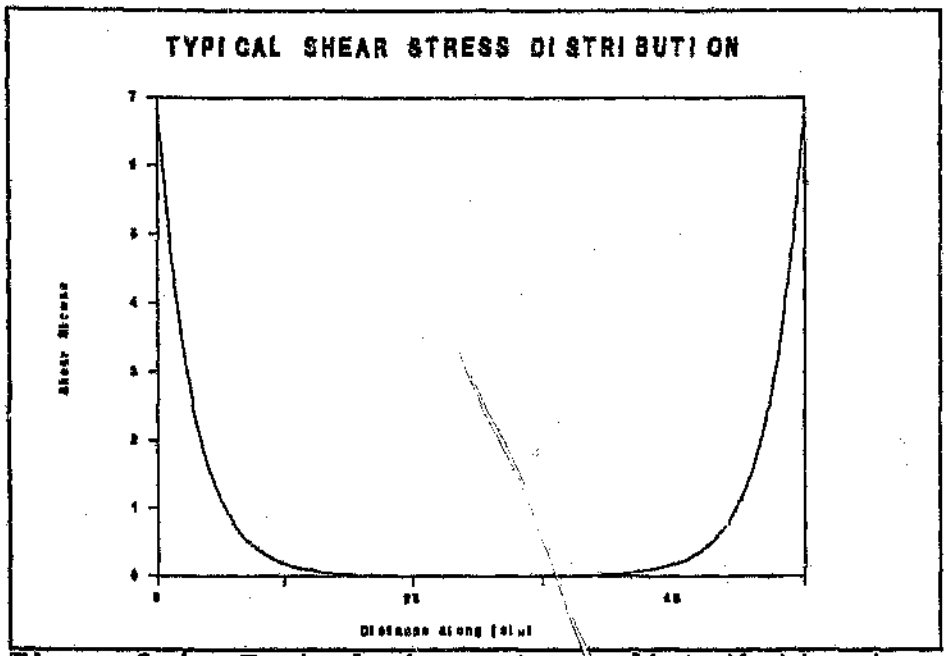

Figure 3.4 : Typical shear stress distribution in a lap shear joint.

The maximum shear stress occurs at the ends of the joint. Plotting these maximum shear stresses for a number of joints of different lengths results in the curve shown in figure 3.5.

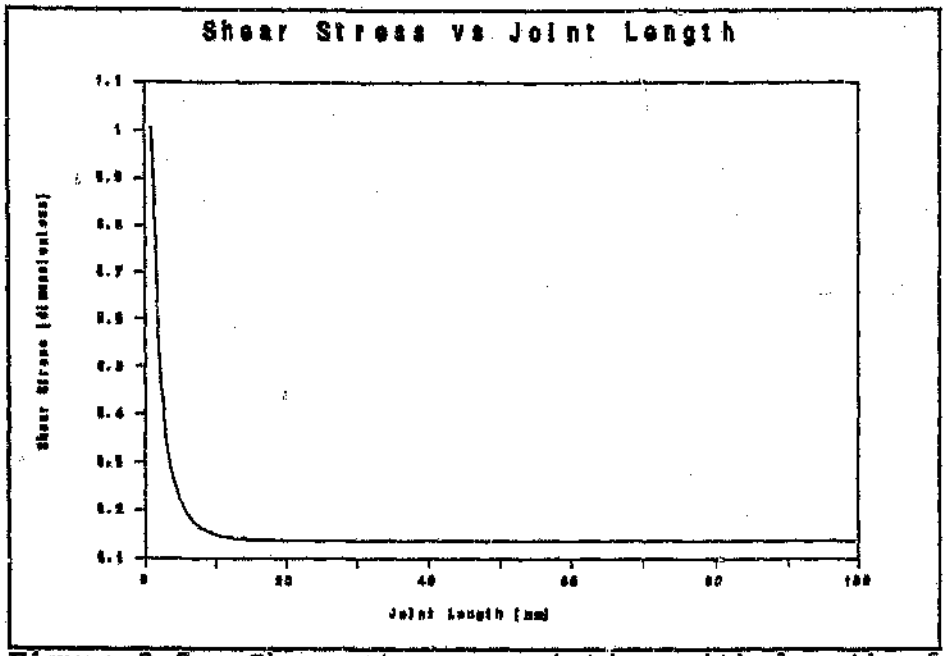

Figure 3.5 : Shear stress variation with length of shear joint.

From figure 3.5 it can be seen that for an adhesive lap joint of constant width there is virtually no increase in strength if the joint length exceeds 15 mm. For practical purposes however this length is too short. Hence a flange length of 50 mm was selected. This means that the adhesive joint will have its maximum strength.

4 EXPERIMENTATION

This chapter outlines the approach adopted in developing the coupling and describes the experimental program used to test each stage of the development phase.

It was decided to do all tests with small diameter pipes. This ensured that the loads were not too high and that the testing machine used (ESH Tensile Testing Machine 250 kN) was able to load the pipes to failure. As outlined in the previous section an internal diameter of 50 mm was chosen with a wall thickness of 8 mm.

4.1 EXPERIMENTAL PROGRAM

The aim of the experimental program was to establish the ultimate load that the coupling can sustain and to establish which factors affect this load. Since the most important part of the coupling is the interface between the pipe and the coupling, the test program was designed to test this interface. Aside from the internal pressure that acts on the pipe, there is an axial force on the flange (caused by the coupling), which opposes the axial force caused by the internal pressure in the pipe. The figure below depicts this loading condition.

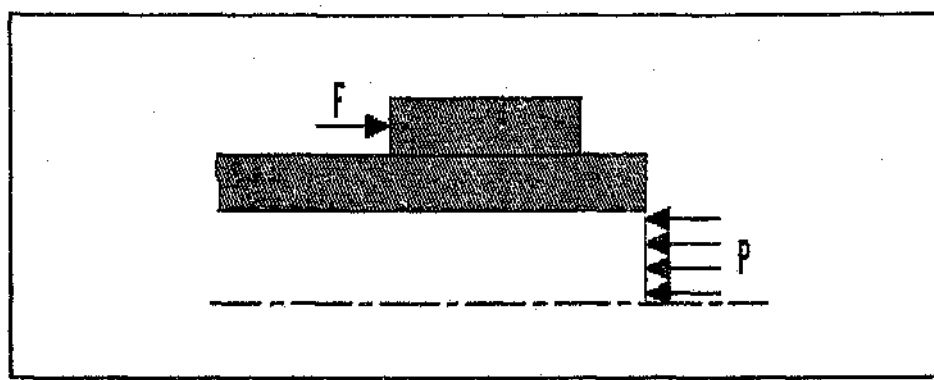

Figure 4.1 : Load applied to flange.

The test program was designed to simulate this loading condition. Hence it was essentially a tensile test that was performed.

4.1.1 TEST SPECIMENS

The test specimens were made of sections of GRP pipe 400 mm in length, 50 mm internal diameter and 8 mm wall thickness. They were filament wound using E-glass fibres impregnated with epoxy resin at a fibre orientation of ±55°. On both ends of the pipe a circumferential step was machined into the outside of the pipe wall. Different step geometries were investigated, the optimum geometry being shown in figure 4.2.

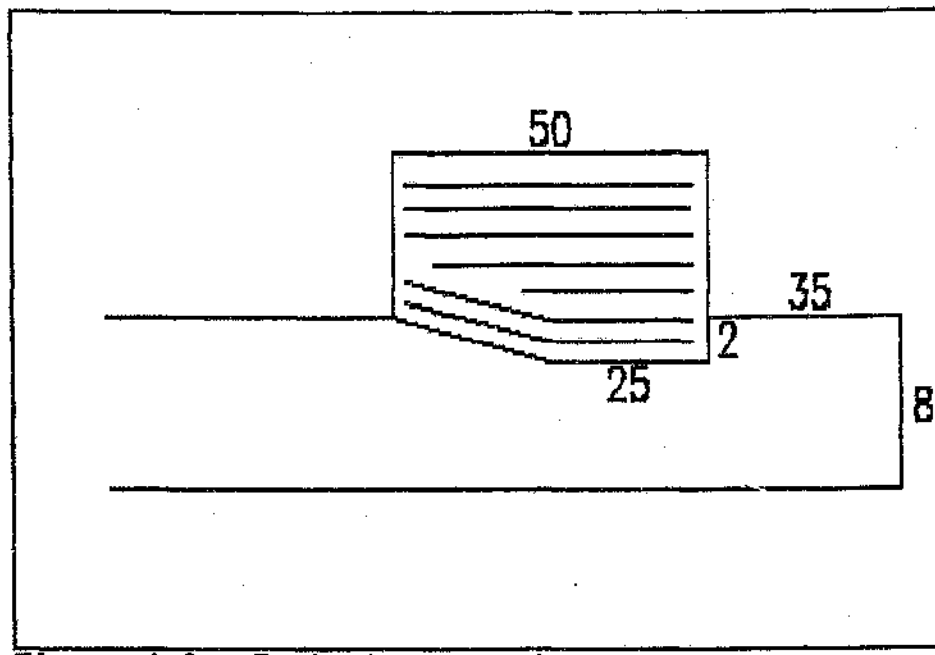

Figure 4.2 : Best step geometry.

Two GRP flanges were laid up directly on the pipe, one on each side. The thickness of these flanges was 10 mm measured from the outside of the pipe. Flanges with different lay-ups of the reinforcement were tested.

The test length of 400 mm was sufficient to ensure that the flanges had a negligible effect on the stress pattern at the middle of the pipe. This was verified using the Finite Element Technique.

For comparison purposes four other pipe/flange combinations were tested. In one instance the pipe was made from steel; in two other cases the flanges were made from steel. Although the purpose of this research was to evaluate GRP couplings on GRP pipes only, it was decided to investigate the effect of a material which is much stiffer and harder than steel on coupling performance. This would give an indication as to how the flange properties should be tailored (by changing the fibre orientations).

The first of these tests used a plain ended GRP pipe without a step. A GRP flange was wound directly onto the pipe. This arrangement derives its strength from the tubular lap joint between the pipe and the flange.

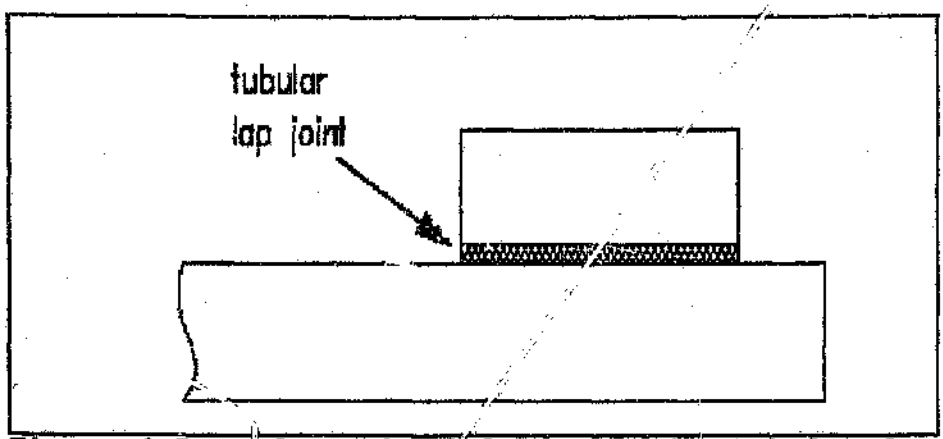

Figure 4.3 : Flange bonded to pipe by tubular lap joint.

The second configuration tested had a step machined into the pipe. But instead of using a GRP flange, a steel split ring was used as a flange. The split ring fitted into the step at the end of the pipe and the two halves were held together by a large pipe clamp, as shown in figure 4.4.

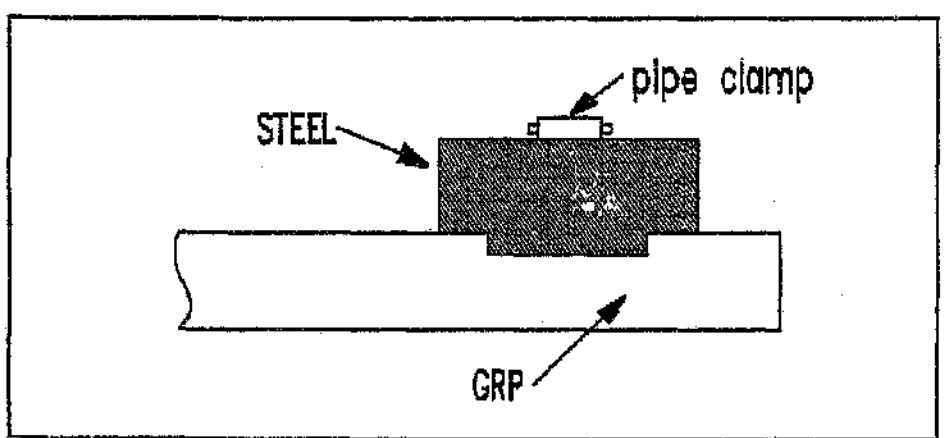

Figure 4.4 : Split steel flange on GRP pipe.

The third test is similar to the previous test described; except that in this case the pipe was manufactured from steel and the GRP flange was manufactured directly on the pipe. In one case the GRP flange was made by wrapping successive layers of resin impregnated chopped strand mat on the pipe. In the other case the flange was made using a bulk moulding compound (BMC) with three dimensional chopped fibres.

The last test, which also utilised a steel flange, derives its strength entirely from the shear strength of the adhesive which was used to bond the flange to the pipe. The pipe has a tapered end, and the flange has an opposite taper on its inside.

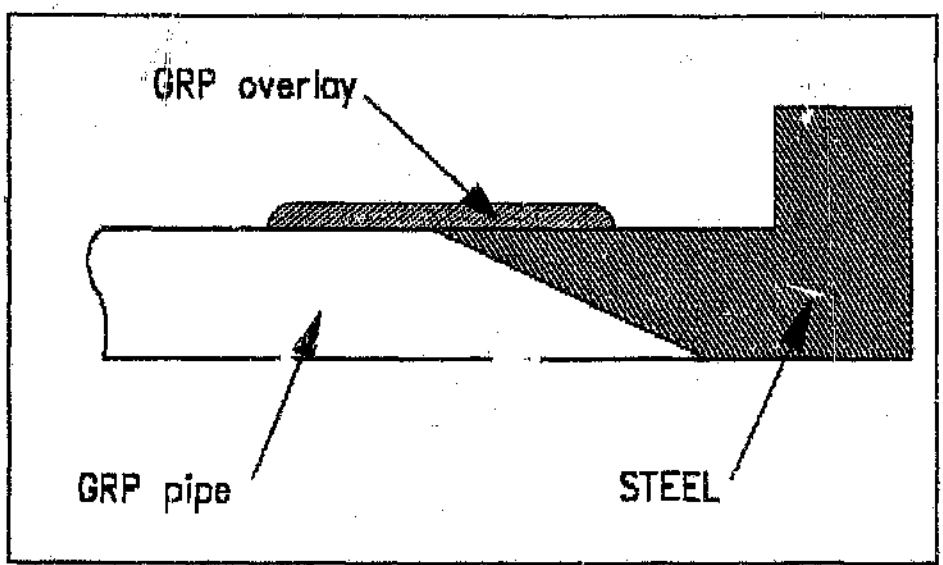

Figure 4.5 : Flange bonded to pipe by scarf joint.



Figure 4.6 : Photo showing pipe and flange with tapered ends.

The two components were simply pushed together with a thin adhesive layer inbetween. This joint could be made even stronger by overwrapping with a few layers of GRP.

4.1.2 TESTING APPARATUS

As stated earlier the type of test performed was essentially a tensile test. A jig was manufactured to clamp the specimen in the testing machine.

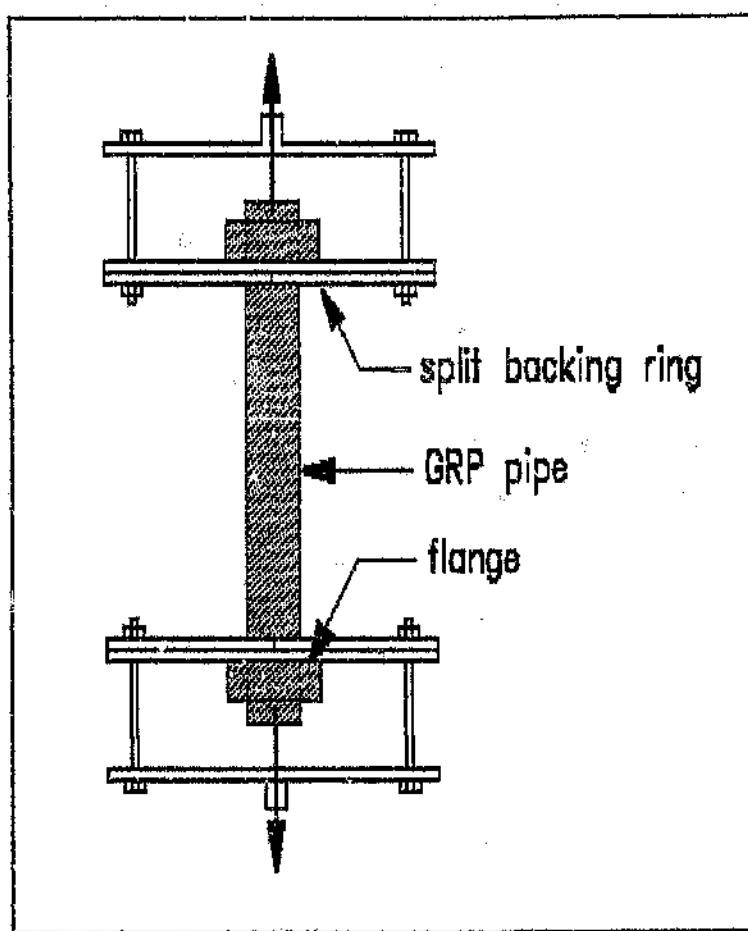

Figure 4.7 : Sketch of test jig.

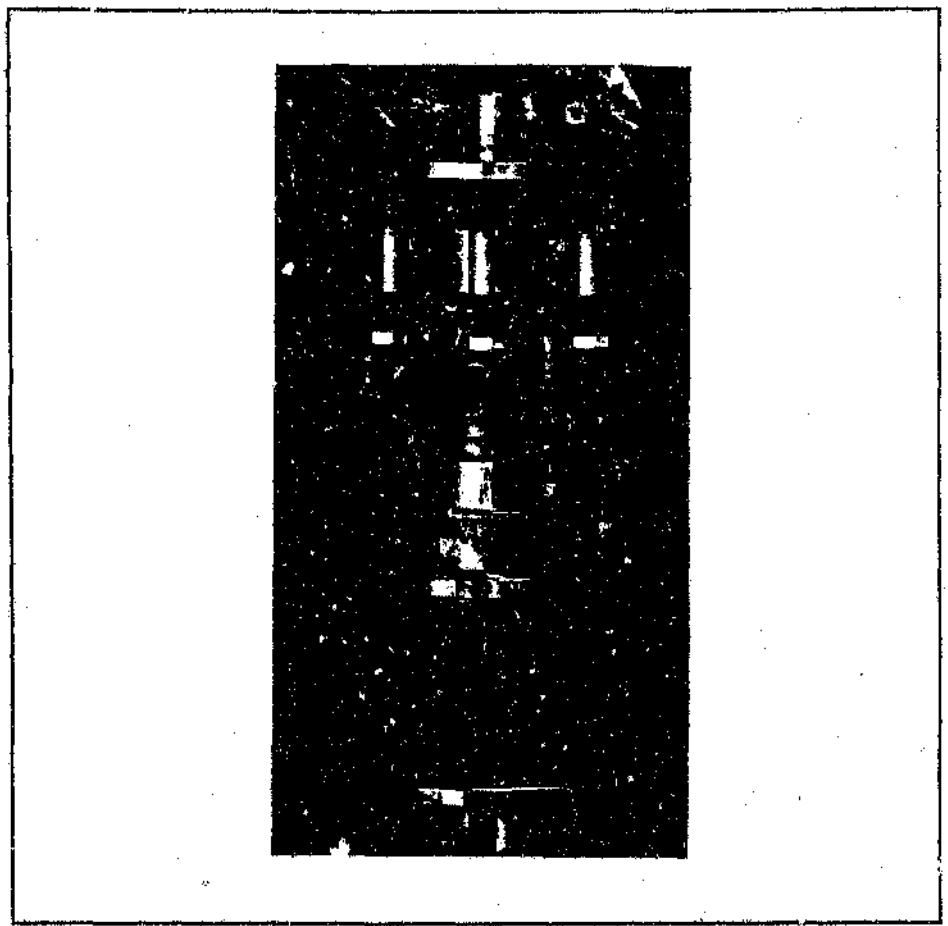

Figure 4.8 : Photo of test jig.

Two steel baseplates are attached to the testing machine (one plate is attached to the piston, the other plate to the loadcell). Two backing rings fit behind each flange and are bolted to the baseplates with four high tensile bolts.

To be able to fit the backing ring behind the flange once this has been manufactured, the ring was made in two halves. Since this type of backing ring is very unstable, a second backing ring was used. The second ring was placed directly behind the first ring, but out of phase by 90°.

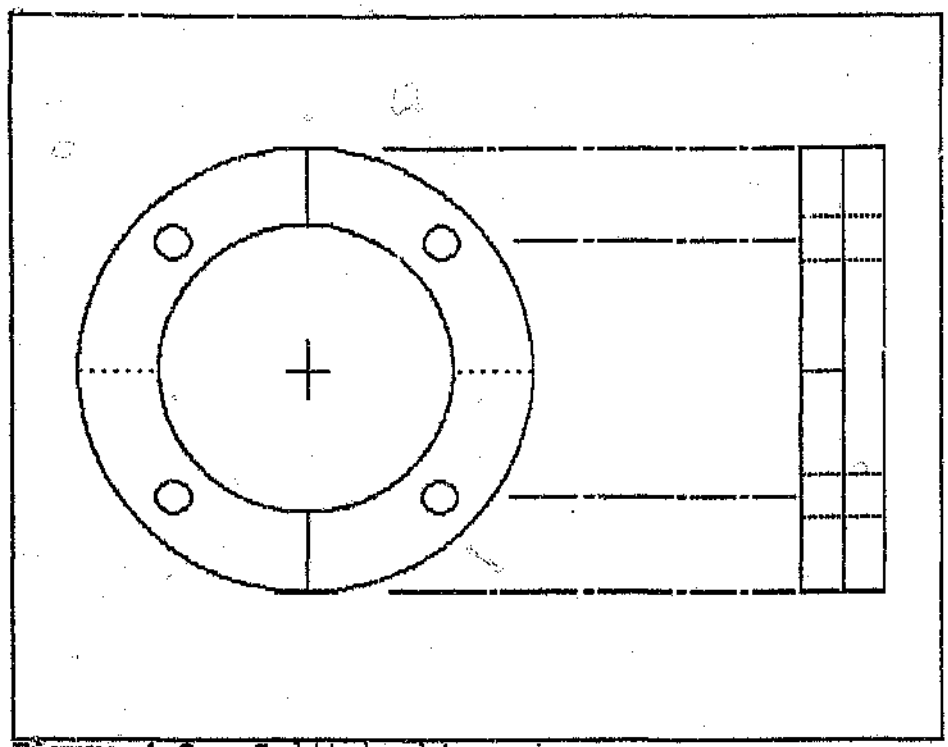

Figure 4.9 : Split backing ring.

With the pipe clamped securely in the testing machine it was now loaded in tension. All pipes were loaded up to failure. Failure of the pipe is represented by either the pipe disintegrating, the flange or the interface failing or a combination of these.

The load was continuously monitored and logged on a pen plotter. Hence the ultimate load was obtained. The shape of the plotted curve gives an indication as to the mode of failure and hence the safety (ie. catastrophic or slow failure) of the coupling.

4.2 RESULTS

This section contains the results of the experimental program as well as the finite element predictions. Some ideas were dismissed as non-feasible on the basis of the finite element results and were consequently not tested experimentally.

4.2.1 EXPERIMENTAL RESULTS

The following diagrams illustrate the different configurations that were tested. The y-axis displays the load (in kN) and the x-axis is a time scale (dimensionless).

The ultimate loads listed were obtained from the tensile tests. The mode of failure of each configuration is shown. The pressures listed are the internal pipe pressures required to produce the ultimate loads shown. These pressures are applicable to the pipes used in the tests, ie. 50 mm internal diameter and 66 mm external diameter.

TYPE I FLANGE

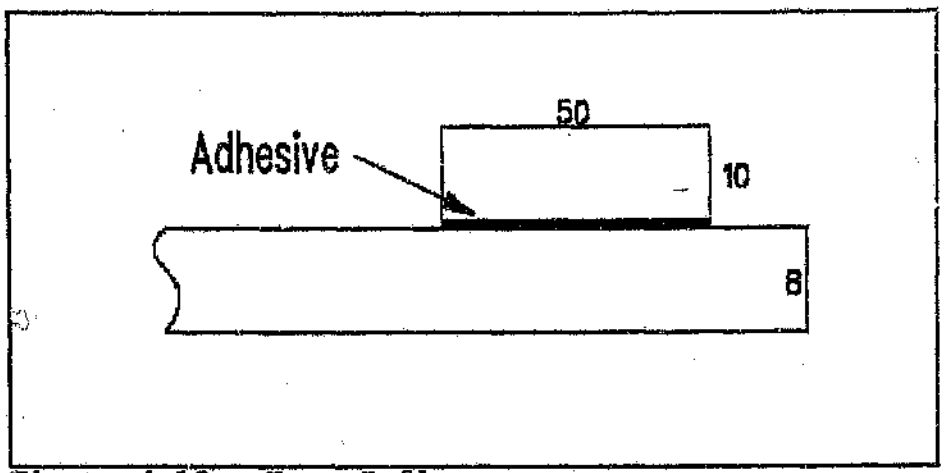

Figure 4.10 : Type I flange.

The ultimate load sustained by the TYPE I flange in figure 4.10 was 29 kN, which is equivalent to an internal pressure of 8.5 MPa. The mode of failure was an adhesive shear failure, which is a catastrophic failure (load bearing capacity drops to zero instantanously), as can be seen from figure 4.11.

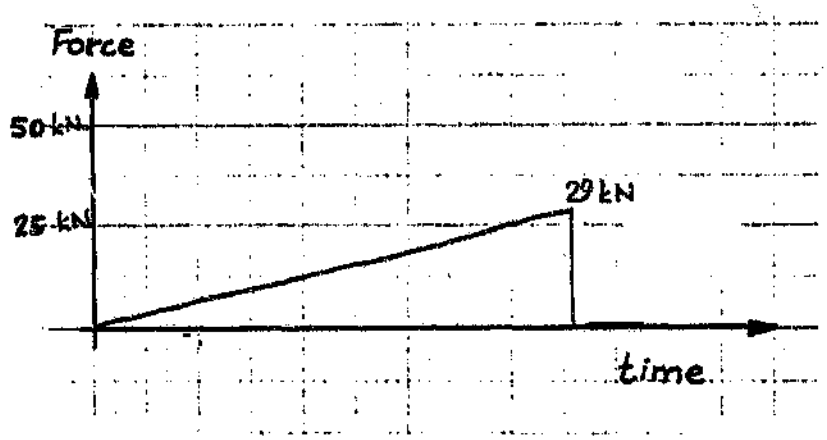

Figure 4.11 : Graph showing the loading on the TYPE I flange.

TYPE II FLANGE

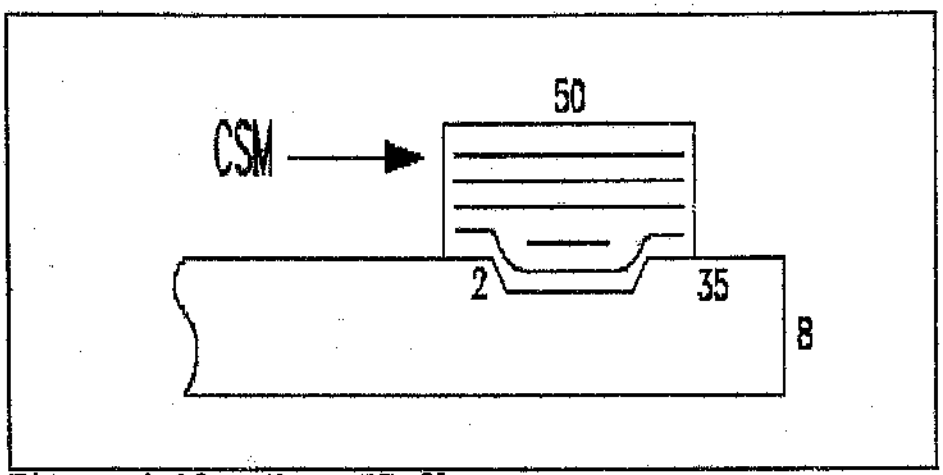

Figure 4.12 : Type II flange.

The load bearing capacity of this configuration results from a combination of the mechanical interaction between the flange and the pipe, as well as adhesive shear stresses along the interface. The flange is made entirely from chopped strand mat. The ultimate load sustained by this flange was 30 kN, which is equivalent to an internal pressure of 9.0 MPa. Failure in this test was due to an expansion of the flange. This is a gradual failure (load bearing capacity drops off very slowly), as can be seen from figure 4.13.

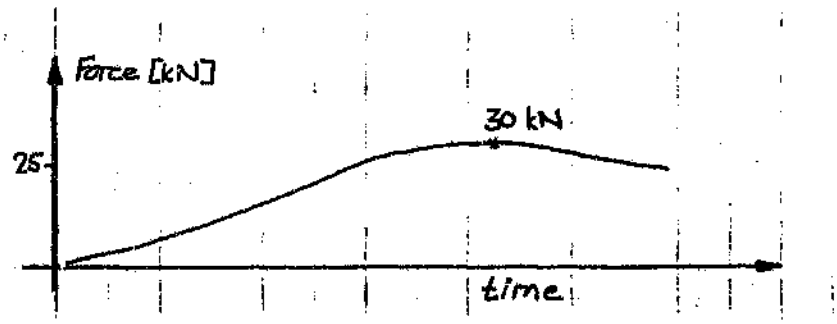

Figure 4.13 : Curve showing the loading and gradual failure of the TYPE II flange.

TYPE III FLANGE

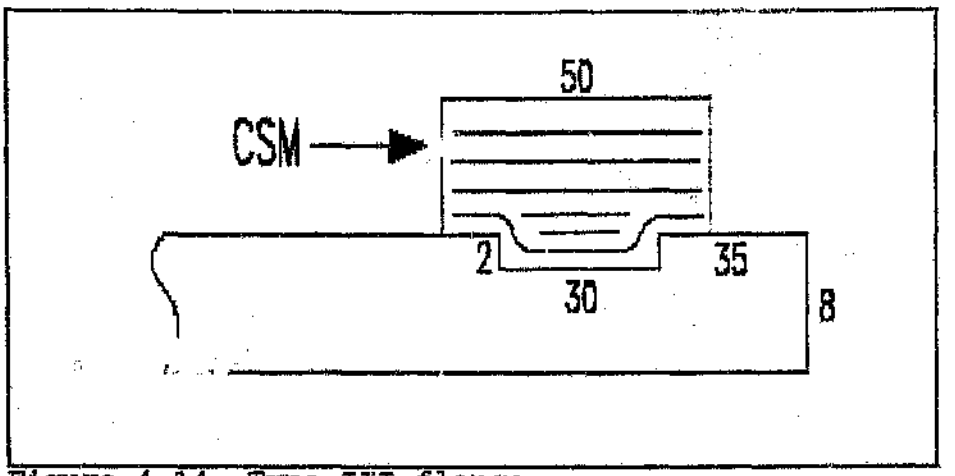

Figure 4.14: Type III flange.

This flange is similar to the TYPE II flange except that the step angle has been increased to 90°. All other dimensions have been maintained. The ultimate load sustained by this flange was 56 kN, which is equivalent to an internal pressure of 16.5 MPa. Failure here was due to crushing of a resin wedge in the corner of the step (in the flange). This is a gradual failure.

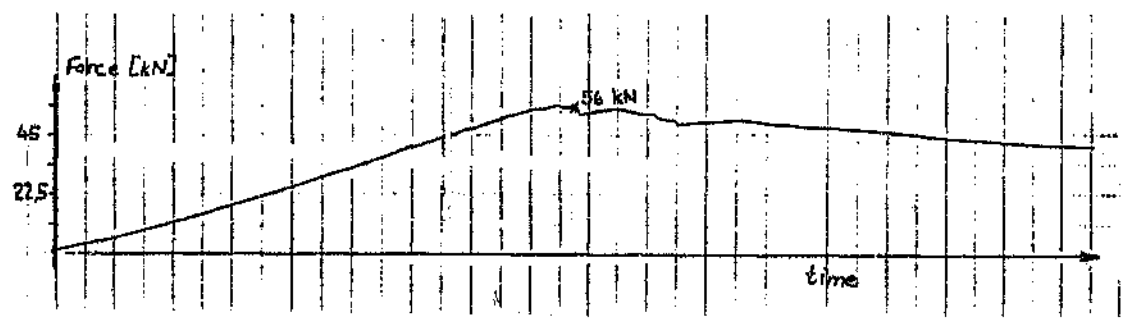

Figure 4.15 : Graph of test result for TYPE III flange.

TYPE IV FLANGE

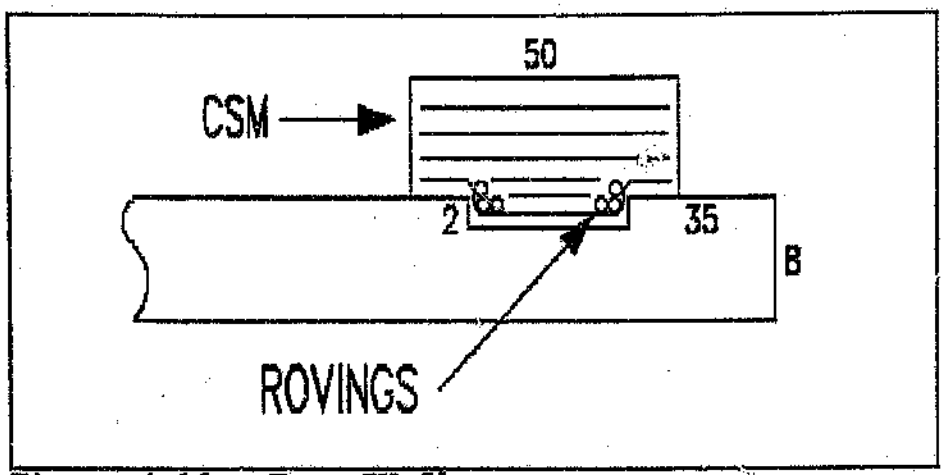

Figure 4.16 : Type IV flange.

This flange and pipe have the same step geometry as the previous combination. The flange is made almost entirely from chopped strand mat, except for the rovings (uni-directional fibres) wound into the corners. The purpose of these rovings was mainly to get rid of the resin wedges which caused the TYPE III flange to fail. The ultimate load sustained by this flange was 65 kN, which is equivalent to an internal pressure of 19.2 MPa. Failure here was due to crushing of the fibres in the corner of the step (in the flange). This is a slow failure, as can be seen by the slow decrease in the load bearing capacity in figure 4.17.

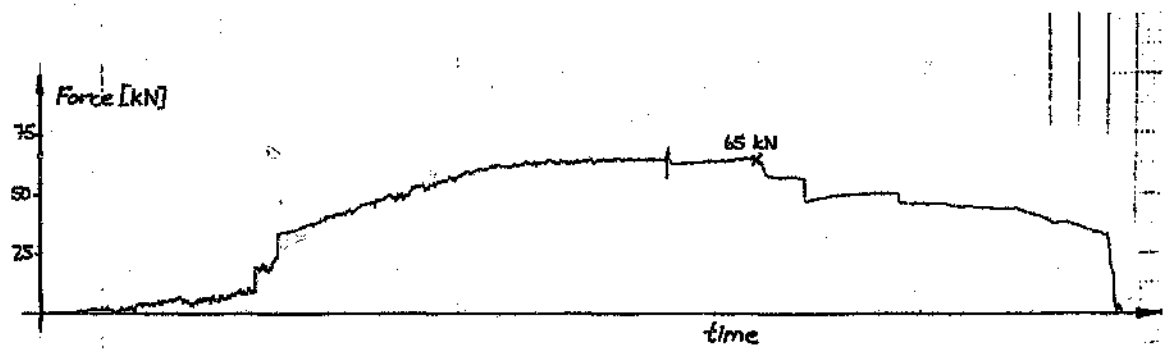

Figure 4.17 : Curve showing the load bearing capacity of the TYPE IV flange.

TYPE V FLANGE

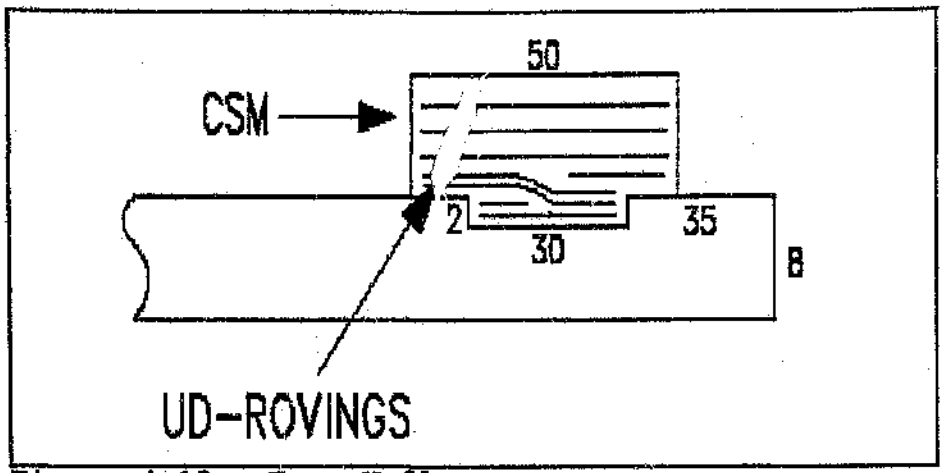

Figure 4.18 : Type V flange.

Two tests with this geometry were done. As opposed to winding uni-directional (UD) rovings in the hoop direction, UD-rovings were aligned in the axial direction to give the flange a higher axial compressive strength at the face of the step. This would also eliminate any excess resin in the corner (at the face of the step). In the first case (type V(a)) the ultimate load sustained was 68 kN, which is equivalent to an internal pressure of 20.0 MPa. Failure here was due to crushing of the fibres in the corner of the step (in the pipe). This is a gradual failure. In the second test (type V(b)) the ultimate load was 72 kN, which equivalent to an internal pressure of 21.1 MPa. This pipe failed due to interlaminar shear. This is a catastrophic failure mode (ie. the load bearing capacity drops to zero instantaneously).

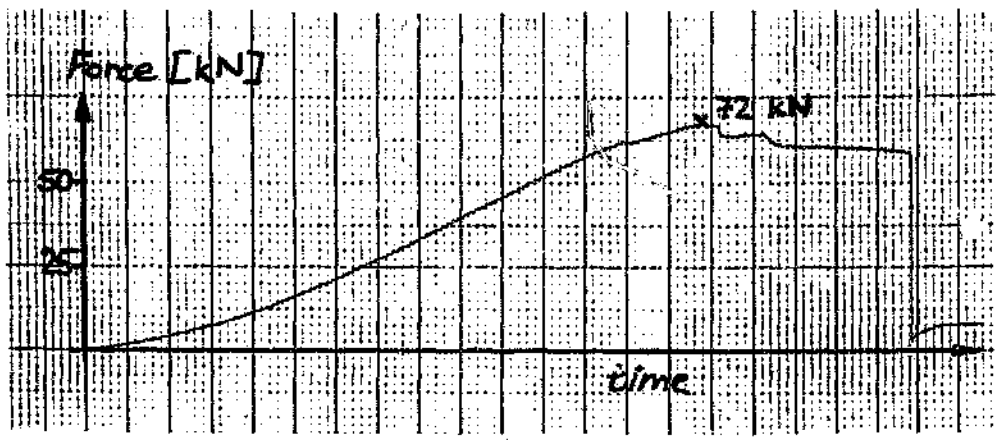

Figure 4.19 : Graph showing the load bearing capacity of the TYPE V(a) flange.

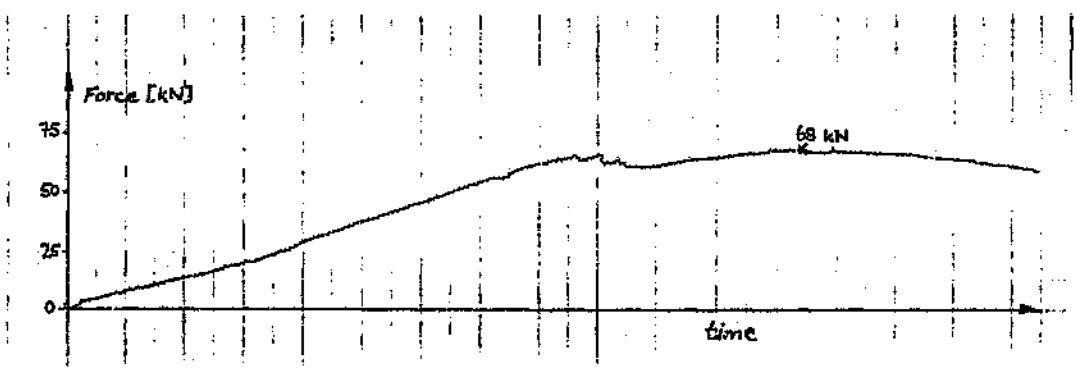

Figure 4.20 : Graph showing the load bearing capacity of the TYPE V(b) flange.

TYPE VI FLANGE

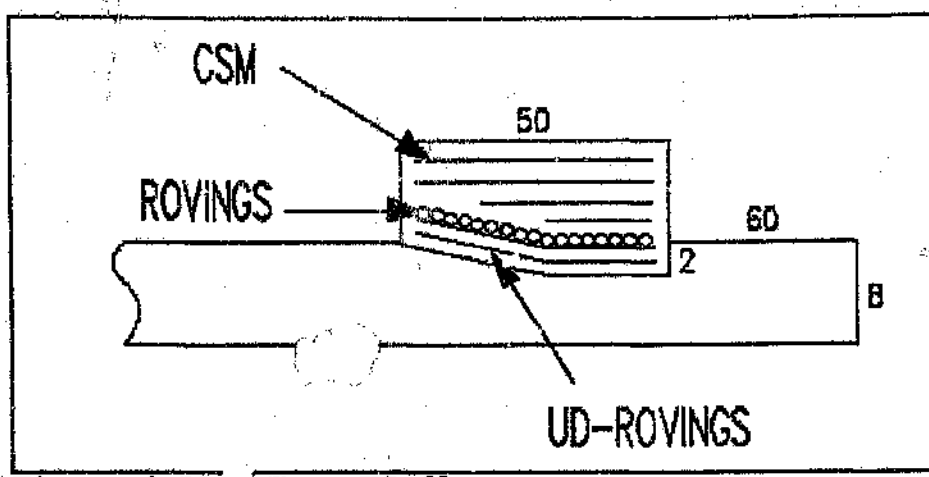

Figure 4.21 Type VI flange.

The rear step was tapered since it did not perform any useful function. It now has the shape of a tubular scarf joint, which is a more efficient joint than the tubular lap joint. The entire joint was moved back from the end of the pipe. The rovings wound in the hoop direction prevent the flange from expanding radially when the load is applied. The ultimate load sustained by this flange was 62 kN, which is equivalent to an internal pressure of 18.2 MPa. Failure here was due to crushing of the fibres in the corner of the step (in the pipe). This is a slow compressive failure.

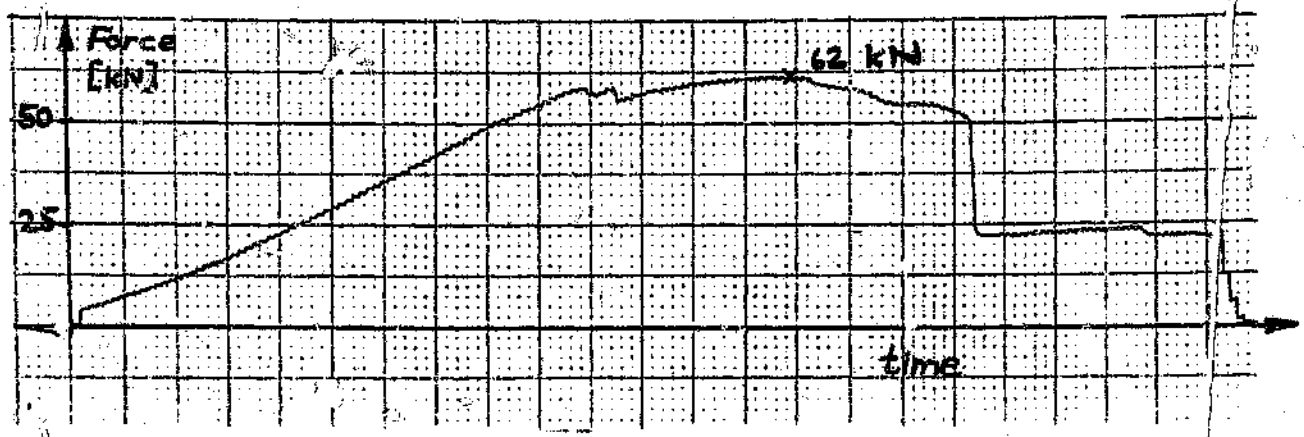

Figure 4.22 : Graph showing the load bearing capacity of the TYPE VI flange.

TYPE VII FLANGE

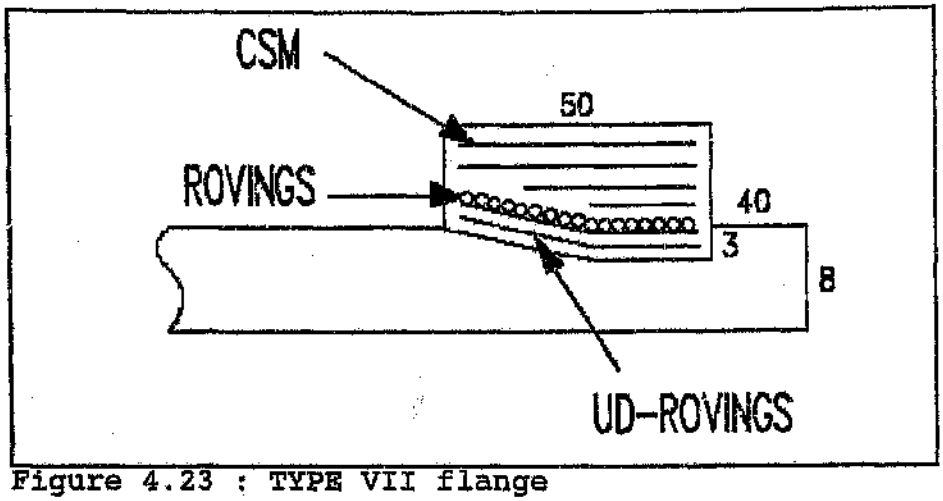

Figure 4.23 : TYPE VII flange

The lay-up is identical to the previous flange, except that the step is slightly deeper and the flange is closer to the end of the pipe. The ultimate load sustained by this flange was 70 kN, which is equivalent to an internal pressure of 20.6 MPa. Failure here was due to buckling of the fibres on the inside of the pipe. This is a slow failure.

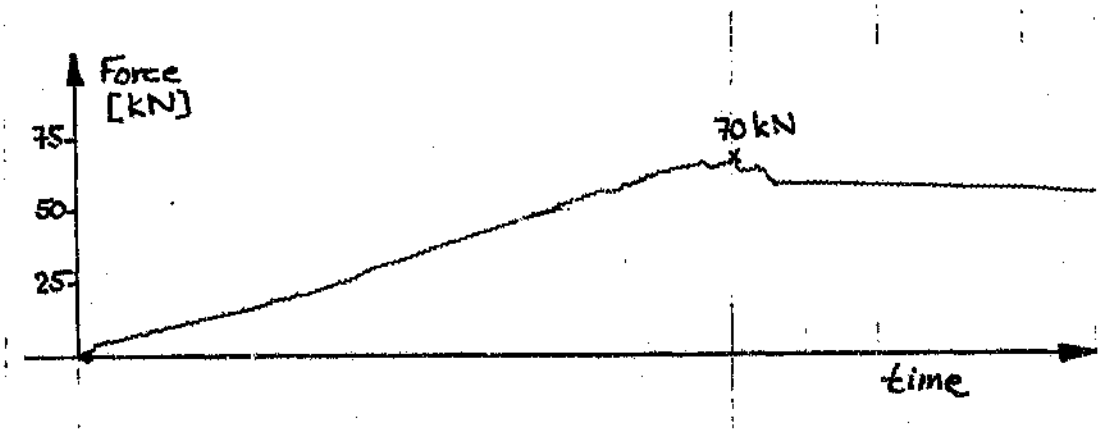

Figure 4.24 : Graph showing the load bearing capacity of the TYPE VII flange.

TYPE VIII FLANGE

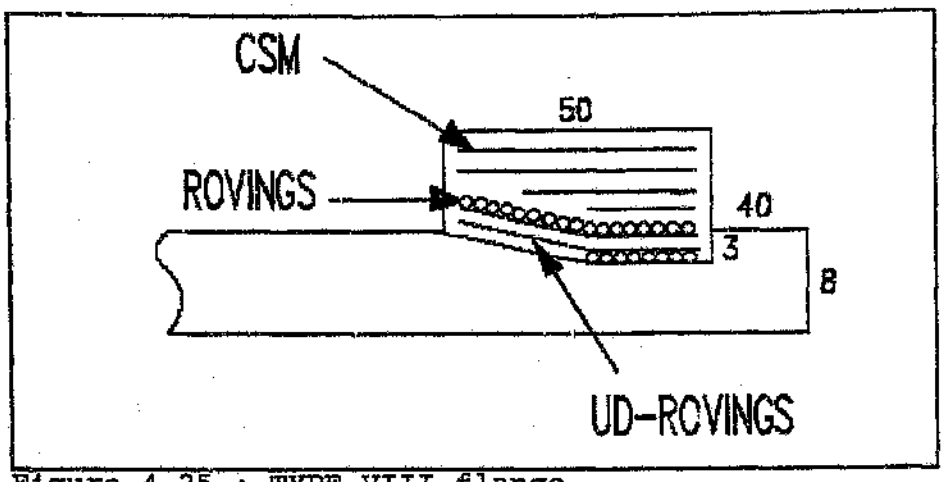

Figure 4.25 : TYPE VIII flange.

The geometry of this flange is identical to the TYPE VII flange with additional hoop reinforcement. The ultimate load sustained by this flange was 75 kN, which is equivalent to an internal pressure of 22.0 MPa. Failure here was due to buckling of the fibres on the inside of the pipe. This is a slow failure.

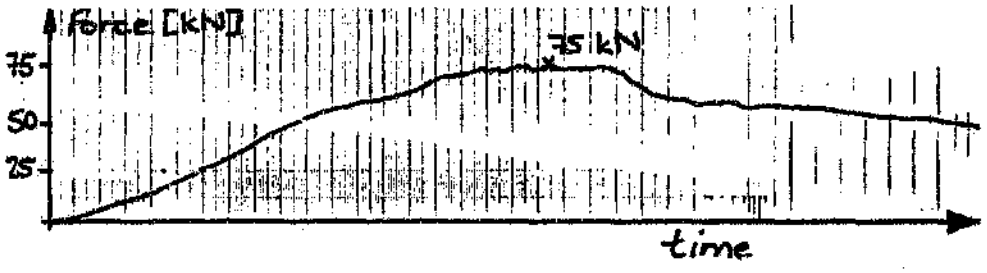

Figure 4.26 : Graph showing the load bearing capacity of the TYPE VIII flange.

TYPE IX FLANGE

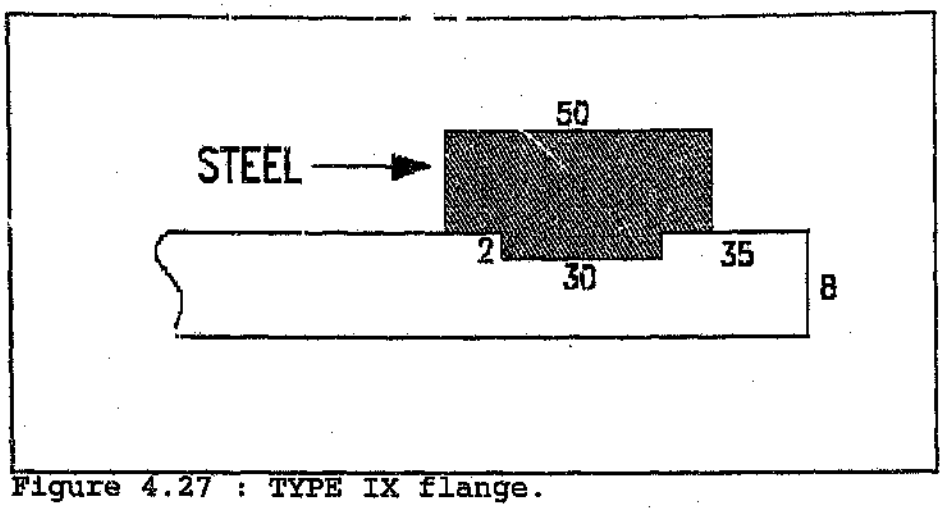

Figure 4.27 : TYPE IX flange.

This flange is made from a split steel ring, resulting in a very high compressive strength (in the flange) at the face of the step. The ultimate load sustained by this flange was 75 kN, which is equivalent to an internal pressure of 22.0 MPa. Failure here was due to interlaminar shear of the pipe. This is a catastrophic failure.

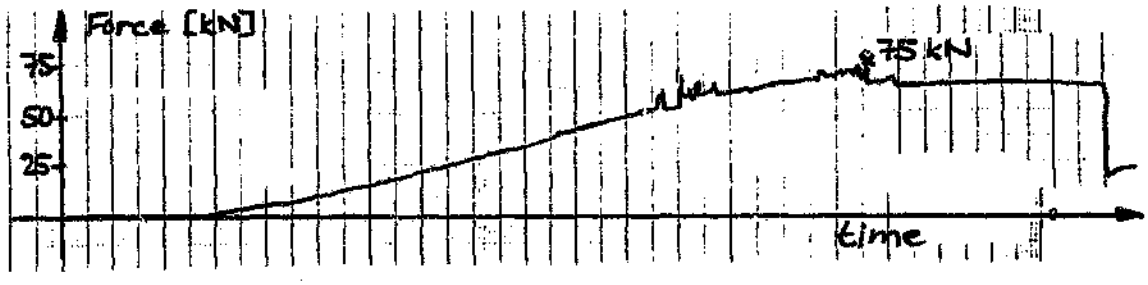

Figure 4.28 : Graph showing the load bearing capacity of the TYPE IX flange.

TYPE X FLANGE

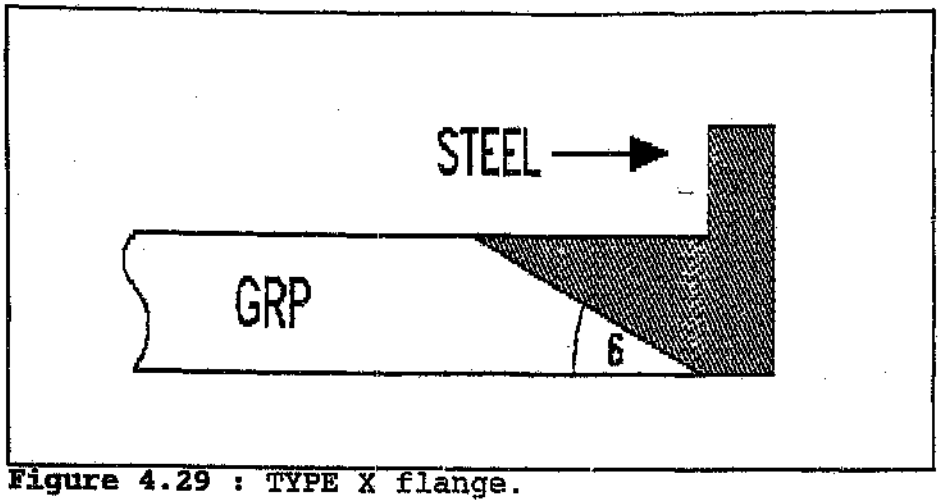

Figure 4.29 : TYPE X flange.

The flange and pipe are both tapered (6°), forming an adhesive scarf joint. This joint derives its strength solely from the adhesive used and the accuracy with which the joint is made. The ultimate load sustained by this flange was 82 kN, which is equivalent to an internal pressure of 24.1 MPa. The mode of failure was an adhesive shear failure, which is a catastrophic failure, as can be seen from figure 4.30.

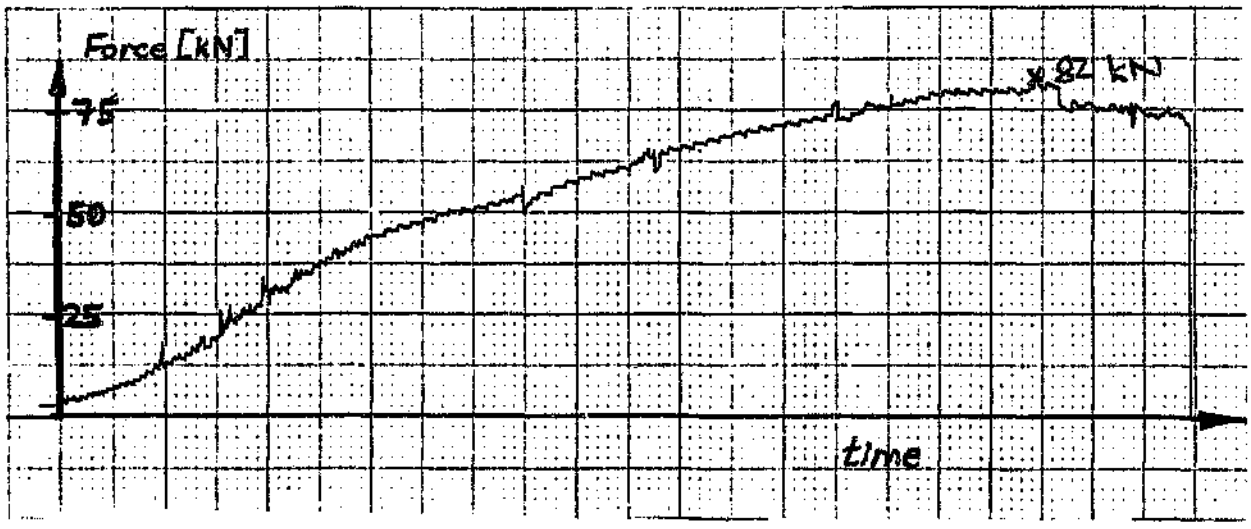

Figure 4.30 : Graph showing the load bearing capacity of the TYPE X flange.

TYPE XI FLANGE

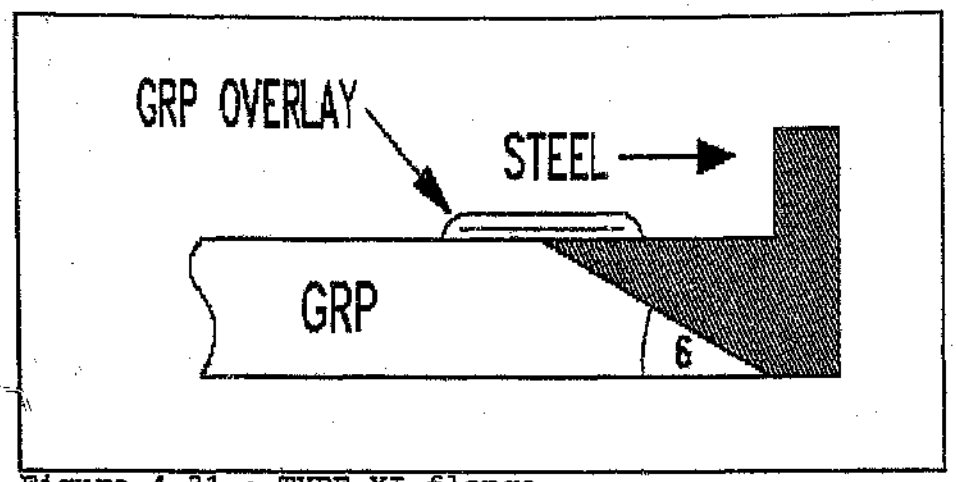

Figure 4.31 : TYPE XI flange.

This flange is similar to the TYPE X flange, except that it has an overwrap which increases the effective shear area of the adhesive. Two tests were done. In the first case (type XI(a)) the ultimate load sustained was 50 kN, which is equivalent to an internal pressure of 14.7 MPa. Failure here was due to adhesive shear. This is a catastrophic failure. In the second test (type XI(b)) the ultimate load was 93 kN, which equivalent to an internal pressure of 27.4 MPa. Failure in this case was also due to adhesive shear.

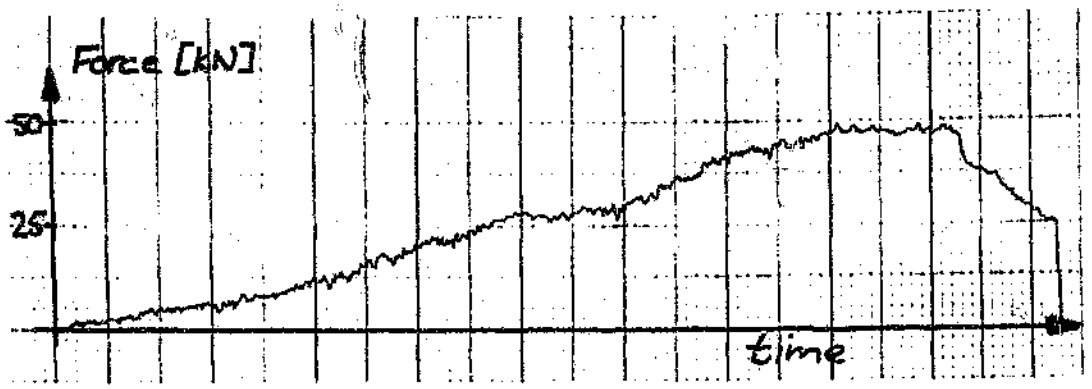

Figure 4.32 : Graph showing the load bearing capacity of the TYPE XI(a) flange.

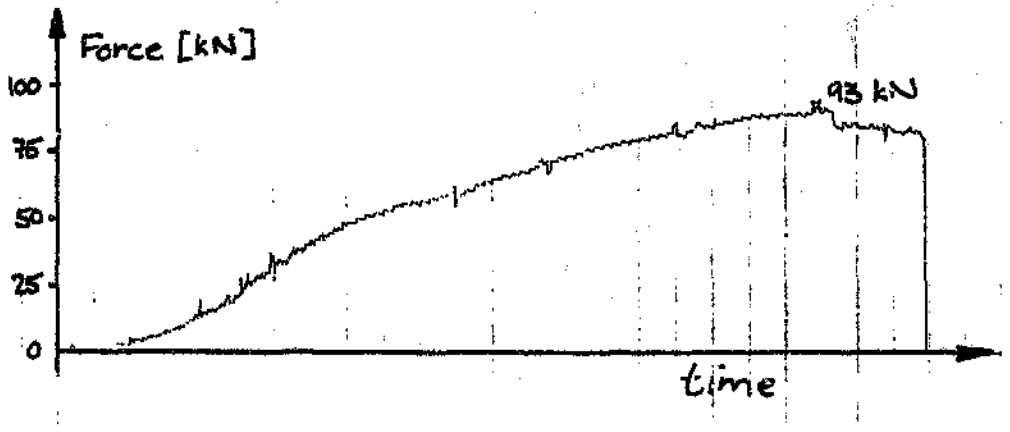

Figure 4.33 : Graph showing the load bearing capacity of the TYPE XI(b) flange.

TYPE XII FLANGE

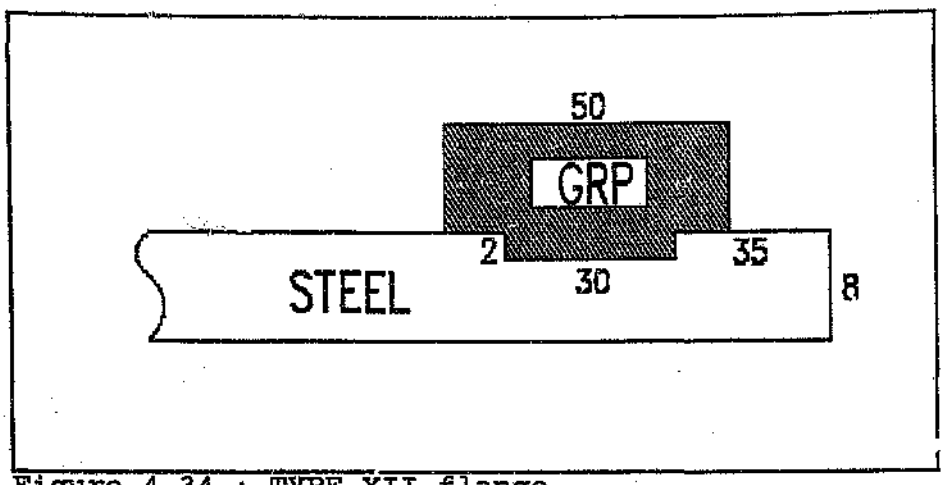

Figure 4.34 : TYPE XII flange.

In this case the pipe is made from steel and the flange is made from GRP, ie. the pipe has a high stiffness compared to the flange. The ultimate load sustained by this flange was 105 kN, which is equivalent to an internal pressure of 31 MPa. Failure was due to crushing of the fibres in the flange. This is a slow failure, as can be seen from figure 4.35.

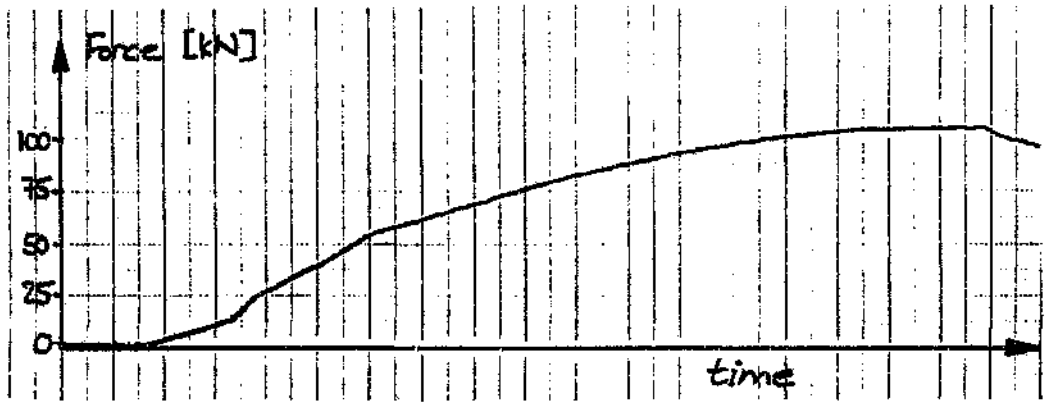

Figure 4.35 : Graph showing the load bearing capacity of the TYPE XII flange.

TYPE XIII FLANGE

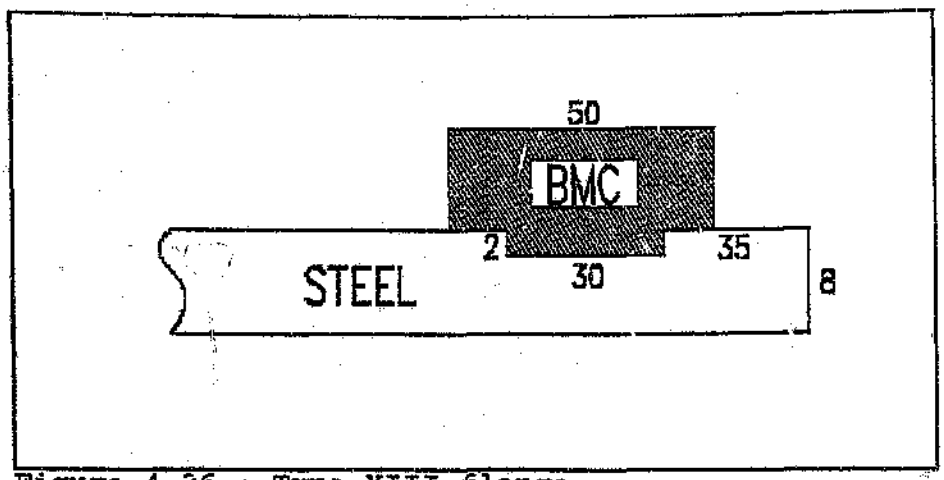

Figure 4.36 : Type XIII flange.

This test has the same geometry as the previous test, except that the material used was a bulk moulding compound with short chopped fibres (6mm length) oriented in all three dimensions. This material has essentially isotropic properties, due to the random orientation of the fibres. The ultimate load sustained by this flange was 70 kN, which is equivalent to an internal pressure of 20 MPa. Failure was due to crushing of the fibres in the flange. This is a slow failure, as can be seen from figure 4.37.

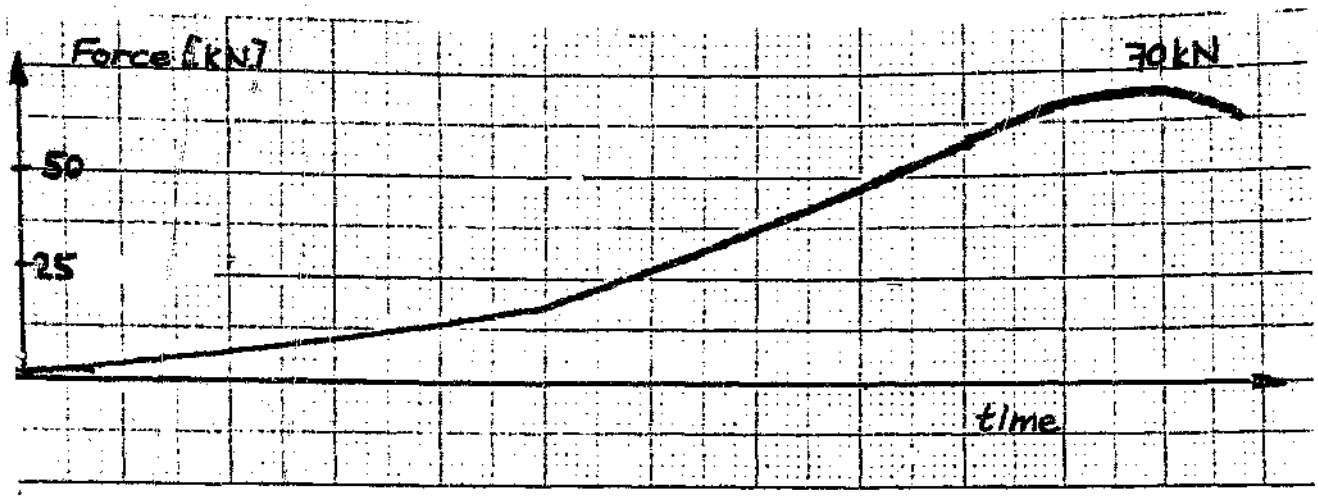

Figure 4.37 : Graph showing the load bearing capacity of the TYPE XIII flange.

4.2.2 FINITE ELEMENT RESULTS

Two of the configurations which were modelled with the finite element technique are shown in the figures below. The meshes of each model are shown in Appendix C.

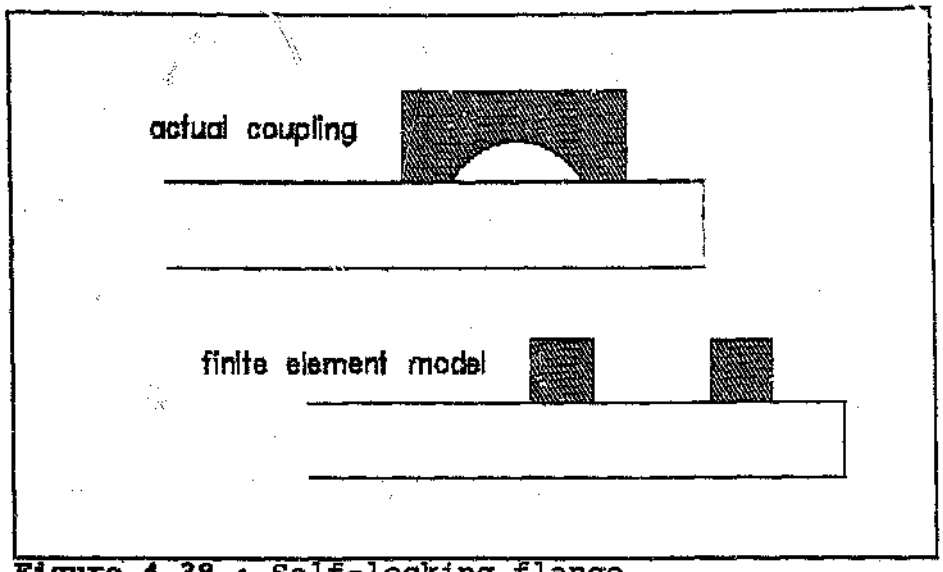

Figure 4.38 : Self-locking flange.

The aim of this model was to determine the radial expansion of the pressurized fibreglass pipe. If the radial expansion between two stiff sections in the pipe (these are the sides of the steel flange) is large, then a mechanical interaction between the pipe and the flange results. This concept of a self-tightening flange could be implemented in the design. The finite element model is simplified by incorporating only two stiff steel rings around the flexible GRP pipe. This is a valid simplification, since the remaining material in the flange does not have much effect on the expansion of the pipe (since the steel rings are much stiffer than the GRP pipe). The following figure is the displacement plot obtained from the finite element software.

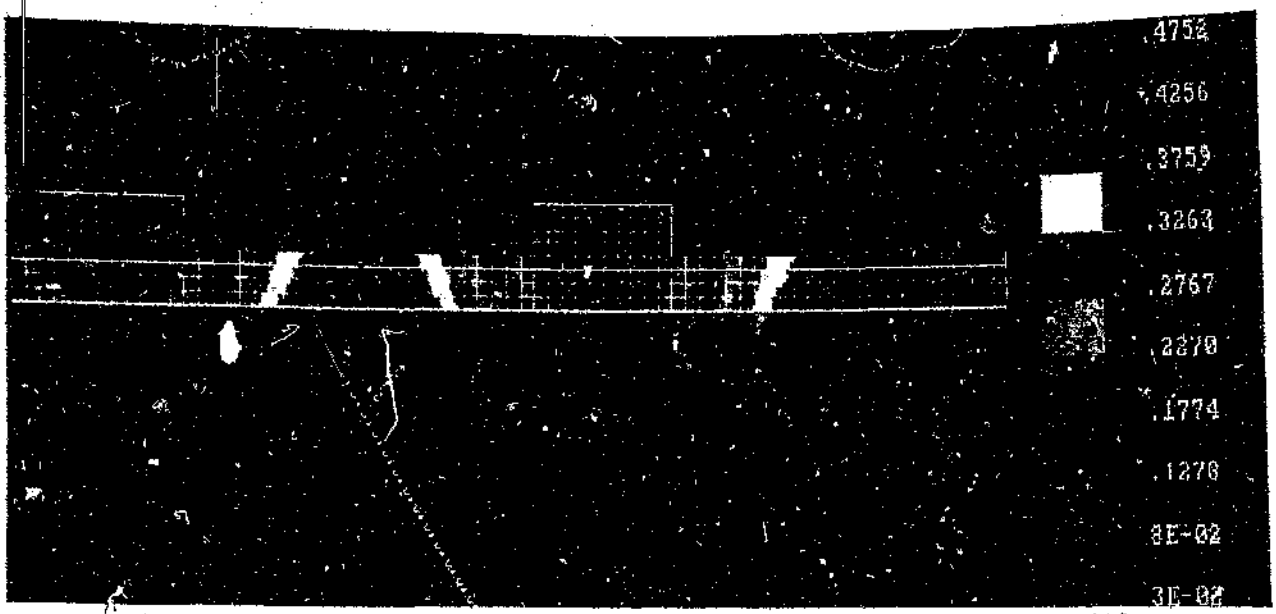

Figure 4.39 : Radial displacement of GRP pipe with two outer stiffening rings.

The output shows the maximum radial expansion between the two stiffening rings to be approximately 0.4[illegible]mm (diametral expansion) at 30 MPa. Although fairly small tolerances can be achieved with the filament winding process, this expansion is not enough to ensure a reliable joint. This configuration was discarded and was hence not tested.

Figure 4.40 shows a pipe with a double flange attached to it. It was thought that by introducing a second step the shear area could be increased sufficiently to affect the load bearing capacity considerably.

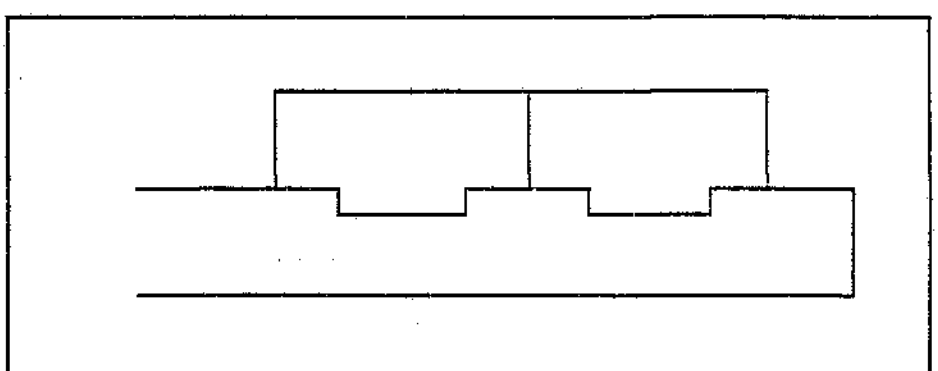

Figure 4.40 : Pipe with a double flange attached to it.

Figure 4.41 shows the axial stresses in a GRP pipe with two GRP flanges.

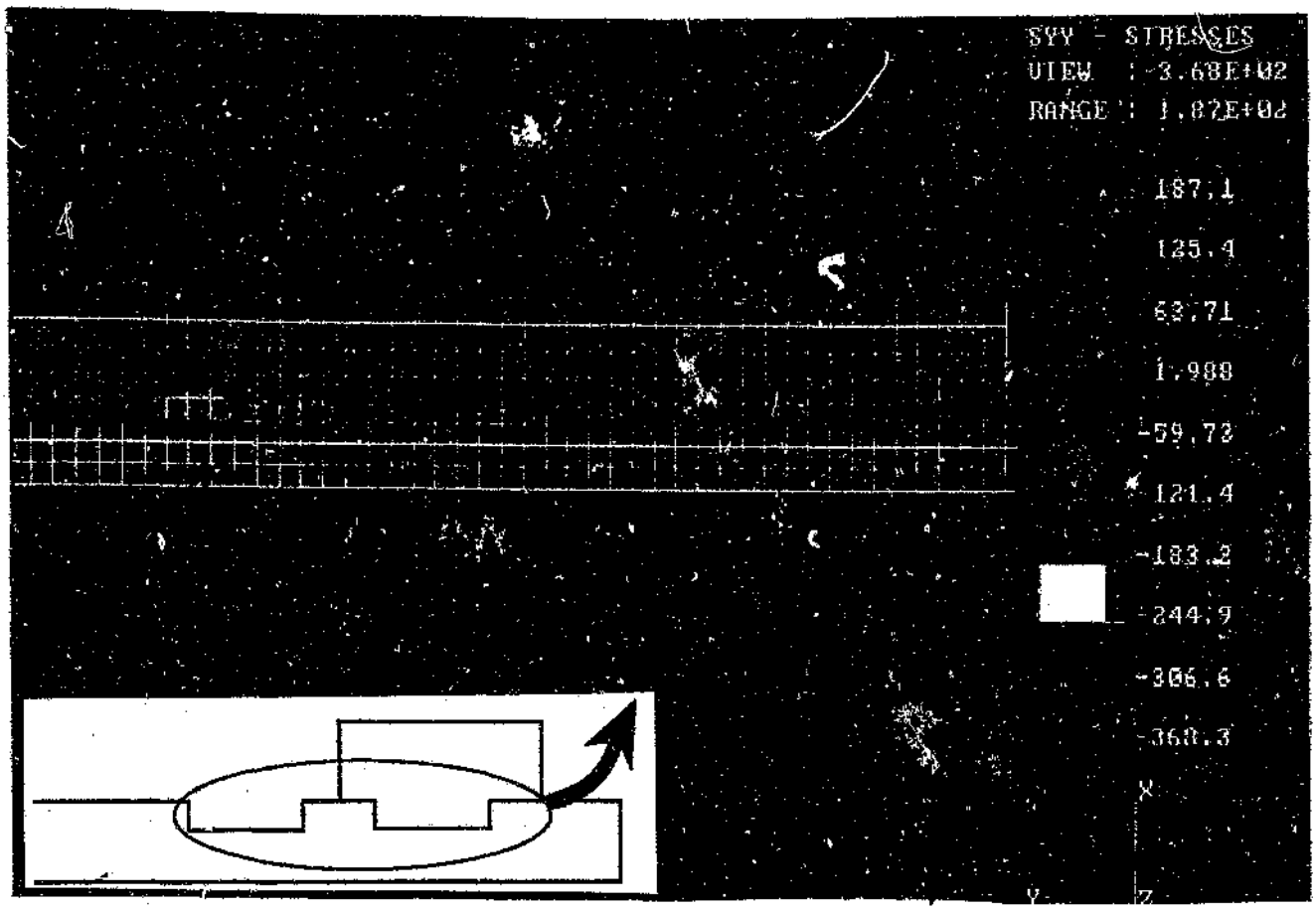

Figure 4.41 : Axial stresses in a GRP pipe with two GRP flanges.

The applied load is equivalent to an internal pressure of 19 MPa. It becomes immediately apparent from the figure that almost the entire force gets transmitted across the first step. Thus very little can be gained by introducing a second step, and hence it was decided not to test this configuration.

Figure 4.42 shows a type XII flange. The pipe is made from mild steel and the flange is made from GRP.

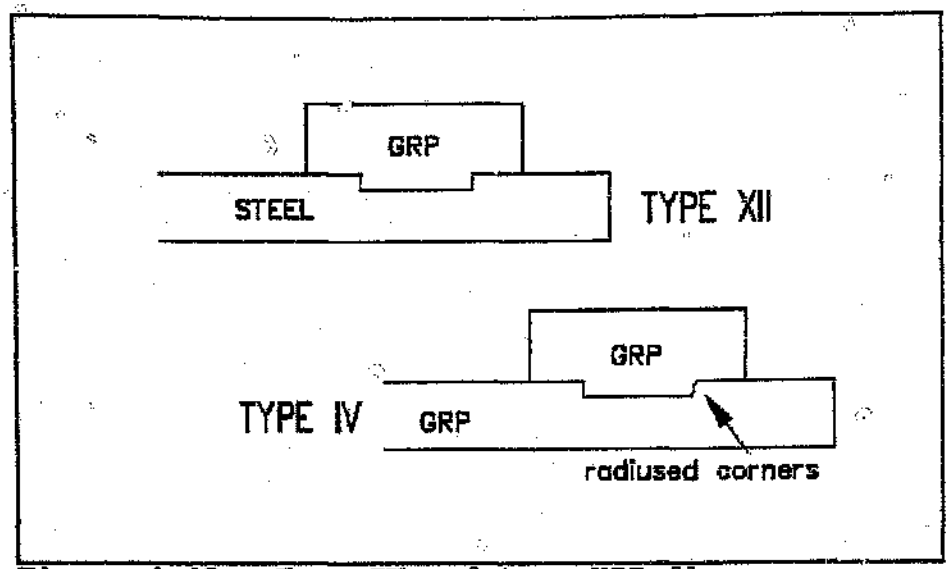

Figure 4.42 : Type IV and type XII flange.

Initially a coarse mesh was used to establish regions with stress concentrations. As expected, the step area was found to be such a region. The mesh was subsequently refined at the front of the step to yield a more accurate solution. Figure 4.43 shows the axial stresses in both the flange and the pipe. The load applied was equivalent to an internal pressure of 31 MPa (ie. the load at which the experimental flange failed). The load was applied as a pressure on the face of the flange.

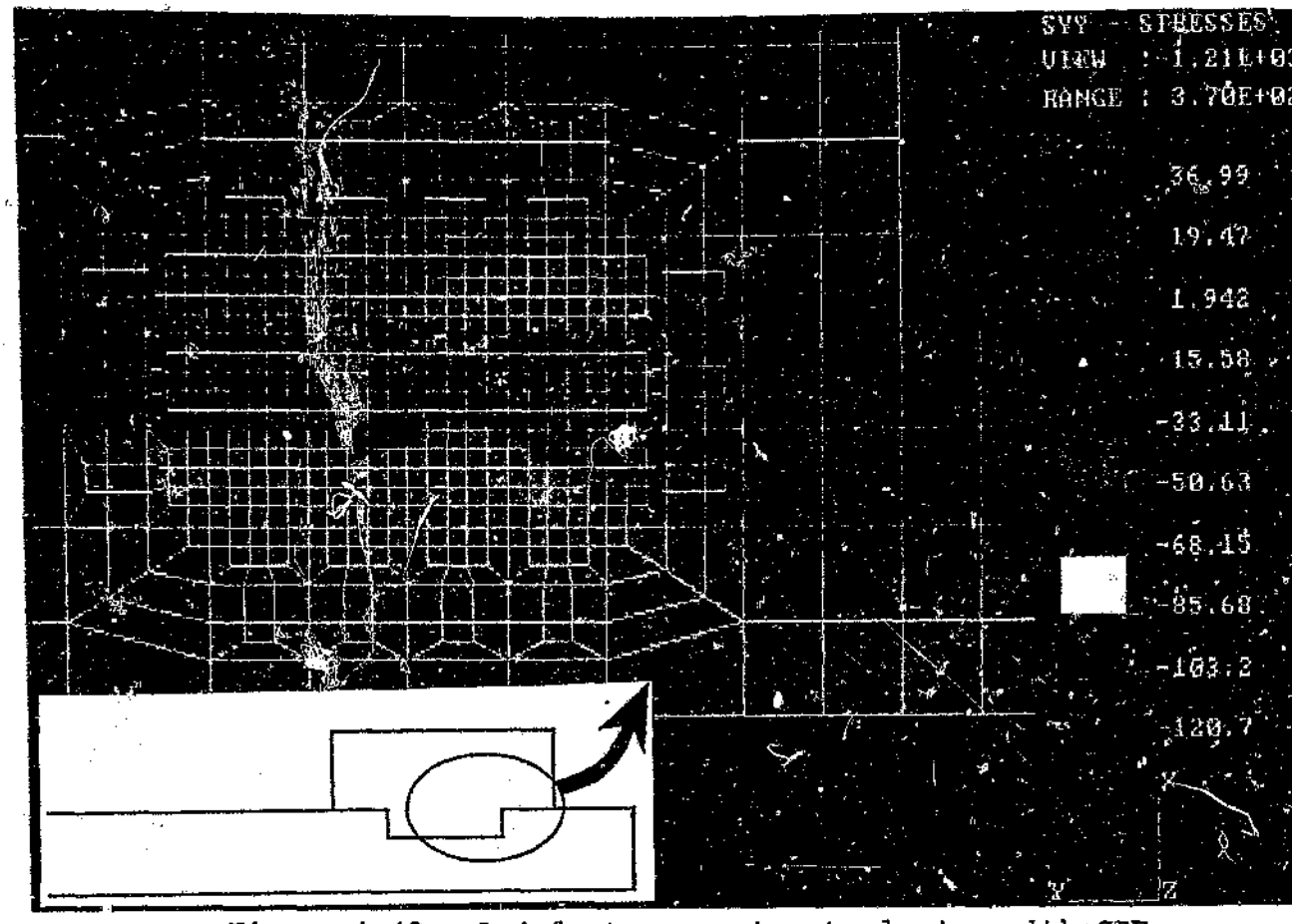

Figure 4.43 : Axial stresses in steel pipe with GRP flange (TYPE XII).

It can be clearly seen that the stress concentration is very localised in the corners and on the surface of the pipe where the flange is in contact with it. Another interesting observation can be made from the above figure. Due to its high stiffness, the steel has a much higher stress concentration than the GRP. Since the steel is strong enough to accomodate this stress concentration, a very high load bearing capacity can be achieved.

The next model has virtually the same geometry, but in this case a GRP pipe is used (TYPE IV). The only difference in the mesh is that the corners were "radiused" to model the actual situation more accurately. The axial stresses are shown in figure 4.44. The load applied was equivalent to an internal pressure of 19 MPa

and was applied as a pressure on the face of the flange.

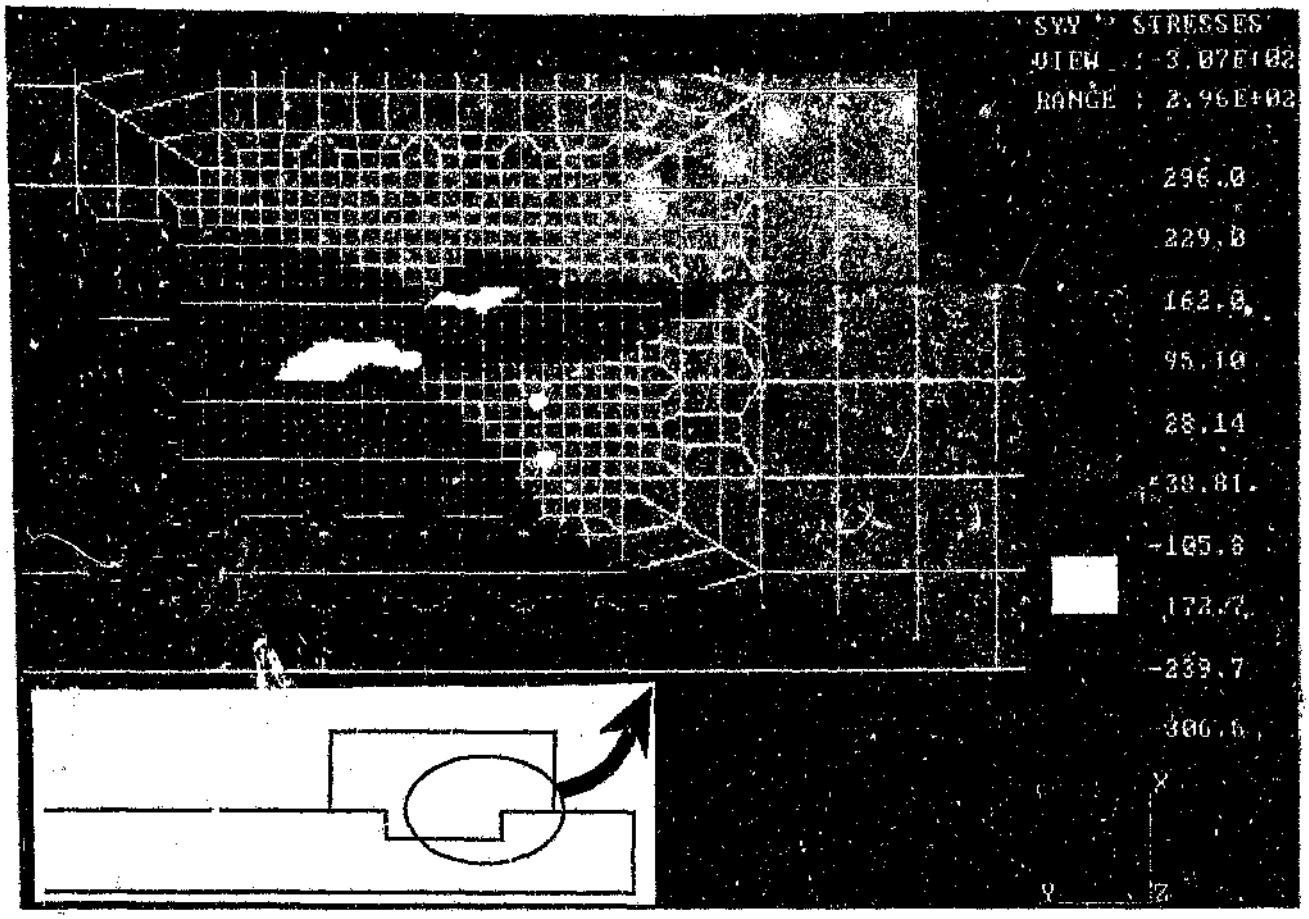

Figure 4.44 : Axial stresses in GRP pipe with GRP flange (TYPE IV).

Clearly here the stress concentration in the GRP flange is much higher than in the previous case, where a steel pipe was used. This shows that the use of a high-stiffness material such as steel will improve the performance of the coupling.

The last two figures do not model any experiments. In this case the type IV flange/pipe was pressurized from the inside to model the pipe in use.

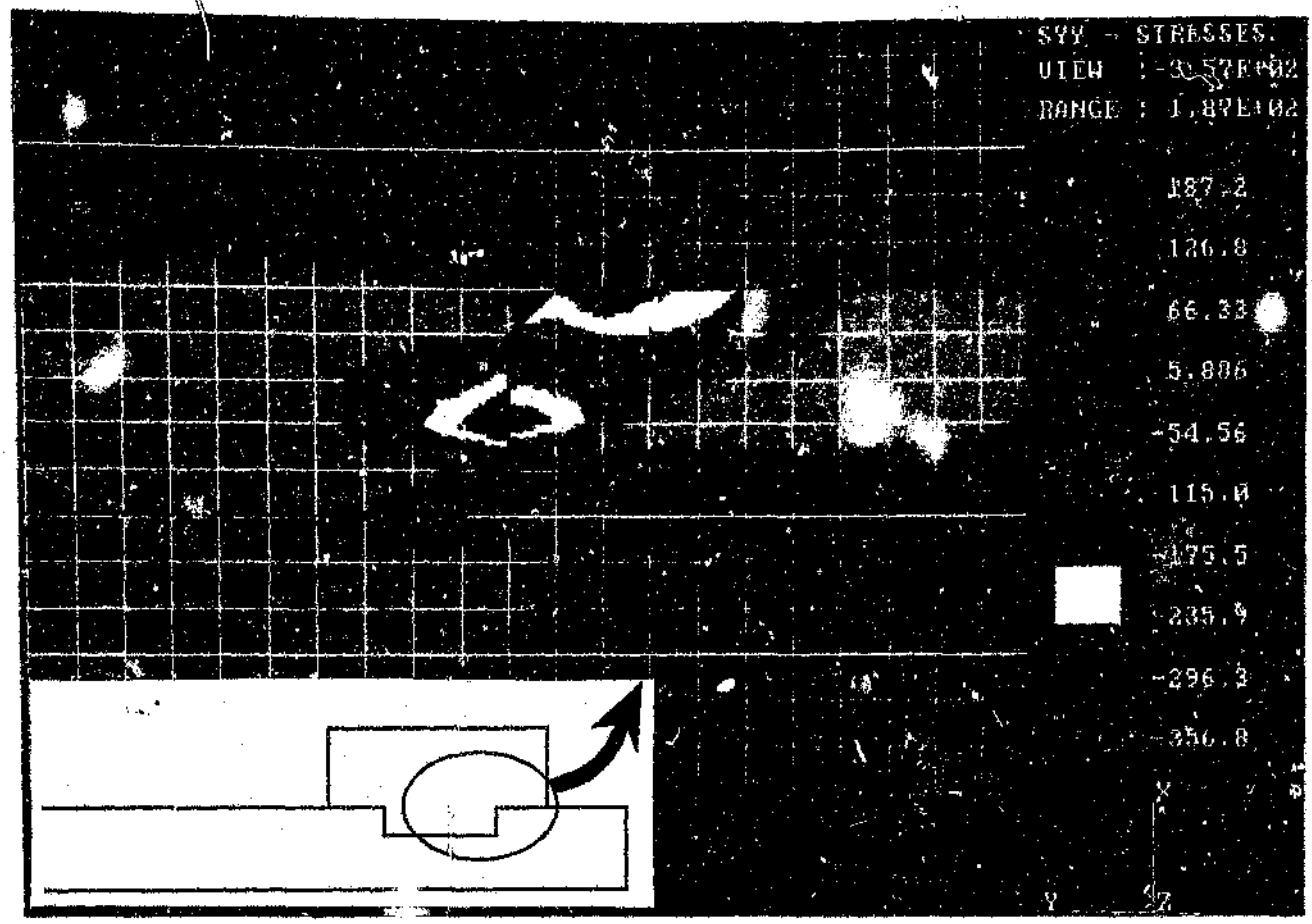

Figure 4.45 : Axial stresses in a "pressurised" GRP pipe with GRP flange.

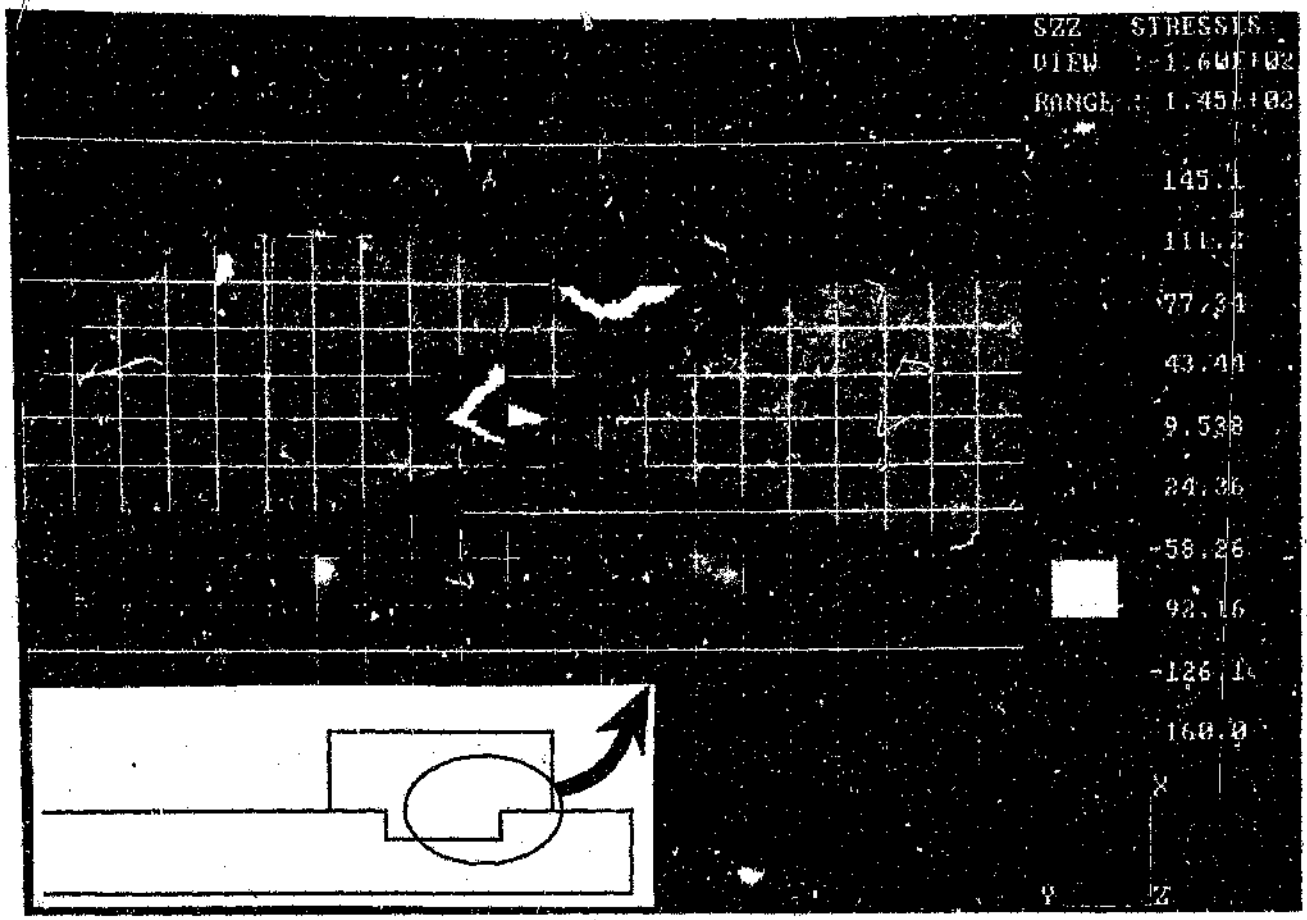

Figure 4.46 : Hoop stresses in a "pressurised" GRP pipe and GRP flange.

The internal pressure applied is 19 MPa, which causes an axial force on the flange of 65 kN (this was the ultimate load in the experiment). From these results the effect of the internal pressure on the stresses can be analysed in comparison to the tensile tests that were done on the test pipes and flanges. These results are discussed in further detail in the following chapter.

5 DISCUSSION

Couplings and joints are a necessary part of any piping installation. Without the pipe being able to be connected to any equipment it would be a worthless system. The coupling design becomes increasingly complex and critical as the operating pressures increase. The coupling cannot simply be designed on its own, since it is an integral part of the pipe and as such needs to be designed together with the pipe. This is especially true for composite pipes, since the pipe design has a large effect on the performance of the coupling.

5.1 COUPLING DEVELOPMENT

The "U"-type rubber ring used in the victaulic coupling is ideally suited to seal high pressure pipes. It does not rely on any bolts or other devices to impose the sealing pressure on it. Instead this seal relies on the hydrostatic pressure to provide the sealing pressure.

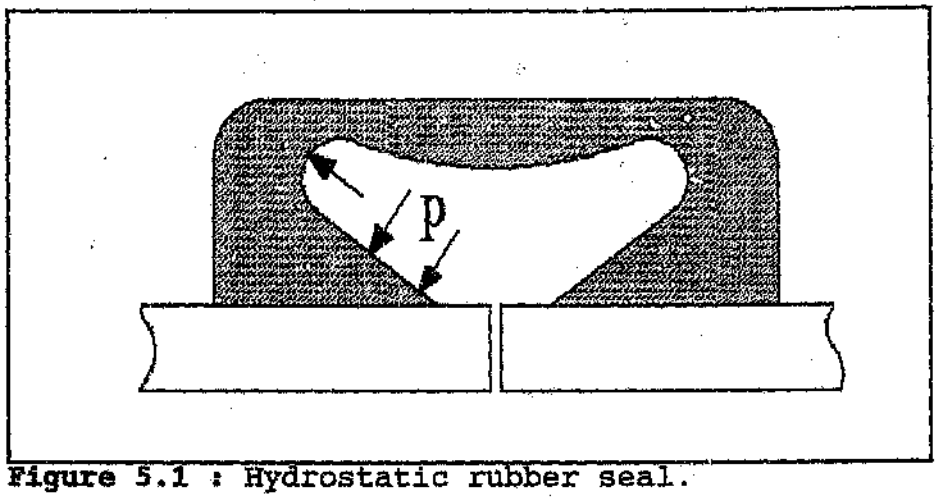

Figure 5.1 : Hydrostatic rubber seal.

As the internal water pressure increases, so the pressure on the lips of the rubber ring increases and hence the sealing pressure is increased. The proposed coupling will use the hydrostatic seal for the sealing function.

The axial force must be transferred somehow from one pipe to the adjacent pipe. This occurs through the coupling, which is built up on the outside of the pipe. Hence the load path is deflected outward from the pipe to the coupling and inward to the next pipe again, as shown in figure 5.2.

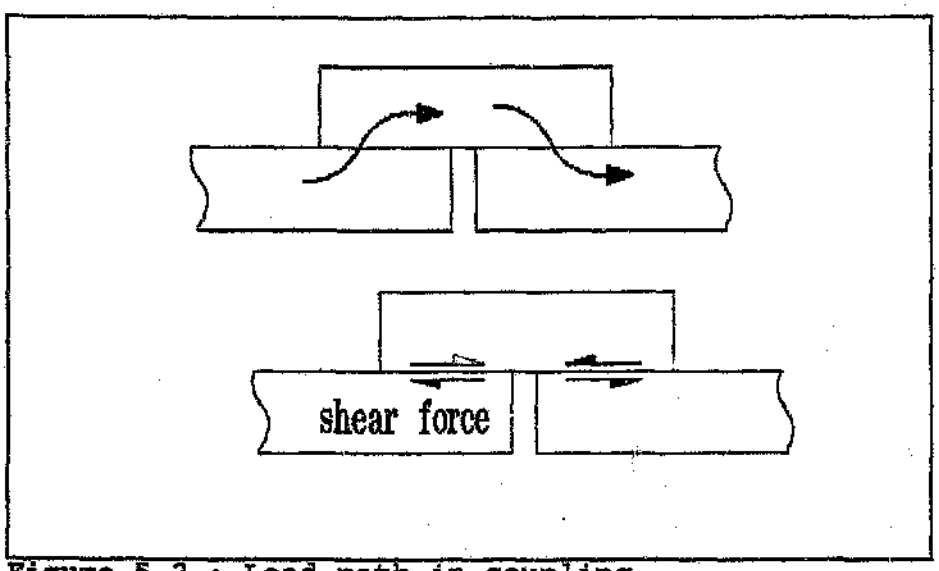

Figure 5.2 : Load path in coupling.

Thus there is essentially a shear load on the pipe and the coupling. This sets up a bending moment in the whole system, as shown in figure 5.3.

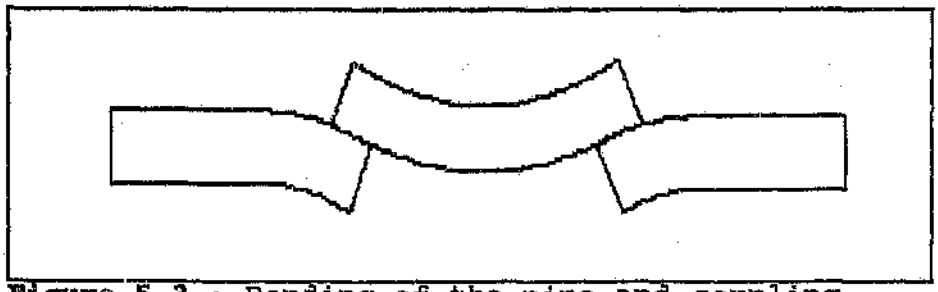

Figure 5.3 : Bending of the pipe and coupling.

Section 2.2.2 described a situation where a flange is either wound directly onto the pipe or a serrated metal ring is pushed onto the pipe and adhesively bonded to the pipe. In both cases there is a distinct interfac ~ between the coupling (flange or serrated ring) and the pipe. A shear force occurs at the interface due to the load being transferred from the coupling to the pipe.

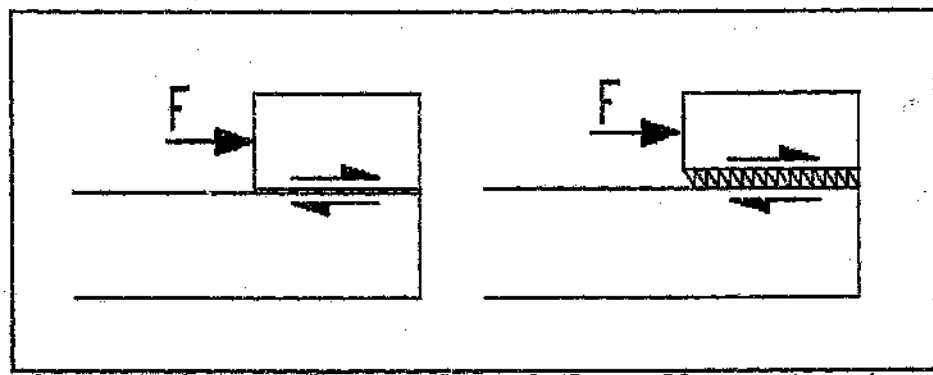

Figure 5.4 : Load transferral from flange to pipe.

A shear stress is set up in the adhesive film between the pipe and the coupling. The load bearing capacity of the coupling thus depends on the strength of the adhesive (assuming that the interlaminar shear strength is higher than the adhesive shear strength).

The quick-connect coupling described in chapter 2 uses a different method to transfer the load from the coupling to the pipe. It utilises a key (steel cable or polypropylene) as the shear member. This concept is illustrated in the figure 5.5.

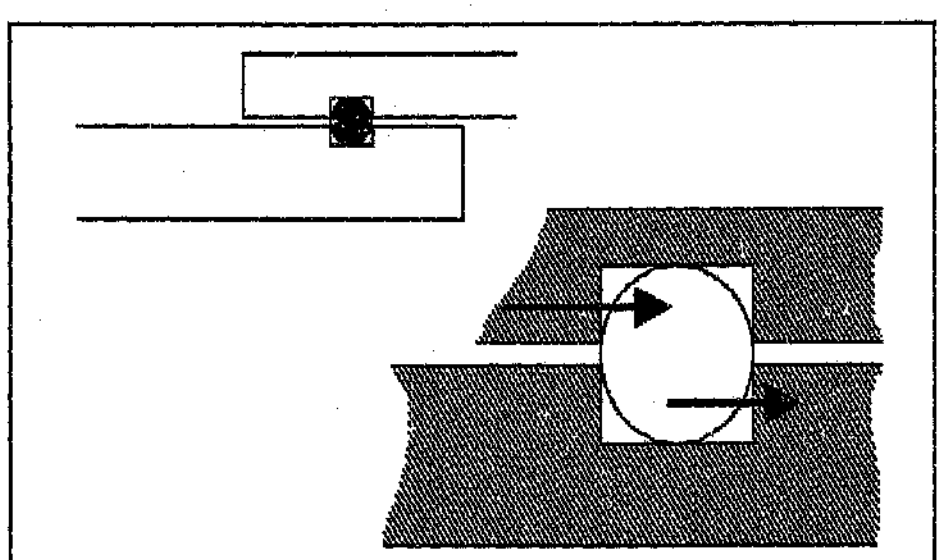

Figure 5.5 : Load transferal method of quick-connect coupling.

As the load increases a shear stress is set up in the key (as well as the coupling and the pipe). The load bearing capacity of this coupling depends to a large extent on the strength of the key. However if a steel key is used, then the stiffness of the key is much higher than the stiffness of the pipe and the coupling; hence failure of one or both of these components may occur.

The coupling uses a combination of two methods of load transferral:
(i) part of the load is transferred through adhesive shear stresses from the flange to the pipe.
(ii) part of the load is transferred mechanically from the flange to the pipe.
The first flange tested had the cross-section shown in figure 5.6 below.

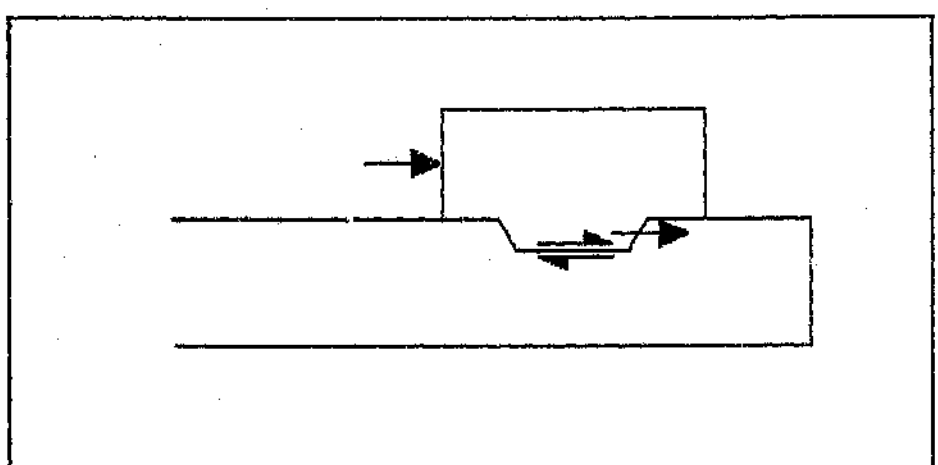

Figure 5.6 : Cross-section of first test flange.

The flange was manufactured by wrapping successive layers of resin impregnated chopped strand mat around a fibreglass pipe which had the step shown above machined into it. Shear stresses exist in the adhesive along the entire contact surface. A "key" effect is achieved by having the step machined into the pipe.

The aim of the tapered step was to minimise the stress concentrations in the corners. Figure 5.7 illustrates the relationship between the two force components and the angle of the step.

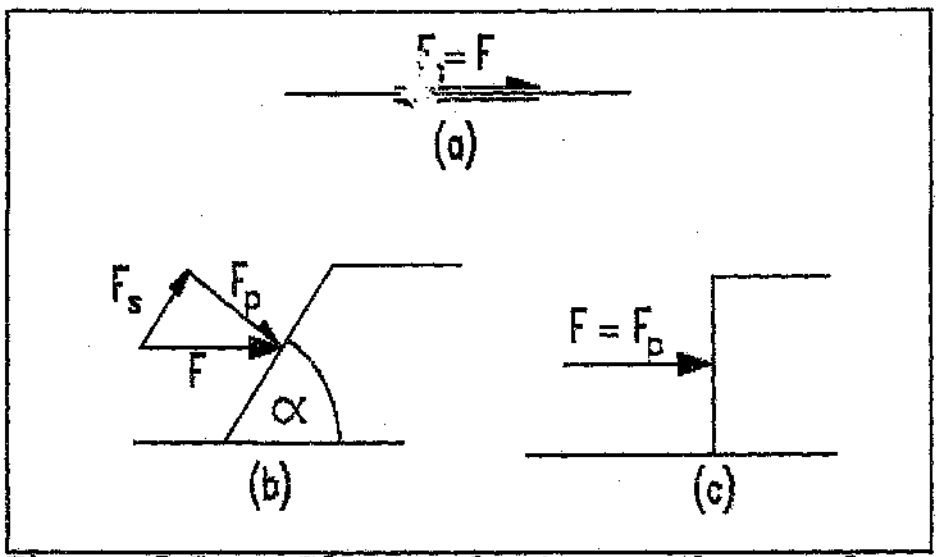

Figure 5.7 : Effect of step angle on force components.

The problem encountered with this geometry, which was also the cause of failure of the flange, was that the force along the surface of the step (F_s) caused excessively high hoop stresses in the flange. These hoop stresses caused the flange to expand and eventually slide over the pipe. The results in section 4.2.1 indicate that this flange (TYPE II, figure 4.12) could sustain a maximum pressure of 9 MPa when used on a pipe with an internal diameter of 50 mm.

One method of increasing the load bearing capacity of this flange is to use a different type of glass reinforcement, eg. unidirectional fibres wound in the hoop direction. This would strengthen the flange in the hoop direction and would minimise its expansion, thus making it more difficult for the flange to

slide over the pipe. It was however felt that the geometry of the pipe/flange interface needed to be changed significantly in order to achieve much higher load bearing capacities.

The two other extremes are a flat pipe with no step at all, in which case the entire load is transferred from the flange to the pipe via adhesive shear stresses, and a step with a right angle, in which case there is a mechanical interaction between the pipe and the flange (see figure 5.7). Both these cases were examined experimentally.

The results show that the combination without the step (TYPE I flange, figure 4.10) is even weaker than the pipe with the tapered step. So although there are no stress concentrations which can damage the pipe or the flange, this combination is very weak because the adhesive is not strong enough. The type of failure that occurs with an adhesive joint is a catastrophic failure. A coupling of this type would show no signs of weakening at all. There would be no water leaks to indicate the onset of failure.

The results for the pipe with a right-angled step (TYPE III flange, figure 4.14) show a significant increase in load bearing capacity. This pipe/flange combination failed at an equivalent internal pressure of 16.5 MPa. The flange was manufactured by winding resin impregnated chopped strand mat directly onto the pipe, as shown in figure 4.14. The reason for this lay-up was that it is probably more difficult to shear "through" a layer of glass reinforcement than to shear this layer off another layer (ie. interlaminar shear). The mode of failure was not by shearing "through" the layer of glass reinforcement, as expected. A different problem arose during the manufacturing phase (see figure 5.8).

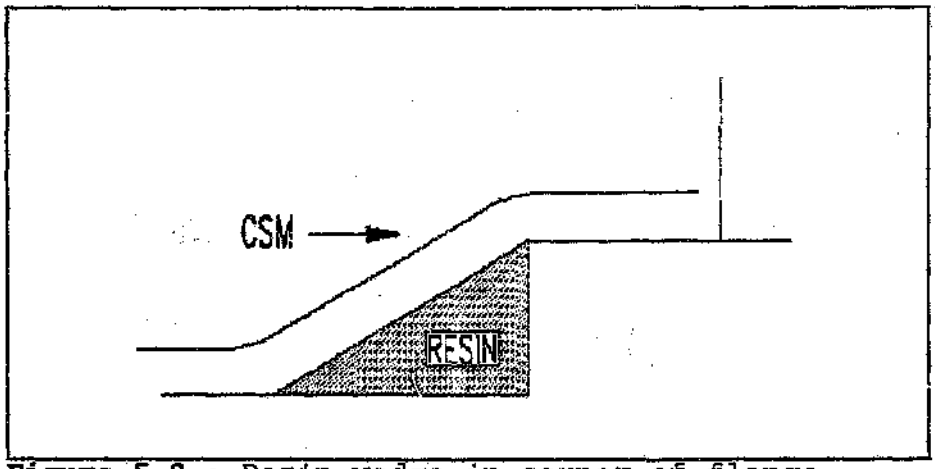

Figure 5.8 : Resin wedge in corner of flange.

Since it is very difficult to lay a coarse chopped strand mat into such a small corner (step depth is only 2 mm), the entire corner was filled with resin only. This resin wedge sheared off the flange, which resulted in a geometry similar to that shown in figure 4.12 (TYPE II flange). This tapered step once again caused excessively high hoop stresses which resulted in the flange expanding and eventually slipping over the pipe.



Figure 5.9 : Photograph of flange expanding and slipping over step.

The next improvement was obviously to get rid of the resin wedge so that premature failure would not occur. The lay-up used for this flange was basically the same as for the previous flange. However, glass rovings were tightly wound into the corners (as shown in figure 4.16, TYPE IV flange) to prevent a resin wedge from forming here. The result was an increase in the load carrying capacity from 56 kN (TYPE III flange) to 65 kN (TYPE IV flange). This flange failed by crushing of the fibres at the face of the step. The fibres at the step (in the flange) were all oriented transversely to the direction of load application and hence were very weak in compression, which is the reason for their failure.

To increase the performance of the flange, the compressive strength of the flange in the axial direction was improved. Since the glass fibres are much stronger in compression along their axis than transverse to their axis they need to be oriented along the axis of the pipe (in the step region) in order to increase the strength of the flange. Figure 4.18 (TYPE V flange) shows how the unidirectional fibres are laid up in the flange to transfer the load to the pipe. Two such tests were performed and in both cases an increase in load bearing capacity was achieved. However, in both cases a new failure mode occurred, and in both cases the pipe failed (interlaminar shear and compression), not the flange.

In the first case (TYPE V flange, test a) the fibres at the face of the step (in the pipe) failed in compression.

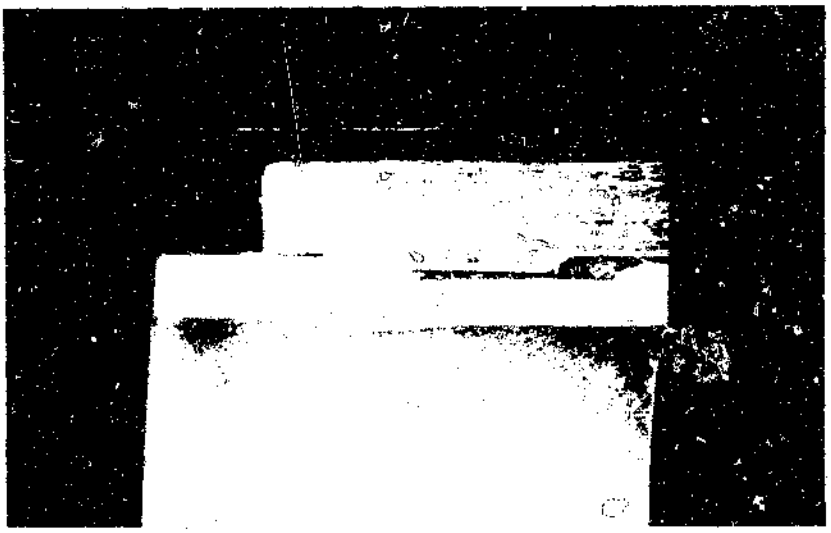

Figure 5.10 : Photograph showing compressive failure of the pipe (step region).

Clearly now the compressive strength of the flange (in the step area) was higher than the compressive strength of the pipe. There is a simple explanation for this. The fibres in the flange were axially oriented (which is also the direction of load application) whereas the fibres in the pipe were oriented at an angle of ±55° to the axis of the pipe, hence these fibres are more transversely loaded than axially. Since the aim was not to optimise the pipe properties, but to keep the pipe as simple as possible with one fibre orientation only (±55°), the geometry and location of the step are the only variables that were altered.

In the second case (TYPE V flange, test b) the pipe failed by interlaminar shear, as shown in the figure 5.11 overleaf.



Figure 5.11 : Photograph showing interlaminar shear failure of the pipe.

Failure here occurred at a slightly higher load than in the first case. This would indicate that the step in the second case was possibly slightly deeper than in the first case, thus decreasing the compressive stress at the face of the step. Otherwise the mode of failure should again have been compression of the fibres. Another useful result of this test is the average interlaminar shear strength of the pipe which is calculated as follows:

$$\tau = \frac{F}{A} = \frac{F}{\pi * d * l} = \frac{72,000}{\pi * 62 * 35} = 10.5\,MPa$$

The previous two tests show clearly that a small change in geometry, for example a marginally deepened step, can have a different failure mode as a result.

After the load has been applied to the coupling, the flange would have been compressed, and in the extreme case would have moved forward relative to the pipe, as illustrated, in the figure 5.12 overleaf.

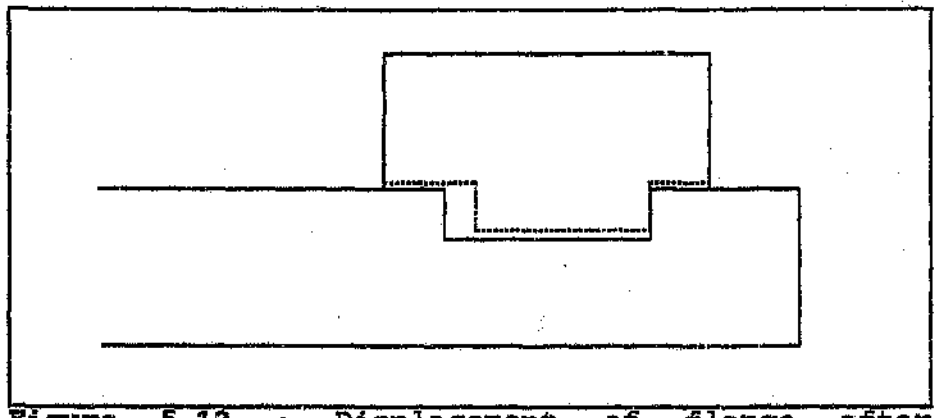

Figure 5.12 : Displacement of flange after compression.

After loading a small gap exists at the rear edge of the step. This indicates clearly that the rear step serves no purpose at all. It also shows that in the extreme case the adhesive may have failed already, but the load can still be carried by the step. The step geometry was changed, as shown in the figure 5.13 below.

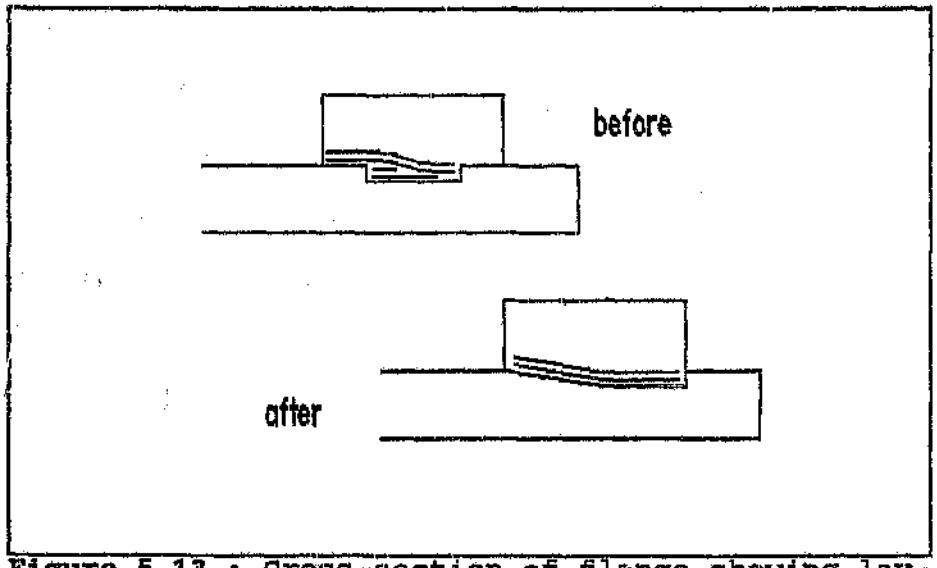

Figure 5.13 : Cross-section of flange showing lay-up.

This geometry is simpler to manufacture and allows the load to follow the path of the fibres more easily since there are no

sharp corners. The load is thus successfully transferred from the coupling to inside the pipe. Because the load is now applied much closer to the centre of the pipe, the bending moment caused by the flange is also reduced. The tapered area of the step represents a tubular scarf joint which is more efficient than a straight tubular joint. For this test the step was machined further back from the end of the pipe. The purpose of this was to increase the interlaminar shear area in the pipe. If the interlaminar shear mode of failure could be induced in the pipe, then it would be easy to predic the coupling performance. Fairly high load bearing capacities should be achieved if this mode of failure is induced.

The new dimensions are shown in figure 4.21 (TYPE VI flange). Evidently the shear area was increased too much and once again the pipe failed by compression of the fibres in the step area. The failed pipe is shown in the figure below.

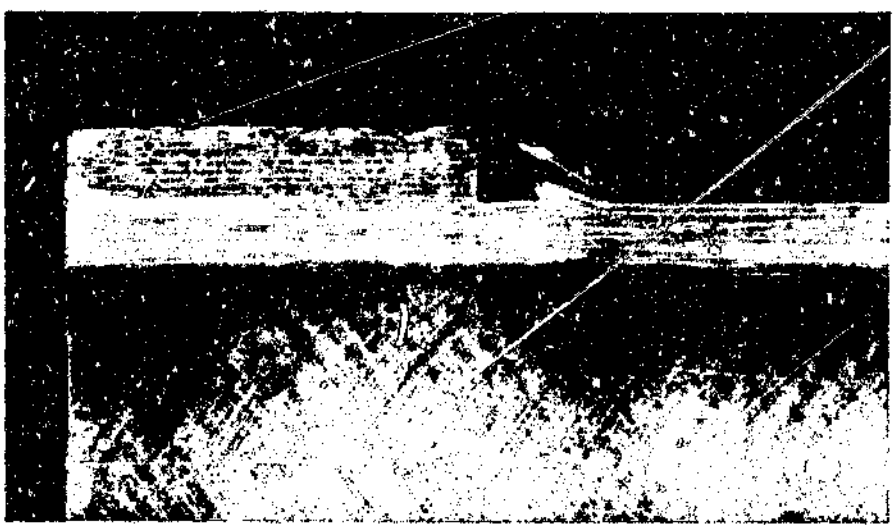

Figure 5.14 : Photograph showing compressive failure of the pipe (new flange cross-section).

Another observation (which can be seen as a lightly coloured patch on the photo) is the delamination on the inside of the pipe. This has probably come about due to the high bending

moment cause by the flange. It indicates another weak area in the pipe and could possibly cause another mode of failure, viz. buckling of the pipe.

The shear area had obviously been increased too much in the previous test, and it was decided to decrease this again. In addition to this the step depth was increased, thus decreasing the compressive stress on the face of the step due to the larger cross-sectional area. The reason for this alteration was that the compressive failures had consistently occurred at lower loads than the interlaminar shear failures. Hence it was desirable to induce an interlaminar shear failure in the pipe.

The new dimensions are shown in figure 4.23 (TYPE VII flange). The fibres wound in the hoop direction (circles on the diagram) prevent the flange from expanding at the back. As can be seen from the results, failure occurred at a load of 70 kN, which is equivalent to the force produced by an internal pressure of 20.6 MPa (for a pipe outside diameter of 66 mm). This is very close to the previous result where the pipe failed by interlaminar shear. However neither of the previous two failure modes occurred here. In this case the pipe failed by buckling. The buckling occurred on the inside of the pipe, and is visible as a lightly coloured delaminated patch on the photograph in figure 5.15.

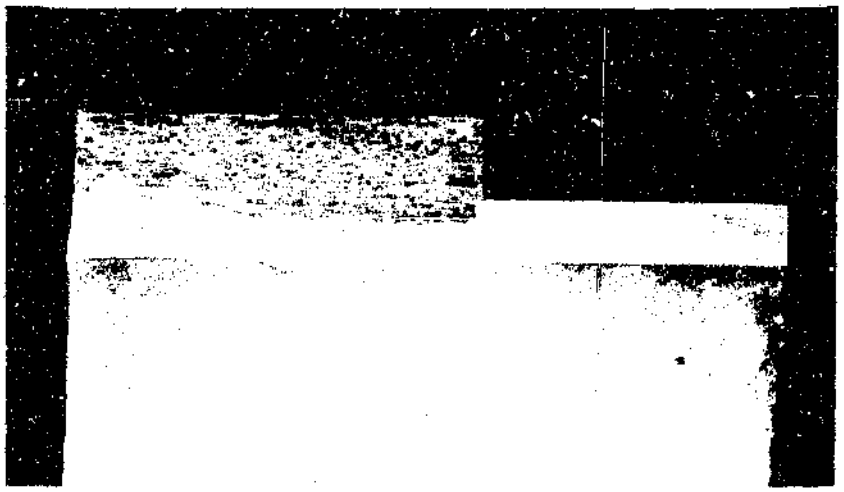

Figure 5.15 : Photograph showing a buckling failure of the pipe (lightly coloured patch on the inside of the pipe).

This type of failure can come about due to very high bending moments set up in the pipe by the flange. If the pipe wall is thin or if the flange is very large (and hence the load is applied far from the centre of the pipe), this bending moment can easily cause failure in the pipe.

To further increase the strength of the coupling the pipe was strengthened in the hoop direction to prevent buckling (TYPE VIII flange, figure 4.25). For this purpose a 3 mm deep step (rather than a 2 mm deep step) was machined into the pipe, as in the previous test. The unidirectional fibre reinforcement was wound perpendicular to the axis of the pipe to a thickness of approximately 0.5 mm. The remaining construction of the flange was virtually identical to the previous flange. The results showed a slight increase in the load bearing capacity to 75 kN, which is equivalent to an internal pressure of 22.0 MPa. This was the highest load obtained for a GRP pipe/GRP flange combination. The mode of failure here was buckling of the fibres on the inside of the pipe.

Five other tests were performed for comparative purposes. These

tests involved both GRP pipes with a mild steel flange attached to them and steel pipes with a GRP flange attached to them. The first of these pipes had a simple rectangular step machined into it (figure 4.27, TYPE IX flange).

The dimensions of this step are the same as in the TYPE III flange. The flange was machined from mild steel and was in the form of a split ring. The two halves of the flange were fitted over the pipe and held together by means of a hose clamp. The pipe in this test failed by interlaminar shear and the load obtained (75 kN) was 4% higher than the load obtained for the equivalent test using a GRP flange. This difference is most probably due to a slight difference in the size of the steps (inaccuracy in the machining process).

In the second of these tests the mild steel flange was adhesively bonded to the pipe using a scarf joint (figure 4.29, TYPE X flange). A taper of 6° was machined into the pipe, with the steel flange having a matching taper. This contact area forms the scarf joint.



Figure 5.16 : Photograph showing the tapered section which makes up the scarf joint.

The strength of this joint is derived solely from the strength of the adhesive. The scarf joint is inherently a very strong and efficient joint, as described in section 3.3. This can be seen from the very high load that was obtained (82 kN). An important feature of the mode of failure of this coupling is that it is a catastrophic failure, ie. the load carrying capacity instantaneously drops to zero when the adhesive fails. There are no warnings that indicate the onset of failure.

The next geometry tested (TYPE XI, figure 4.31) is virtually identical to the previous one, with the exception of an additional strap joint (tubular lap joint) on the outside. This joint is made by simply wrapping successive layers of resin-impregnated glass reinforcement around the outside of the pipe and flange. This effectively increases the area over which bonding takes place. Two tests were performed with this geometry, and two completely different results were obtained. In the one test the highest load (93 kN) of all the tests was obtained. This load is equivalent to the load caused by an internal pressure of 27.4 MPa. In the second test one of the lowest loads (50 kN) was obtained. The cause of this was perhaps

that the adhesive joint was not properly prepared (it was either dirty, or the tapered surfaces did not match properly). These two results indicate that this type of joint is very unreliable. Extreme care has to be taken to prepare the joint properly, and even then one cannot guarantee a strong joint.

In the last two tests a steel pipe was used, which had the step machined into it. In one case the flange was made from chopped strand mat (TYPE XII, figure 4.34) which was laid up directly onto the pipe. The highest load of all tests was obtained here, viz. 105 kN, which is equivalent to an internal pressure of 31 MPa. Due to the high stiffness of steel compared to GRP, the stress concentration at the step occurs in the pipe and not in the flange, as can be seen in the finite element model in figure 4.43. The flange, which had the fibres axially aligned at the step, failed due to compression of the fibres at the step. The steel pipe is also able to resist the bending moment imposed on it by the flange and hence the buckling failure dos not occur. The effect of a high strength, high stiffness material in the pipe/flange assembly can be seen here, viz. an increase in the load bearing capacity.

In the last case (TYPE XIII flange, figure 4.36) the flange was made from a bulk moulding compound (BMC) with short fibres (6 mm length) oriented in all directions. However due to the low glass content (approximately 20% by mass, compared to 35% for the chopped strand mat flange) the load bearing capacity was accordingly lower at 75 kN, which is equivalent to an internal pressure of 22 MPa.

The remainder of the coupling is as described in chapter 2. A cylindrical split ring clamps around the flanges on adjacent pipes. The hydrostatic rubber seal is located between the pipe surface, the edge of the flange and the inside of the split ring (see figure 5.17).

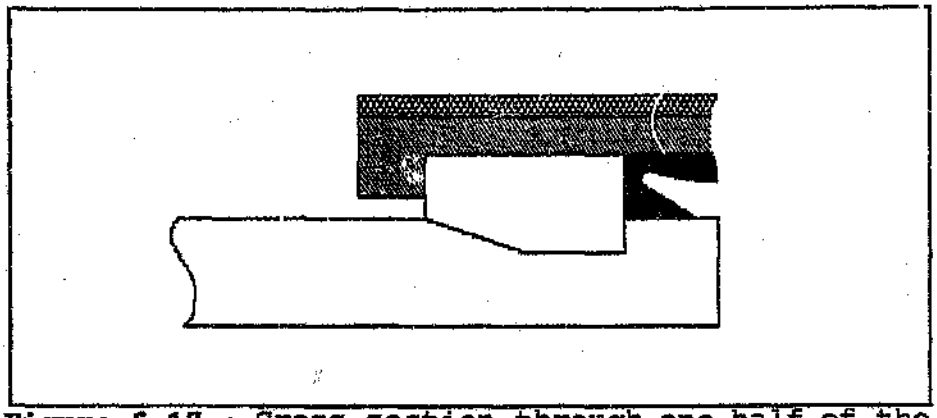

Figure 5.17 : Cross-section through one half of the GRP coupling.

The two halves of the split ring are held together by a thin GRP sleeve.

The critical area of the coupling is the connection of the flange to the pipe, ie. the interface between the flange and the pipe, because the load is transferred across this interface. The size of the split ring and the external sleeve can easily be increased to accommodate an increase in the load, whereas there are geometrical limitations on the interface, eg. the depth of the step cannot be increased indefinitely to decrease the compressive stress.

5.2 FACTORS AFFECTING THE COUPLING PERFORMANCE

There are evidently three different modes of failure of the pipe:

- compressive failure of the fibres on the face of the step.
- interlaminar shear failure where a thin cylinder (thickness of the step) shears off the pipe.
- buckling failure on the inside of the pipe.

These three modes of failure are closely related to the depth *t* of the step and its distance *l* from the end of the pipe (see figure 5.18 below).

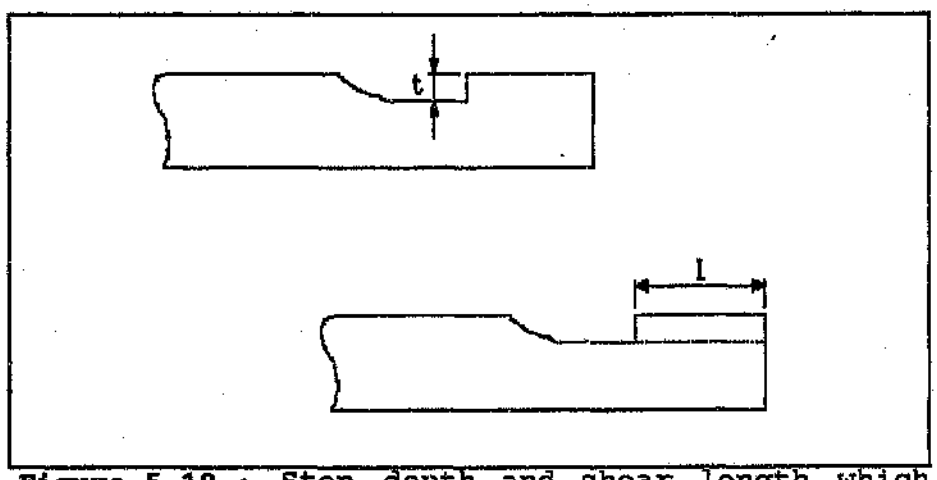

Figure 5.18 : Step depth and shear length which affect coupling performance.

In general, an increase in the depth of the step *t* decreases the possibility of the fibres failing in compression, since the cross-sectional area of the step increases and consequently the compressive stress decreases. As the distance *l* of the step from the end of the pipe decreases, so the interlaminar shear area decreases and the possibility of an interlaminar shear failure increases. These tendencies occur if the pipe is the component that fails, not the flange. This is ususlly the case, because the flange can be made much stronger in compression than the pipe, since the pipe's fibres are oriented at an angle to the direction of load application (hence the compressive strength is much lower).

The buckling failure depends on various variables. If the flange is excessively thick, ie. if the load is applied too far away from the centre of the pipe, then a very high bending moment is set up in the pipe and a buckling failure may result. Also, if the step is very deep, then the pipe strength is reduced considerably and a buckling failure may result. Hence there is obviously a limit to the depth of the step. Naturally, if the step is very close to the end of the pipe, then the pipe may still fail due to interlaminar shear, even if the step is very deep.

The three modes of failure can be shown in terms of the step depth *t* and step length *l* in the form of a failure mechanism map.

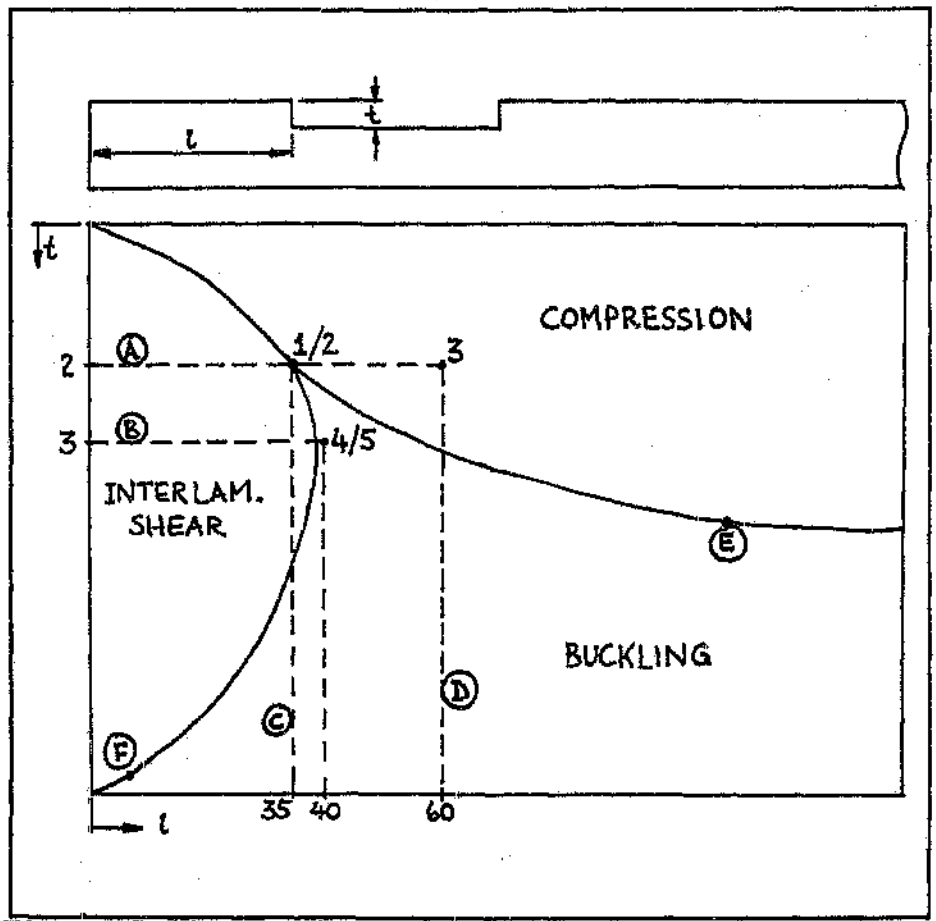

Figure 5.19 : Failure mechanism map of the GRP pipe and coupling.

Three different regions are shown in the figure. These regions represent the different modes of failure that can occur in the pipe:

- compressive failure of the fibres on the face of the step. This failure mode results in a slow decrease in the load bearing capacity, and will show signs of failure by weeping or leakage. If failure should occur, then this is a desirable mode of failure, since there are warning signs and the necessary precautions can be taken.
- interlaminar shear failure of the pipe. This is a catastrophic failure since the load bearing capacity drops to zero instantaneously; hence this mode of failure is not desirable.
- buckling failure on the inside surface of the pipe. This is also a gradual mode of failure, since the load bearing capacity decreases slowly. Warning signs (such as weeping) of an impending failure may be visible; hence this is also a desirable mode of failure.

It appears as if the highest loads are obtained if all three failure modes are just about to occur. In this instance the optimum relationship between step depth, pipe wall thickness and the distance between the step and the end of the pipe is achieved. Only a slight increase in the step depth would cause the pipe to fail due to buckling, or, by moving the step closer to the end of the pipe an interlaminar shear failure would be induced.

Line 'A' represents a case of constant step depth t where shear failure will occur if the shear length l is not too large. With an increase in shear length, the tendency is towards a compressive failure (compare types V(b) and VI in section 4.2.1).

Line 'B' is a case where the step depth is fairly deep. The initial mode of failure here is also interlaminar shear. However as the shear length is increased the tendency is towards a buckling failure.

Lines 'C' and 'D' both represent cases where the shear length is kept constant. The initial mode of failure for a very shallow step is compression of the fibres on the face of the step (for both case 'C' and 'D'). As the step depth is increased, the mode of failure changes to either an interlaminar shear failure (as in case 'C' where the shear length is fairly short) or to a buckling failure (as in case 'D' where the shear length is fairly long).

Points '1' and '2' on the above figure represent a case of the TYPE V flange (shown in figure 4.18). Two tests with this flange were done and in both cases a different failure mode resulted. In one case failure was due to compression of the fibres at the face of the step, in the other case failure was due to interlaminar shear of the pipe. The step geometry of these pipes was virtually identical (there may have been very slight differences due to machining). This shows how in some cases two different failure modes are just about to occur, and it is hence difficult to predict the mode of failure in some cases.

Point '3' on the above figure represents a case of the TYPE VI flange (shown in figure 4.21). Clearly here the distance between the step and the end of the pipe is too large for interlaminar shear to occur, and the thickness of the pipe at the step is still great enough to resist buckling.

Points '4' and '5' on the figure above represent a case of the TYPE VII and TYPE VIII flange (shown in figures 4.23 and 4.25 respectively). In this case the step depth is deep enough (ie. the cross-sectional area of the step is large enough) to decrease the compressive stress so that this mode of failure will not occur. The pipe's thickness at the step has been decreased too much so that a buckling failure has resulted.

It is apparent from the figure that there is a "cut-off" point (marked point 'E'). At this step depth t an increase in the length l will have no further effect on the failure modes. Only

a slight variation in the step depth t will swing the failure mode from a compressive failure to a buckling failure or vice versa. Another interesting point is marked 'F' on the figure. Here the remaining pipe wall thickness is negligible. Depending on the length l either a buckling failure or a shear failure may result. The load bearing capacity of the coupling will obviously be negligible in this case.

The previous figure will change if the flange has a different thickness. An increase in flange thickness will have as a result a larger bending moment in the pipe, and hence buckling will be the primary mode of failure. A change in material properties will also affect the relationship between the three failure modes.

To achieve the highest possible load, the flange's and pipe's stiffness must be as high as possible. Since the pipe's stiffness is determined by the fibre orientation during the filament winding process (and is constant for these experiments), the flange must be made at least as stiff as the pipe. The critical area here is at the face of the step, not the entire flange.

For this reason the fibres on the inside of the flange are aligned with the pipe axis, since they have the highest stiffness in this direction. These unidirectional fibres now have the shape of a cone which has little strength in the radial and hoop directions. The purpose of the rovings wound in the hoop direction over this cone is hence to strengthen the cone in the hoop direction. The remaining part of the flange is not highly stressed and can easily be made up from chopped strand mat.

From the results it can be seen that in all cases where the above lay-up sequence was used for the flange, the strength and stiffness of the flange were high enough to prevent failure of the flange. Virtually the same loads were obtained as for the steel flange (TYPE IX). The small difference in the ultimate

a slight variation in the step depth *t* will swing the failure mode from a compressive failure to a buckling failure or vice versa. Another interesting point is marked 'F' on the figure. Here the remaining pipe wall thickness is negligible. Depending on the length *l* either a buckling failure or a shear failure may result. The load bearing capacity of the coupling will obviously be negligible in this case.

The previous figure will change if the flange has a different thickness. An increase in flange thickness will have as a result a larger bending moment in the pipe, and hence buckling will be the primary mode of failure. A change in material properties will also affect the relationship between the three failure modes.

To achieve the highest possible load, the flange's and pipe's stiffness must be as high as possible. Since the pipe's stiffness is determined by the fibre orientation during the filament winding process (and is constant for these experiments), the flange must be made at least as stiff as the pipe. The critical area here is at the face of the step, not the entire flange.

For this reason the fibres on the inside of the flange are aligned with the pipe axis, since they have the highest stiffness in this direction. These unidirectional fibres now have the shape of a cone which has little strength in the radial and hoop directions. The purpose of the rovings wound in the hoop direction over this cone is hence to strengthen the cone in the hoop direction. The remaining part of the flange is not highly stressed and can easily be made up from chopped strand mat.

From the results it can be seen that in all cases where the above lay-up sequence was used for the flange, the strength and stiffness of the flange were high enough to prevent failure of the flange. Virtually the same loads were obtained as for the steel flange (TYPE IX). The small difference in the ultimate

load can be attributed to slight inaccuracies during machining of the step.

The maximum load obtained for this type of flange on a filament wound pipe (± 55° fibre orientation) with an inside diameter of 50 mm and an outside diameter of 66 mm is 75 kN. This load is equivalent to the load caused by an internal pressure of 22 MPa. Given the present materials, there are two ways of increasing the load bearing capacity:

- decrease in flange thickness: this will cause the load to be applied closer to the centre of the pipe and will hence decrease the bending moment set up in the wall of the pipe. However the flange thickness cannot be decreased indefinitely, since the actual coupling still has to clamp around the flanges on adjacent pipes. A small flange will have a high contact stress and will in turn cause a high contact stress on the coupling.
- increase in pipe thickness: the pipe's thickness only needs to be increased at the ends where the flanges are located. An increase in the wall thickness means that the step depth can be increased without affecting the hoop strength of the pipe. Thus the buckling strength of the pipe as well as the compressive strength at the face of the step can be increased simultaneously. However an increase in wall thickness also increases the distance between the pipe axis and the line of load application. Thus an increase in wall thickness brings with it an increase in the bending moment.

The interlaminar shear failure is a catastrophic failure. The load bearing capacity of the coupling drops to zero virtually instantaneously. This type of failure is in most cases undesirable from the point off view that there are no previous indications of an impending failure, and hence no precautions can be taken. The compressive and buckling failures however are very slow failures, ie. the load bearing capacity decreases very slowly as failure of the pipe occurs. In these cases the pipe would most probably start weeping and the coupling would start

leaking before there is a drastic decrease in load bearing capacity.

As can be seen from the results the TYPE X and TYPE XI flanges obtained the highest strengths. The high strength can be attributed mainly to the high efficiency of the scarf joint, which was used to bond the flange to the pipe. This flange obviously had no problems with shear failures, since the shear strength of mild steel is an order of magnitude greater than the interlaminar shear strength of GRP. There is also no risk of the flange section buckling (at least at these small diameters). The high stiffness of steel aids the performance of the adhesive joint, since there are no large strains in the adhesive. This joint can unfortunately not be reproduced in GRP due to the anisotropic material properties and the low stiffness.

A major problem occurs if this type of joint (TYPE X and TYPE XI) is not properly prepared. This is clearly visible by the two results of the TYPE XI flange; one test yielded a load bearing capacity of 93 kN, the second test only 50 kN. Premature failure can easily come about if slightly aged adhesive is used or if the surfaces are slightly dirty. It is impossible to tell in advance if this joint is strong or not. The fact that the failure is also a catastrophic failure (as in the interlaminar shear failure) is another disadvantage of this type of coupling.

The results obtained from the experiments are only valid for this specific pipe size. Since the end thrust in a closed, pressurized pipe is proportaional to the square of the diameter ($F \propto d^2$), the stresses in the pipe would soon exceed the material's strength if the pipe diameter is increased too much. There is very little that can be done about this. To a certain extent the pipe's thickness could be increased to increase its strength. However this would most likely be very uneconomical. As was shown in the section 3.3 on adhesive stresses, the strength of a tubular adhesive joint can be increased to a certain extent by increasing the length of the joint. Thereafter

an increase in strength can only be achieved by increasing the diameter of the pipe, and this is very uneconomical. This is one of the many reasons why high pressure piping is limited to small diameters (this is also the case for steel pipes).

5.3 CORRELATION BETWEEN EXPERIMENTAL AND THEORETICAL RESULTS

The results of the finite element analysis correlate well with the experimental results. The figures 4.44 to 4.46 (GRP pipe with GRP flange) clearly show two regions where elevated stresses occur. One region is the stress concentration at the face of the step, the other area is on the inside of the pipe directly in line with the step. The two figures below superimpose the stress contours from the finite element analysis on a photograph of the pipe/flange cross-section. In the first case shown the pipe failed by compression of the fibres at the face of the step. In the second case the pipe failed by buckling on the inside surface.



Figure 5.20 : Photograph of pipe and flange superimposing the axial stress contours.



Figure 5.21 : Photograph of pipe and flange superimposing the hoop stress contours.

The stress contours imposed on the first photograph (fig 5.20) are the axial stresses in the pipe and the flange. On the second photograph (fig. 5.21) the hoop stresses are superimposed.

In figure 5.20 two stress concentrations of approximately equal magnitude are clearly visible - one in the flange and one in the pipe. The load applied on the flange in the finite element model in this case was 65 kN, which is the load at which the pipe failed experimentally (TYPE IV flange). The axial compressive stress at the face of the step ranges from approximately 40 MPa to 100 MPa (see figure 4.44). The fibres in the flange can resist this stress since they are directly in line with the applied force. However the fibres in the pipe are not aligned with the force; they are oriented at an angle of ±55° to the line of force and are hence much weaker in compression. The average compressive strength of the pipe (80% glass content by mass, 20% epoxy resin by mass) is approximately 250 MPa. Using the Classical Lamination Theory the compressive strength for such a laminate, with the fibres oriented at ±55° to the loading axis, is found to be 90 MPa. This is in the range of stresses predicted by the finite element analysis at the face of the step.

Hence the possibility of a compressive failure in the pipe is evident from figure 4.44.

Figures 5.21 and D.1 show that the hoop stresses below the step change from tensile to compressive. The buckled failure region on the inside of the pipe coincides with these stress contours. The hoop stresses are due to the bending moment set up by the flange.

The results obtained are only valid for pipes with an internal diameter of 50mm and a wall thickness of 8 mm. The equation governing the endload is

$$F = \frac{\pi}{4} \cdot d_o^2 \cdot P$$

where F is the ultimate load, P is the constant internal pressure and d_o is the outside diameter (the outside diameter is used because the seal is located on the outside of the pipe). According to this equation the endload increases with the square of the diameter.

The area A_c of the step over which the compressive force is applied is given by

$$A_c = \frac{\pi}{4} \cdot (d_o^2 - d_c^2)$$

and the interlaminar shear area given by

$$A_s = \pi \cdot d_c \cdot l$$

where d_c is the diameter measured to the bottom of the step and l is the length of the shear area. The relationship between the two diameters is

$$d_c = d_o - k$$

where k is a constant.

Thus the areas A_c and A_s can be written as

$$A_c = \frac{k\pi}{4}(2d_o - k)$$

$$A_s = \pi(d_o - k)\, l$$

Clearly the areas increase with an increase in diameter (but not with the square of the diameter as is the case with the endload).

This explains why high pressure pipes normally have small diameters. A coupling may work well on a small pipe at a high pressure, but will fail if the pipe diameter is increased too much.

5.4 PERFORMANCE PREDICTION USING THE FINITE ELEMENT METHOD

Two different flange/pipe combinations were modelled using the NISA II PC finite element software. These two combinations are shown in figure 5.22.

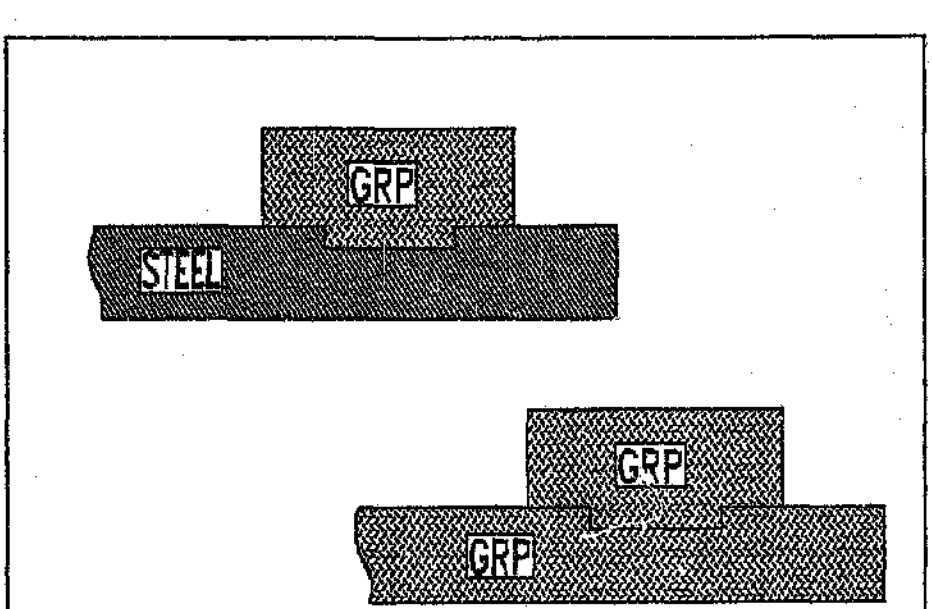

Figure 5.22 : Flange/pipe combinations modelled using NISA II PC.

By introducing the model with the steel pipe, the effect of the steel's high stiffness on the performance of the coupling can be shown clearly. This can be correlated with the experimental results.

Initially a coarse grid was used for the model. This gave an indication of the stress pattern, and any stress concentrations could then be identified. The mesh was then refined in areas where there was a stress concentration, to obtain a more accurate result and to show how localised the stress really is. The final mesh is shown in appendix C.

For all models axisymmetric solid elements were used. These elements may be used with orthotropic material properties [REF. 7], which is sufficient for the pipe and flange. The material properties used for the theoretical analysis are listed in the table below. They were obtained from previous tests done on these materials [REF. 8].

Table 5.1 : Material properties used in FE analysis

	Filament wound pipe (±55°)	Hand laid-up flange	Steel pipe
Ex [GPa]	6.5	6.6	200
Ey [GPa]	10.8	10.0	---
Ez [GPa]	17.8	10.0	---
Gxy [GPa]	4.0	3.8	---
Gyz [GPa]	9.4	4.0	---
Gxz [Gpa]	6.6	3.8	---
v	0.35	0.32	0.3

These material properties apply for a chopped strand mat flange and a filament wound pipe with a fibre angle ± 55° to the axis of the pipe. The axis-system (as reqquired by the finite element software) is as follows:

- x-axis is through-thickness
- y-axis is along the axis of the pipe
- z-axis is along the circumference of the pipe.

For simplicity these properties are assumed to be constant throughout the pipe and the flange.

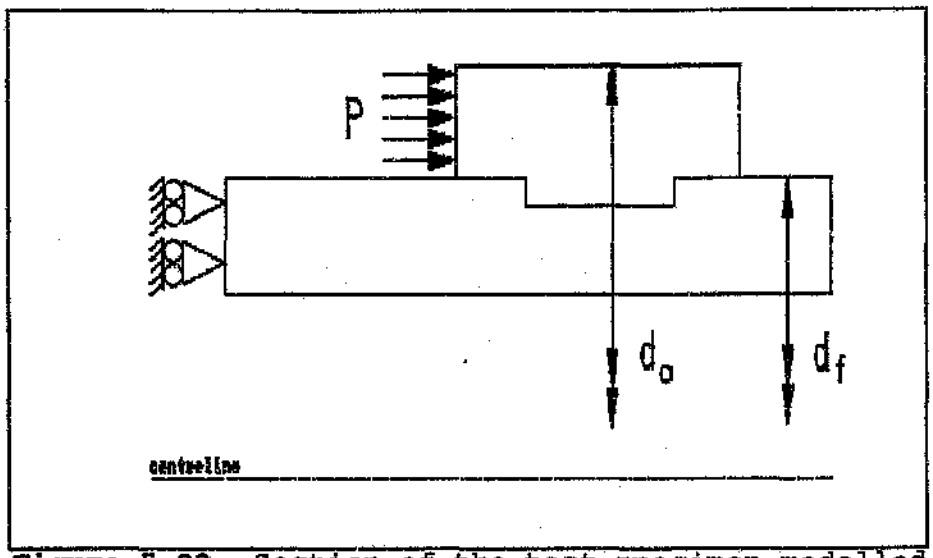

Figure 5.23 : Section of the test specimen modelled using the finite element technique.

The test specimen, as well as being axi-symmetric, has another axis of symmetry at the middle of the pipe; hence only one half of the pipe needs to be modelled. The model is constrained in the axial direction on one side. It is however free to contract or expand in the radial direction. The load is applied as a pressure P on the face of the flange. This simulates the experiment where the tensile force is applied in the form of a distributed load over the face of the flange by the split backing rings. The pressure P is related to the internal pressure P_i as follows:

$$P = P_i \cdot \frac{A_i}{A}$$

where A_i is the cross-sectional area of the pipe (this is the cross-sectional area up to the outside of the pipe) and A is the cross-sectional area of the flange.

To model the experiment as accurately as possible, the finite element model must essentially consist of two separate parts: the flange and the pipe. Initially the flange and the pipe are adhesively bonded together. As the load is applied, a certain

deformation takes place in the flange as this gets compressed against the step in the pipe.

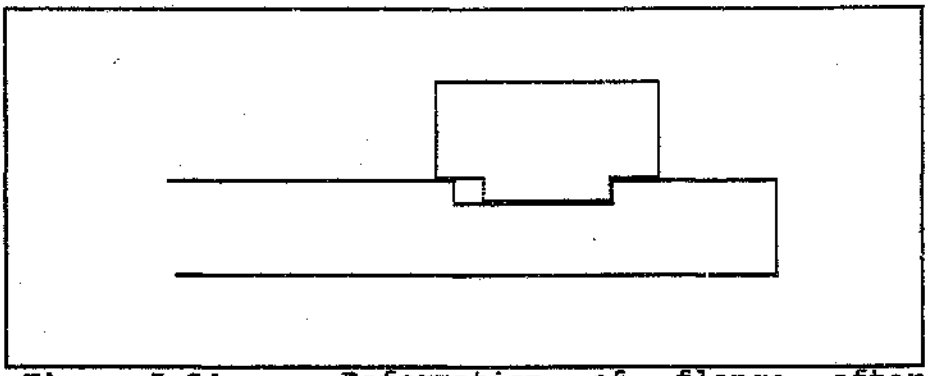

Figure 5.24 : Deformation of flange after compression.

In the extreme case the adhesive fails entirely and there is only the mechanical interference at the step. The model catered for this case in that it allowed the flange to move freely in the axial direction, except at the step. This is shown in figure 5.24 above. The flange is also allowed to expand in the radial direction.

The element meshes used for the finite element models are shown in appendix C. As mentioned earlier a refined mesh is used in the region of the step to cater for very localised stress concentrations. A further refinement in the GRP pipe/GRP flange model is the use of triangular elements at the front of the step. These elements help to model the small radius in a sharp corner due to the machining process. The force used in the each of these theoretical analyses is equivalent to the ultimate load obtained in the relevant experiments. The results obtained from these analyses were already discussed briefly in the previous chapter. The stresses predicted in the relevant failure regions (these regions were visible on the test specimens) correspond fairly well to the material failure stresses.

Model of GRP pipe with GRP flange

The compressive strength of a GRP laminate with the fibres oriented at ±55° to the loading axis was found to be approximately 90 MPa (using the Classical Lamination Theory). This is in the region of the compressive stresses predicted by the theoretical analysis at the front of the step.

The shear stress in the GRP pipe (figure D.2 in appendix D) is very high and localised in the corner at the bottom of the step. This is an area where a crack can be initiated. The crack will however not grow perpendicular to the stress contours, as it would in an isotropic material. Since a laminate is a layered material with a distinct interface between each layer, the crack will tend to grow along one of these interfaces. This mode of failure is referred to as interlaminar shear. The interlaminar shear strength of the filament wound pipes used in the experiments was found to be approximately 10.5 MPa. This value is close to the average shear stress (in the region of 7 MPa) in the end of the pipe as obtained from the theoretical analysis (see figure D.2).

In figure D.1 the increase in the hoop stress at the front of the flange can clearly be seen. This increase is due to the bending moment caused in the pipe by the flange. In figure 4.44 (axial stresses) there is an indication of an increase in compressive stresses on the inside of the pipe directly below the step, and also slightly infront of the step. These stress contours coincide with the failure regions of the buckled pipe. Although the particular pipe/flange combination that was modelled here did not fail by buckling, this failure mode was nevertheless imminent, as can be seen by the lightly-coloured delaminated patch on the inside of the pipe in figure 5.14.

The close correlation of the theoretical and experimental results shows that the finite element technique can be used as a tool to predict failure in fibreglass pipes.

Model of steel pipe and GRP flange

The same mesh was used for the steel pipe/GRP flange combination. The axial stresses are shown in figure 4.43. There is a very localised stress concentration on the surface of the pipe at the step. The stress concentration that was present in the flange in the previous model (GRP pipe/GRP flange) has virtually completely disappeared. This is due to the high stiffness of the steel pipe (the stiffness of steel is one order of magnitude higher than the stiffness of GRP). Since the steel has such a high stiffness and also a high shear strength, it will not fail easily due to buckling, compression or shearing. The fact that the stress concentration has been transferred almost entirely to the steel means that the load bearing capacity can be increased. The experiment yielded an ultimate load of 105 kN, which is considerably higher (60%) than the equivalent test using a GRP pipe.

Model of GRP pipe with double GRP flange

Figure 4.40 shows a double flange arrangement. This analysis was done to establish the effect of two flanges on the load bearing capacity.

A very coarse mesh was used. The material properties in this case were taken as simply isotropic, which is acceptable for a first estimate. The axial stresses are shown in figure 4.41. Here it is clearly visible that the entire stress concentration occurs at the back step. The front step serves no purpose whatsoever, since by this stage virtually the entire force has been transferred to the pipe already. The conclusion of this analysis is that nothing is gained by using two steps. The only thing that happens practically is that the size of the coupling is increased.

Th nite element technique seems tc work well for some cases and it has been validated for this purpose as being a useful and reliable tool to predict stresses, it can possibly be used to model those pipe/flange configurations that are too involved to test experimentally. In particular, the finite element model can easily be used to simulate pressure loads that would occur in practice, whereas experimental hydrostatic pressure testing at such high pressures is fairly involved.

To be able to compare the pressurised model to the un-pressurised model, the axial load on the interface between the flange and the pipe is kept constant, ie. 65 kN. The constraints on this model were changed considerably. Instead of the end of the pipe being axially constrained, the one side of the flange is now constrained, as shown in figure 5.25.

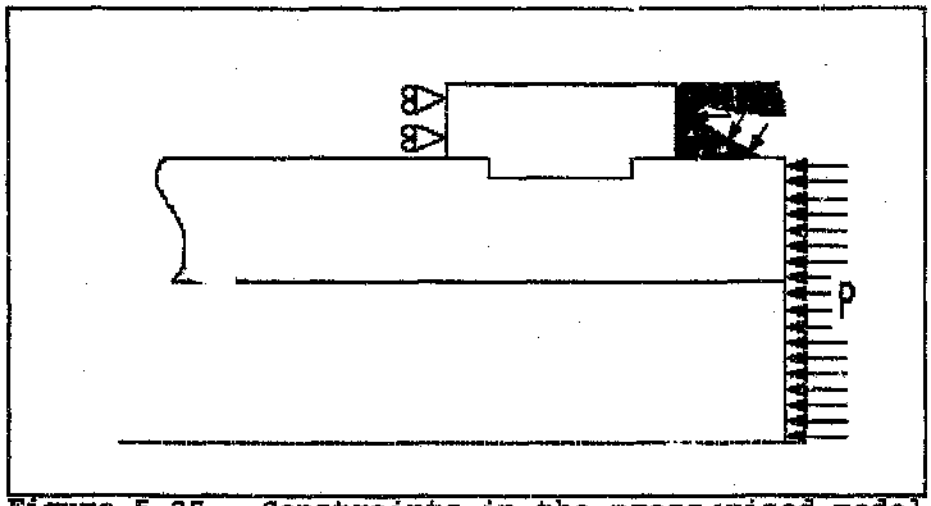

Figure 5.25 : Constraints in the pressurised model

Figure 5.25 shows that the internal pressure acts over the entire cross-sectional area, as well as inside th- "U"-seal which is located on the outside of the pipe. Clearl, t : pressure inside the seal has no effect on the axial endload (and hence on the axial force on the interface) since it is acting directly through the flange onto the constraints. Hence the pressure acting over the cross-sectional area of the pipe only must cause the required

endload of 65 kN. The required pressure P is thus calculated as follows:

$$P = \frac{F}{A_o}$$

where F is the endload and A_o is the cross-sectional area to the outside of the pipe. Using this equation the required pressure is found to be 19 MPa. Figure 5.26 shows how this pressure is applied on the model.

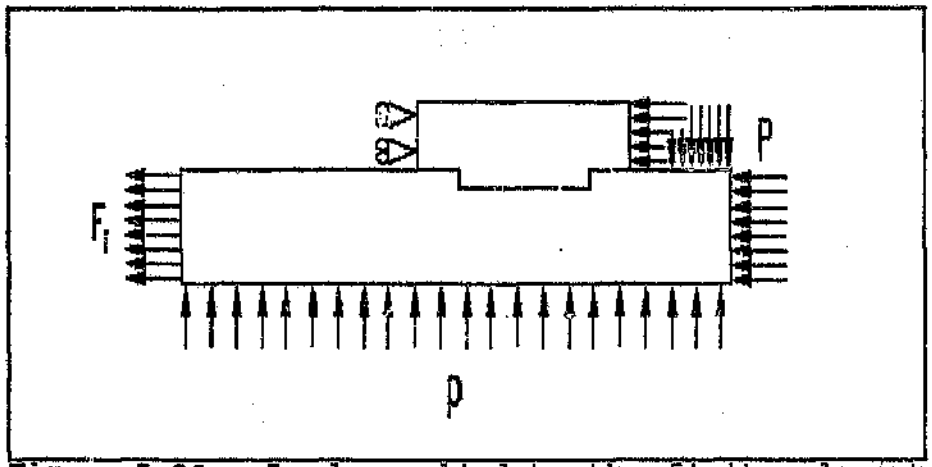

Figure 5.26 : Loads applied to the finite element model.

The internal pressure is applied through the seal to the outside of the pipe and the end of the flange. This causes compressive stresses in both the flange and the pipe. The pressure acting across the wall thickness of the pipe is applied as such and causes part of the axial load. The pressure acting axially on the inside of the pipe is applied as a force F_i on the end of the pipe. The force F_i is computed as follows:

$$F_i = P \cdot A_i$$

where A_i is the cross-sectional area on the inside of the pipe. Lastly, the internal pressure acts radially outwards.

The figures 4.45 and 4.46 show the axial and hoop stresses respectively of the pressurised model. Some differences exist between these results and the results for the un-pressurised model. Due to the additional pressure on the flange, the axial stresses have become more compressive, as expected. The moment caused by the flange is increased due to the pressure acting inwards through the seal. However the pressure acting radially tends to counteract this moment. The hoop stresses on the inside of the pipe are no longer compressive, but tensile stresses. This means that in this case buckling is no longer a problem.

However the pressure has introduced another stress concentration in the pipe and the flange at the face of the step. High axial compressive stresses act here, predominantly due to the pressure acting axially on the pipe wall. The stresses are considerably higher than in the un-pressurised case.

Pressurisation obviously has the effect of increasing the axial compressive stresses and decreasing the hoop stresses. Thus a different design approach should be taken for a pressurised pipe. To minimise the possibility of a compressive fibre failure, the step depth should be increased to increase the step's cross-sectional area. Although this may increase the possibility of a buckling failure (according to figure 5.19), this is to a certain extent not a problem since the compressive stresses have been decreased significantly by the internal pressure.

If the step depth was to be increased by 50% to 3 mm, the cross-sectional area would be increased by 48% . The compressive stress would consequently be decreased by approximately one third. Hence they would be in the region of the compressive axial stresses of the un-pressurised model. The hoop stresses would naturally increase. However the general stress pattern would be very similar to the un-pressurised case.

This means that with a few changes in the step dimensions a very similar load bearing capacity can be achieved as in the normal tensile case.

5.5 GENERAL CONSIDERATIONS

With a thin flange attached to the pipe (as is the case with all the configurations), various methods of joining adjacent pipes are possible. A split collar could be used as a backing flange (similar to the split ring used in the tensile test) with tie bolts holding the pipes together. Various sealing methods could be used, as discussed in chapter 2.

The coupling and sealing method which is suggested as being the best is shown in figure 5.27.

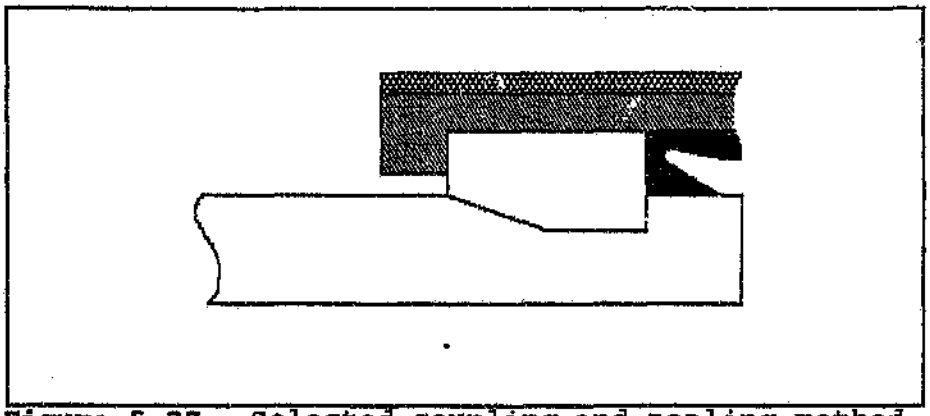

Figure 5.27 : Selected coupling and sealing method.

The hydrostatic rubber "U"-seal has been proved to be a very reliable seal and is currently being used with the Victaulic coupling to join steel pipes. One pre-requisite for this seal is that the pipe surface must be smooth, otherwise water can penetrate underneath the lips of the seal. This would have an adverse effect on the sealing capability.

Since it is desirable to have the entire coupling made from GRP, it was decided not to use any bolts. The danger with using bolts is that they can easily be overtightened. GRP can be damaged easily in this manner and may crack.

The coupling should be easily and quickly installed. For this reason the split ring is suggested. The two halves are simply clamped over the adjacent two flanges (of the adjacent pipes) and the sleeve is slid over the split ring to hold it together. Uncoupling the pipe is the reverse of this process: the outer sleeve is slid off and the two coupling halves fall apart.

As was mentioned earlier, the strength of the coupling depends on the strength of the interface between the pipe and the actual coupling (in this case it is the flange). This is also the limiting factor in the coupling design, since the interface cannot be made infinitely strong. The split ring on the other hand can always be increased in size to take the loads imposed on it.

One problem is envisaged, however, and that is that the fibres at the end of the pipe are exposed to the water. This is an area where the water can easily penetrate into the laminate under high pressures. Degradation of the laminate could start here and be the cause of weeping. Thus the pipe should be sealed somehow. In the TYPE X and TYPE XI flanges this would not be a problem since the steel flange extends up to the inside of the pipe and there are hence no exposed fibres. It might prove necessary to line the entire pipe with a thermoplastic liner (eg. PVC or polypropylene) to seal the inside of the pipe properly. (The need for this lining can however only be established through extensive testing). If the pipe is lined on the inside, then the liner can be extended over the end of the pipe and the exposed fibres can be sealed.

This coupling (shown in figure 5.27) satisfies most of the requirements laid down in section 1.1. One drawback of this coupling is that it does not permit angular or axial movement of the pipes. Any angular movement could possibly damage the coupling, although watertightness is not necessarily lost immediately.

One requirement was that the pipe's longitudinal strength at the joint should be at least equivalent to the remaining pipe's longitudinal strength. This is difficult to achieve in a GRP pipe (due to its anisotropic material properties and due to the fact that it is a layered material). By introducing the coupling, the stresses in both the flange and the pipe are increased significantly, which may cause the pipe to fail prematurely by a failure mode not related to the longitudinal strength of the pipe. Hence this requirement is difficult to achieve.

This coupling is nevertheless easily and quickly assembled and disassembled in limited working space, and with the minimum of individual adjustment. The coupling also maintains the constant internal diameter, so that the build-up of deposits does not occur. It is a "sexless" coupling, which has important advantages in confined spaces where the pipes cannot be turned around if they are oriented in the wrong direction.

On pull-wound pipes this coupling might be stronger than on filament wound pipes. The filament winding process creates a pipe with constant material properties throughout the pipe wall. The pull-winding process on the other hand has distinct layers with different material properties, ie. in one layer the fibres might be axially aligned giving this layer a high axial compressive strength, whereas another layer might have fibres aligned in the hoop direction giving this layer a high hoop strength. Thus the fibres in the step region (in the pipe) might be axially aligned, giving the step a higher compressive strength than in the filament wound pipe. This would result in a higher load bearing capacity.

Naturally the filament wound pipe could also be tailored in the step region (by aligning fibres at a different angle than ±55°) to take account of the loads imposed on it by the coupling. This would however require the use of a sophisticated filament winding machine, in order to achieve varying winding angles in the pipe.

6 CONCLUSIONS

Figure 6.1 shows four of the pipe/flange combinations that were tested.

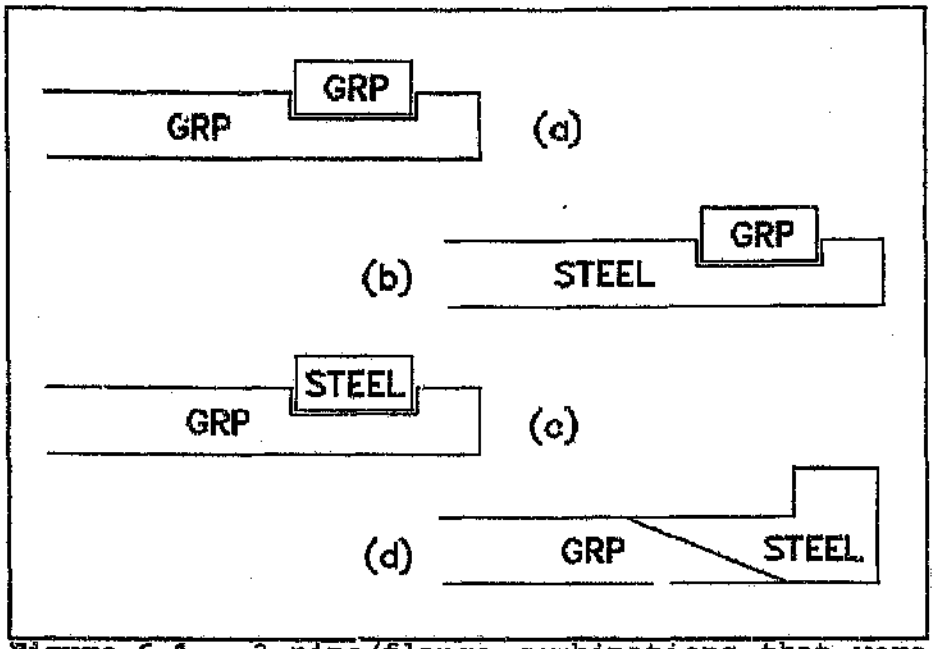

Figure 6.1 : 3 pipe/flange combinations that were tested.

1) The maximum load obtained with a GRP pipe and GRP flange was 75 kN, which is equivalent to an internal pressure of 22 MPa (see figure 6.1(a)). This result is valid for a pipe of 50 mm internal diameter, 8 mm wall thickness and a fibre orientation of ±55°. The pipe was made from E-glass fibres impregnated with epoxy resin, and the flange was made from E-glass fibres impregnated with polyester resin. The pipe and the flange have equivalent stiffnesses.

2) Three modes of failure can occur if a GRP pipe and GRP flange are used: compressive fibre failure, buckling failure and interlaminar shear failure. The compressive and buckling failures are slow failures and will cause weeping of the joint. The interlaminar shear failure is a catastrophic failure in that

the entire joint shears off instantaneously.

3) The maximum load obtained for the steel pipe with the GRP flange (figure 6.1(b)) was 105 kN, which is equivalent to an internal pressure of 31 MPa. The high strength of this joint can be attributed to the high stiffness of steel, which allows it to accommodate most of the load. It also shows that by tailoring the flange a high strength and stiffness can be achieved. If the GRP pipe (see point (1) above) had been tailored, then a higher load bearing capacity would also have been achieved in this case.

4) The high strength of the GRP pipe with the steel flange (75 kN, figure 6.1(c)) can also be attributed to the high stiffness of steel. In this case however the pipe was not tailored in the step region for this loading condition, and hence it failed earlier than the combination (3) above.

5) The maximum load obtained for the steel flange bonded to the GRP pipe by means of a scarf joint was 93 kN, which is equivalent to an internal pressure of 27 MPa. The performance of this coupling can be attributed to the high performance of the scarf joint. Extreme care must be taken when making the joint to ensure that the surfaces match properly, otherwise premature failure may occur (as in the TYPE XI (a) flange). The mode of failure is catastrophic as in the case of the interlaminar shear failure.

6) The stiffness of each component (pipe and flange) has a marked effect on the overall performance of a GRP coupling. An increase in stiffness brings with it an increase in load bearing capacity. Since the pipe was not tailored and hence its stiffness remained constant throughout the experiment, this effect is limited. In this case the flange was much stiffer than the GRP pipe, and hence the pipe was the member that always failed. The mode of failure however depended to a certain extent on the stiffness of the flange.

7) The finite element technique is useful in predicting pipe and coupling performance. It was successfully used to simulate the experiment, and was able to predict the mode of failure of the pipe.

8) The results are only valid for 50 mm pipes with a wall thickness of 8 mm. Since the endload increases quadratically with the diameter, the pressure capability drops very quickly as the diameter increases.

9) A lot of effort is required when designing with GRP in order to obtain the same performance of a steel coupling. Careful tailoring of both the pipe and the coupling is necessary in order to achieve high load bearing capacities.

10) The failure mechanism map shown in figure 5.19 is useful in that is shows which failure mode can be expected for a certain geometry. This failure map is particular to a pipe with an internal diameter of 50 mm and a wall thickness of 8 mm, but a similar map can be produced for any size of GRP pipe. From this failure map the relationship between the step depth t and the distance l of the step from the end of the pipe can be seen. As mentioned in (2) above, three different failure modes can occur in a GRP pipe. The failure map shows a point where all three modes are just about to occur. Here the relationship between the step depth and the distance of the step from the end of the pipe is such that the highest load bearing capacity is achieved.

11) The requirement for the design pressure (as stipulated in section 1.1) was 30 MPa for a pipe and coupling manufactured entirely from GRP. This requirement was not achieved. The highest load obtained for a GRP pipe with a GRP coupling during this research was 75 kN, which is equivalent to an internal pressure of 22 MPa (for a pipe with 50 mm internal diameter). This results in a safety factor of 1.1 (instead of the customary 1.5 for flexible pipes) on the target operating pressure of 20 MPa.

12) The guidelines for coupling design listed in section 1.1 were adhered to. From this point of view the research was a success, since it was the pipe that failed and not the pipe coupling.

7 RECOMMENDATIONS

1) Since the pipe is the member that fails when the load gets too high (between 65 kN and 75 kN), it is the pipe that needs to be strengthened in order to achieve higher loads. This can be done by optimising the fibre orientation at the end of the pipe, ie. by tailoring the pipe to take the loads imposed on it by the flange.

2) Optimisation of the pipe can also be done by incorporating a different material such as steel. The effect of a high strength, high stiffness material was dicussed in the report. By incorporating a steel member in the filament wound pipe, the end of the pipe could be substantially strengthened.

3) Alternatively one could simply build up the ends of the pipe. This extra thickness will increase the buckling strength of the pipe end. The step depth can then also be increased to increase the compressive strength at the pipe/flange interface.

4) Based on the results of the experiments it is recommended that a high strength, high stiffness material such as steel be incorporated into the design of a pipe coupling for operating pressures in excess of 20 MPa. It appears to be impossible to use a pipe with constant properties throughout (as is the case with a filament wound pipe with only one winding angle). Hence it is advisable that any sort of flange be incorporated into the pipe. This means that the pipes have to be manufactured to the correct lengths, and cannot be simply cut and joined.

REFERENCES

1) **ASTM Standards and Literature References for Composite Materials**, ASTM, Philadelphia, USA, 1987.
2) O.C. Young, J.J. Trott, **Buried Rigid Pipes: Structural design of pipelines**, London Elsevier, 1984.
3) E.W. Godwin, F.L. Matthews, P.F. Kilty, **The design of bolted flange joints in GRP**, Plastics and Rubber Processing and Applications, volume 6, number 2, 1986.
4) G.H. Ryder, **Strength of materials**, The Macmillan Press Ltd., London, 1982.
5) R.M. Jones, **Mechanics of composite materials**, McGraw-Hill Book Company, New York.
6) I. Skeist, **Handbook of Adhesives**, van Nostrand Reinhold Company, New York, 1977.
7) **E.M.R.C. NISA** element library, Finite Element software manual.
8) **Materials database of the RP/Composites Facility**, University of the Witwatersrand, Johannesburg, South Africa.
9) N.P. Cheremisinoff, **Fibreglass reinforced plastics handbook**, Ann Arbour Science, New York, 1977.
10) B. Jay Schrock, **Underground Plastic Pipe (International Conference on)**, American Society of Civil Engineers, New York, 1981.
11) **Duropenta: Durolok, Duroquick**, trade pamphlet, Durban.

APPENDIX A – CLASSICAL LAMINATION THEORY

This theory assumes a plane stress state for laminate with orthotropic material properties, ie.

$$\sigma_3 = 0 \qquad \tau_{23} = 0 \qquad \tau_{31} = 0$$

where the direction 1 is along the fibre axis, direction 2 is transverse to the fibre direction and direction 3 is through the thickness.

The strain-stress relations can be written as

$$\begin{Bmatrix} \epsilon_1 \\ \epsilon_2 \\ \gamma_{12} \end{Bmatrix} = \begin{bmatrix} S_{11} & S_{12} & 0 \\ S_{12} & S_{22} & 0 \\ 0 & 0 & 2*(S_{11}-S_{12}) \end{bmatrix} \begin{Bmatrix} \sigma_1 \\ \sigma_2 \\ \tau_{12} \end{Bmatrix}$$

where

$$S_{11} = \frac{1}{E} \quad \text{and} \quad S_{12} = -\frac{\nu}{E}$$

and the stress-strain relations are

$$\begin{Bmatrix} \sigma_1 \\ \sigma_2 \\ \tau_{12} \end{Bmatrix} = \begin{bmatrix} Q_{11} & Q_{12} & 0 \\ Q_{12} & Q_{11} & 0 \\ 0 & 0 & Q_{66} \end{bmatrix} \begin{Bmatrix} \epsilon_1 \\ \epsilon_2 \\ \gamma_{12} \end{Bmatrix}$$

where

$$Q_{11} = \frac{E}{1-\nu^2} \quad \text{and} \quad Q_{12} = \frac{\nu E}{1-\nu^2} \quad \text{and} \quad Q_{66} = \frac{E}{2(1+\nu)} = G$$

To obtain the stress strain relations for a lamina of arbitrary orientation the transformation matrix is used, viz.

$$\begin{Bmatrix} \sigma_x \\ \sigma_y \\ \tau_{xy} \end{Bmatrix} = \begin{bmatrix} \cos^2\theta & \sin^2\theta & -2\sin\theta\cos\theta \\ \sin^2\theta & \cos^2\theta & 2\sin\theta\cos\theta \\ \sin\theta\cos\theta & -\sin\theta\cos\theta & \cos^2\theta-\sin^2\theta \end{bmatrix} \begin{Bmatrix} \sigma_1 \\ \sigma_2 \\ \tau_{12} \end{Bmatrix}$$

which results in

$$\begin{Bmatrix} \sigma_x \\ \sigma_y \\ \tau_{xy} \end{Bmatrix} = \begin{bmatrix} \overline{Q_{11}} & \overline{Q_{12}} & \overline{Q_{16}} \\ \overline{Q_{12}} & \overline{Q_{22}} & \overline{Q_{26}} \\ \overline{Q_{16}} & \overline{Q_{26}} & \overline{Q_{66}} \end{bmatrix} \begin{Bmatrix} \epsilon_x \\ \epsilon_y \\ \gamma_{xy} \end{Bmatrix}$$

where

$$\overline{Q_{11}} = Q_{11}\cos^4\theta + 2(Q_{12}+2Q_{66})\sin^2\theta\cos^2\theta + Q_{22}\sin^4\theta$$

$$\overline{Q_{12}} = (Q_{11}+Q_{22}-4Q_{66})\sin^2\theta\cos^2\theta + Q_{12}(\sin^4\theta+\cos^4\theta)$$

$$\overline{Q_{22}} = Q_{11}\sin^4\theta + 2(Q_{12}+2Q_{66})\sin^2\theta\cos^2\theta + Q_{22}\cos^4\theta$$

$$\overline{Q_{16}} = (Q_{11}-Q_{12}-2Q_{66})\sin\theta\cos^3\theta + (Q_{12}-Q_{22}+2Q_{66})\sin^3\theta\cos\theta$$

$$\overline{Q_{26}} = (Q_{11}-Q_{12}-2Q_{66})\sin^3\theta\cos\theta + (Q_{12}-Q_{22}+2Q_{66})\sin\theta\cos^3\theta$$

$$\overline{Q_{66}} = (Q_{11}+Q_{22}-2Q_{12}-2Q_{66})\sin^2\theta\cos^2\theta + Q_{66}(\sin^4\theta+\cos^4\theta)$$

APPENDIX B – TABLE OF RESULTS FOR FIGURE 3.3

The following table lists thicknesses (calculated with the Classical Lamination Theory) for various pipe sizes and internal pressures. These calculations are based on a minimum tensile strength of 500 MPa and 250 MPa compressive strength. These are conservative figures as quoted by material suppliers. With a stronger fibre the wall thickness would be decreased.

The straight line equation calculated from this data is

$$t = \frac{1}{455} * P * D$$

WALL THICKNESSES FOR VARIOUS PIPE SIZES AND PRESSURE RANGES (AXIAL STRESS = 500 MPa, COMPRESSIVE STRESS = 250 MPa)

INTERNAL DIAMETER [mm]	WALL THICKNESS [mm]			
	P=10 MPa	P=15 MPa	P=20 MPa	P=25 MPa
10	—	—	0.44	—
20	0.44	0.64	0.88	1.12
30	—	—	1.32	—
40	0.88	1.32	1.76	2.20
50	1.12	—	2.20	—
60	1.32	2.00	2.64	3.32
70	1.56	—	3.08	—
80	1.76	2.64	3.52	4.40
90	2.00	—	3.96	—
100	2.20	3.32	4.40	5.50
110	2.40	—	4.84	—
120	2.64	3.96	5.28	6.60
130	2.88	—	5.72	—
140	3.08	4.64	6.16	7.70
150	3.32	—	6.60	—
160	3.52	5.28	7.04	8.80
170	3.76	—	7.48	—
180	3.96	5.96	7.92	9.90
190	4.20	—	8.36	—
200	4.40	6.60	8.80	11.00

APPENDIX C — ELEMENT MESHES

Figure C.1 shows the element mesh used in the finite element analysis. The mesh is fairly coarse in the regions of low stress concentration, and is fine in the regions of high stress concentrations such as the front of the flange.

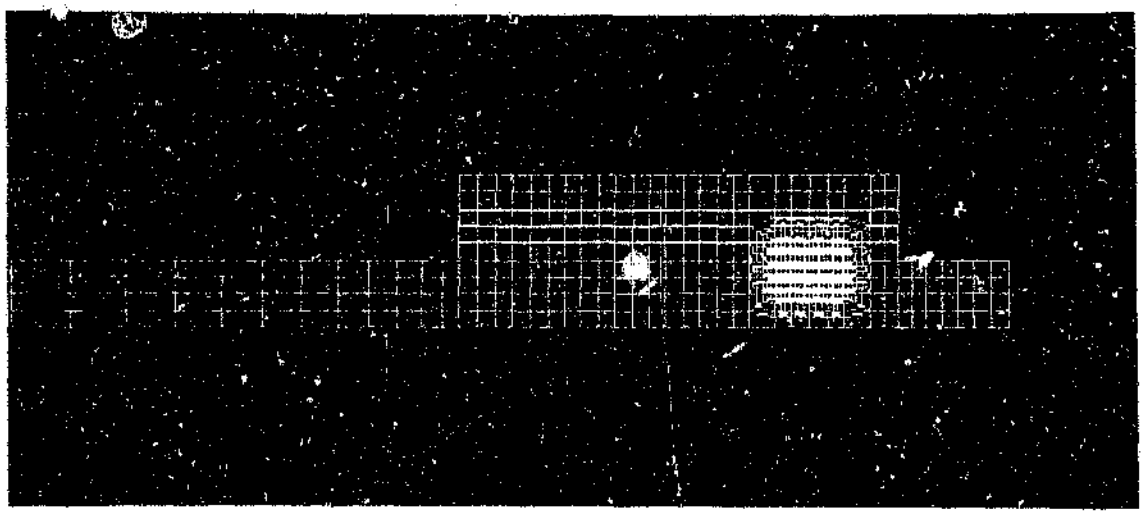

Figure C.1 : Finite element mesh of flange and pipe.

The figure C.2 shows the refined mesh at the front of the flange (step region). The triangular elements were used to simulate the small radius which occurs in the corners of the step due to the machining process.

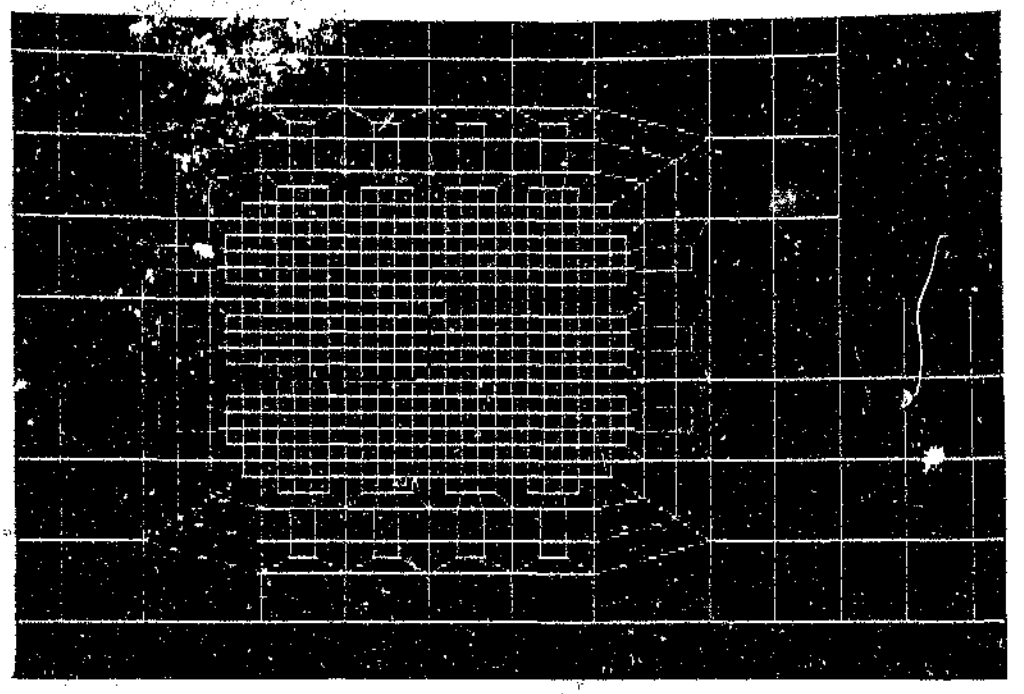

Figure C.2 : Refined mesh at step.

APPENDIX D – FINITE ELEMENT RESULTS

The following two figures are additional stress contours (hoop and shear) of the TYPE IV flange (figure 4.44 shows the axial stress contours).

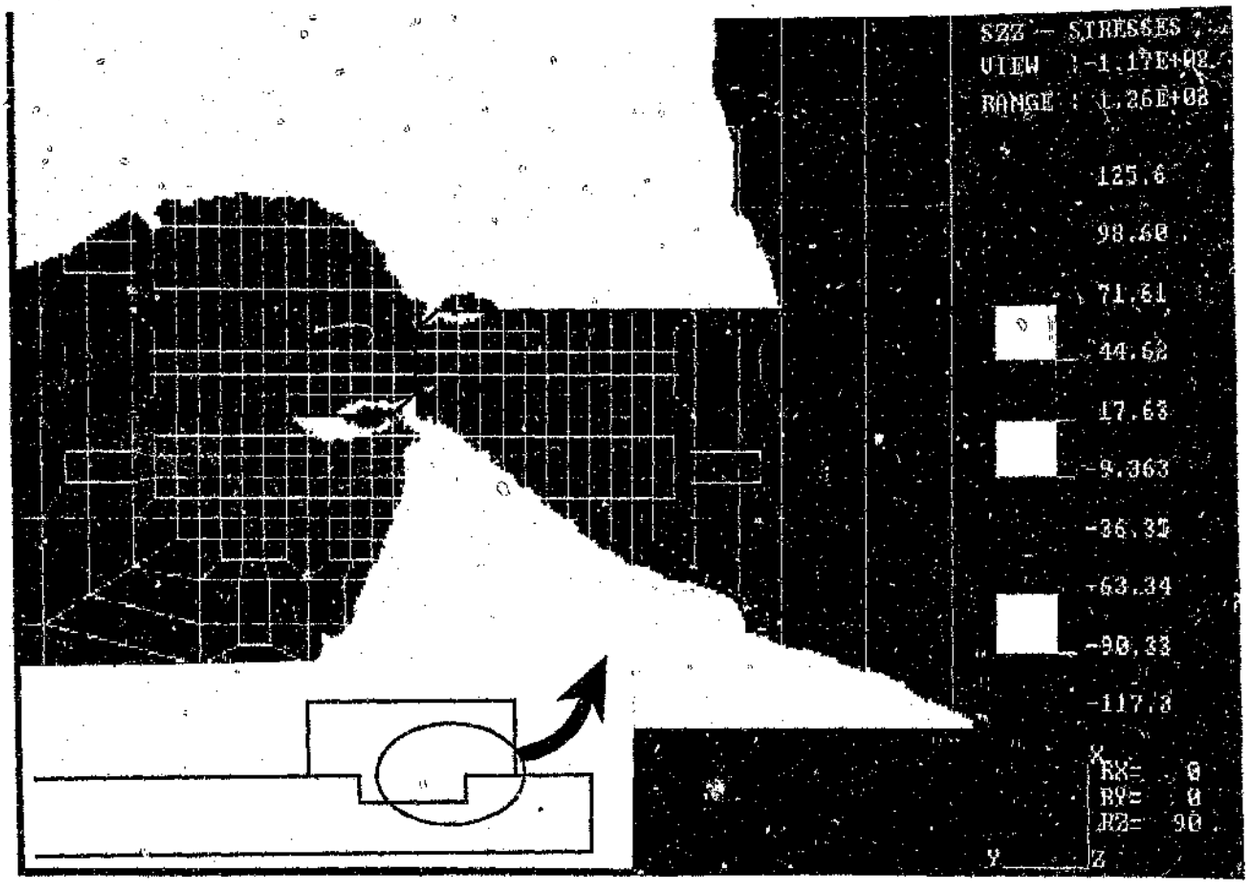

Figure D.1 : Hoop stresses in GRP pipe with GRP flange (TYPE IV).

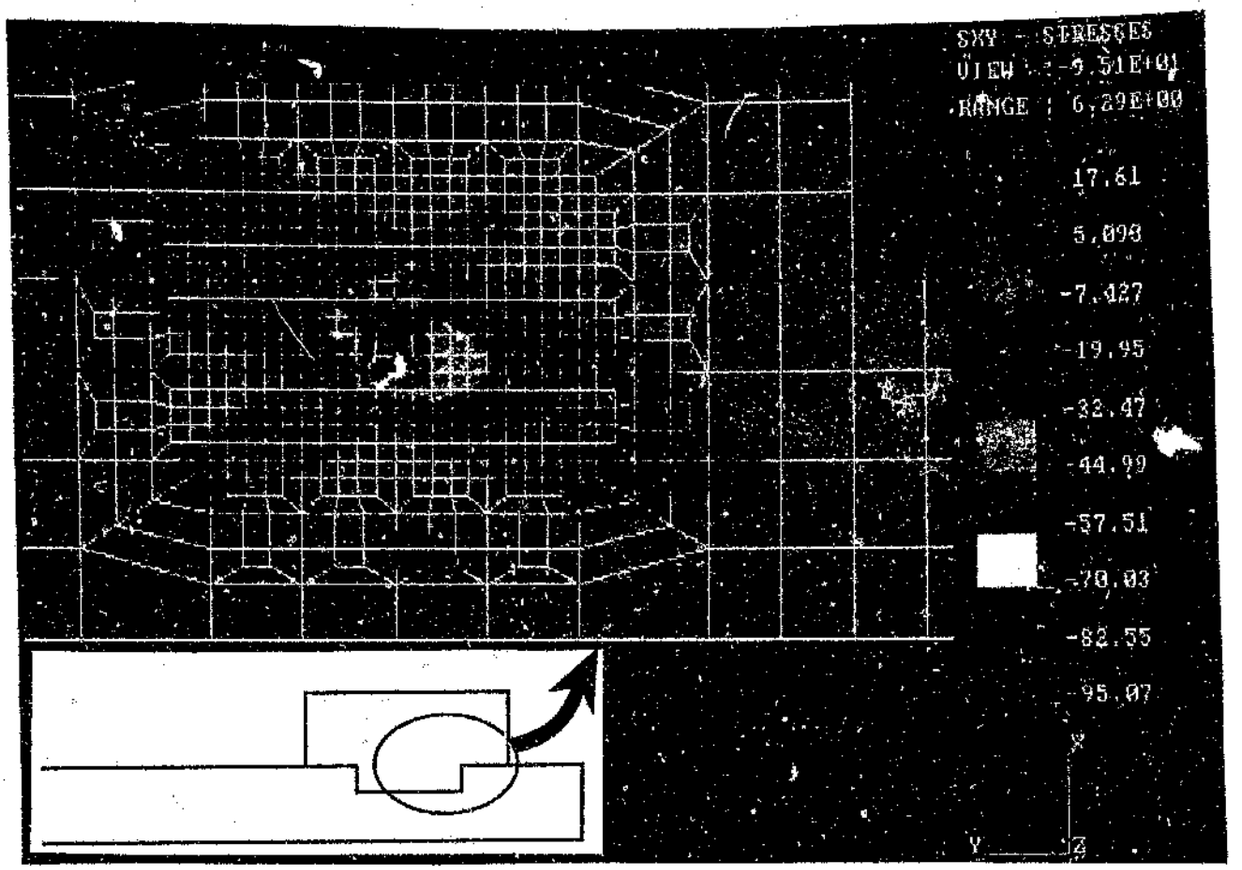

Figure D.2 : Shear stresses in GRP pipe with GRP flange (TYPE IV).

Author: Gutmayer Johannes.
Name of thesis: Evaluation of glassfibre reinforced plastic pipe couplings for high pressure applications.

PUBLISHER:
University of the Witwatersrand, Johannesburg
©2015

LEGALNOTICES:

Copyright Notice: All materials on the University of the Witwatersrand, Johannesburg Library website are protected by South African copyright law and may not be distributed, transmitted, displayed or otherwise published in any format, without the prior written permission of the copyright owner.

Disclaimer and Terms of Use: Provided that you maintain all copyright and other notices contained therein, you may download material (one machine readable copy and one print copy per page)for your personal and/or educational non-commercial use only.

The University of the Witwatersrand, Johannesburg, is not responsible for any errors or omissions and excludes any and all liability for any errors in or omissions from the information on the Library website.